Carboranylphosphinic acids: A New Class of Purely Inorganic Ligands to Generate Polynuclear Compounds and Multifunctional Nanohybrid Materials for Biomedical Applications

Elena Oleshkevich

Universitat Autònoma de Barcelona

Carboranylphosphinic acids: A New Class of Purely Inorganic Ligands to Generate Polynuclear Compounds and Multifunctional Nanohybrid Materials for Biomedical Applications

Elena Oleshkevich

TESI DOCTORAL

Programma de Doctorat de Química

Directora: Prof. Clara Viñas i Teixidor

Tutor: Dr. Lluis Escriche Martinez

Departament de Química

Facultat de Ciències

2017

Memòria presentada per aspirar al Grau de Doctor per

Elena Oleshkevich

Vist i plau

Prof. Clara Viñas i Teixidor (Directora)

Dr. Lluis Escriche Martinez (Tutor)

Bellaterra, 11 de Maig de 2017

La Professora CLARA VIÑAS i TEIXIDOR, Professora d'Investigació del Consejo Superior de Investigaciones Científicas a l'Institut de Ciència de Materials de Barcelona

CERTIFICA

Que en Elena Oleshkevich, llicenciat en Enginyeria Química, ha realitzat sota la meva direcció la Tesí Doctoral que porta per títol "*Carboranylphosphinic acids: A New Class of Purely Inorganic Ligands to Generate Polynuclear Compounds and Multifunctional Nanohybrids Materials for Biomedical Applications*" i que recull aquesta memòria per optar al títol de Doctor en Química per la Universitat Autònoma de Barcelona.

I, perquè consti i tingui els efectes corresponents, signa aquest certificat a Bellaterra, a 11 de Maig de 2017.

Prof. CLARA VIÑAS i TEIXIDOR

ICMAB (CSIC)

Campus de la Universitat Autònoma de Barcelona
08193 Bellaterra, Catalunya, Espanya
Telf.: +34 935 801 853
Fax.: +34 935 805 729
http://icmab.es/

Aquest treball de recerca ha estat finançat per la Comisión Interministerial de Ciencia y Tecnología, CICYT, mitjançant els projectes CTQ2013-44670-R i CTQ2016-75150-R; per la Generalitat de Catalunya amb el projecte 2014/SGR/149 i al projecte concedit per l'ALBA (ref.: 2015091372). Agraïr la beca de Formació de Personal Universitari (FPU, ref.: AP-2012-3828) concedida pel Ministerio de Ciencia e Innovación, durant el període maig del 2013 al abril del 2017.

Aquest treball d'investigació, amb la data de defensa del 23 de Juny de

2017 , té com a membres del tribunal a:

- President: Prof. Olivier Diat, Investigador CEA, Institut de Chimie Séparative de Marcoule.

- Secretari: Dra. Mercé Capdevila, Professora Titular d'Universitat de la Universitat Autònoma de Barcelona.

- Vocal: Dra. Fernanda Marujo Marques, Investigador científic, Departamento de Ciências e Tecnologias Nucleares, Campus Tecnológico e Nuclear, Instituto Superior Técnico da Universidade de Lisboa.

Com a membres suplents:

- Suplent 1: Prof. Joan Suades Ortuño, Catedràtic de la Universitat Autònoma de Barcelona.

- Suplent 2: Dra. Montserrat Rodríguez, Professora Titular de Química de la Universitat de Girona.

ACKNOWLEDGEMENTS

To begin I would like to point that I am in debt to many people for the accomplishment of this PhD thesis. First of all I want to thank Prof. Clara Viñas, my PhD director, who accepted me with lots of care, who always believed in me, who always encouraged me, always gave lots of scientific ideas and supported mines, so I had a chance to learn many techniques, participate in many conferences and training scientific schools, and work on application part of ligands synthesized in this PhD thesis. I would also like to thank Prof. Francesc Teixidor, who also supported, motivated, and directed me during these 5 years of PhD thesis, for his predisposition to solve any of my doubts at any moment. To both of them I would like to express my appreciation!

To Dr. Rosario Núñez and Dr. José Giner for their collaboration and kind advices.

To Dr. Anna Rosell, thank you for accepting our collaboration with all your passion (and incredible energy) for research. To Dr. Anna Morancho, who performed many biological tests for us, it was a great pleasure to learn from you. To Dr. Koen Galenkamp, who also realized many biological studies for us with cancer cells, thank you for the many ideas and explanations you provided me during our collaboration.

To Dr. Lluis Escriche from Universitat Autònoma de Barcelona for accepting to be my PhD tutor.

To Dr. Ana Paula Candiota from Universitat Autònoma de Barcelona for being so welcome always and providing autoclave sterilization of our samples.

To Dr. Xavier Fontrodona, Prof. Reijo Sillanpää, DR. Duane Choquesillo-Lazarte, Prof. Matti Haukka for the resolution of the crystalline structures presented in this work, in spite of some of them were really challenging.

Special thanks to Dr. Isabel Romero García! Your help was essential for the work with coordination polymers! Thank you also for being so helpful and providing me many explanations and experience during our work, for the private advices as well.

I am thankful to Prof. Xavier Obradors, the director of ICMAB for accepting me in the institute and giving me the opportunity to use all the services within the institute as well as to all the ICMAB´s personnel for doing their best for me.

I wish also to thank to Anna Fernández for all the patience in doing and sometimes repeating NMR analysis, for her advices and nice atmosphere always in her “lab”, and to Jordi Cortés, without him the work in the laboratory would not be possible! Gracias Jordi!!!

To my colleagues who became my friends also! To Radu Popescu for training me in the lab and explaining many details about NMR and chemistry in general, to Màrius Tarrés for his help in the lab always and with catalan, motivation in general and funny company in SAF, to Ivy and Adnana for their attention and friendly talks that made my days in the lab. Especially to Adnana, you taught me to be patient! To Arpita and Abhishek, thank you both for help with English! Also to Arpita and Ines (my students ☺) who became good friends for me! To Isa and Bego for their support, funny talks and help with catalan. And all other students in our group (Albert, Ana Cioran, David, Ana Daniela, Marius Lupu, Flavia, Lei, Mahdi, Victor, Justo) for all your collaboration and good atmosphere in the group! I wish also to give thanks to Elena Laukhina, for her taking care of me and encouraging me.

Also my thoughts bring to my friends (Katia, Jane, Stamatis, Pablo) and one's nearest and dearest (Victor), who made my life last 5 years, and motivated in difficult moments. To Victor, who always supported me and has been there with me, for me in good, in bad. Thank you moi miliy! Вите, которому я благодарна за его терпение и за то, что он рядом!

The last, but one of the most important to my mother, without whom I would not be who I am now. Мама, спасибо за все терпение и поддержку, понимание и любовь!

Thank you all for you've done for me and for all I've learnt!

ORGANITZACIÓ DEL MANUSCRIT

D’acord amb la normativa vigent i prèvia acceptació de la comissió de Doctorat de la Universitat Autònoma de Barcelona, aquesta Memòria es presenta com a recull de publicacions, que va ser aprovada per aquesta comissió el dia 26 d'abril de 2017 (Addendum I). A més d'incloure les publicacions aprovades, també s'han inclòs els treballs realitzats en el marc d'aquesta tesi doctoral que estan enviats o en procés de elaboració (Addenium II).

Addendum I. Articles publicats i presentats a la Comissió de Doctorat de la Universitat Autònoma de Barcelona al 26 de abril de 2017:

1. “Carboranylphosphinic Acids: A New Class of Purely Inorganic Ligands”. Elena Oleshkevich, Francesc Teixidor, Duane Choquesillo-Lazarte, Reijo Sillanpää, and Clara Viñas. *Chemistry- A European Journal*, **2016**, *22*, 3665-3670.

2. “*m*-Carboranylphosphinate as Versatile Building Blocks to Design All Inorganic Coordination Polymers”. Elena Oleshkevich, Clara Viñas, Isabel Romero García, Duane Choquesillo-Lazarte, Matti Haukka, and Francesc Teixidor. *Inorganic Chemistry*, **2017**, DOI: 10.1021/acs.inorgchem.7b00610.

Addendum II. Articles d'aquesta tesi doctoral que estan enviats o en procés de elaboració:

1. “Merging Icosahedral Boron Clusters and Magnetic Nanoparticles: Aiming towards Multifunctional Nanohybrid Materials”. Elena Oleshkevich, Francesc Teixidor, Anna Rosell and Clara Viñas.

2. ”Biocompatible Fully Inorganic Nanohybrids for Biomedical Applications: Combining Magnetic Nanoparticles and Icosa-hedral Boron Clusters”. Elena Oleshkevich, Anna Morancho, Koen M. O. Galenkamp, Alba Grayston, Joan X. Comella, Francesc Teixidor, Anna Rosell, and Clara Viñas.

Numbering of the compounds

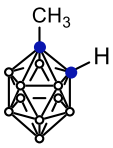

(1)

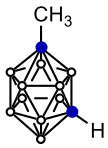

(2)

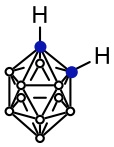

(3)

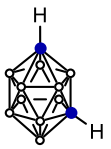

(4)

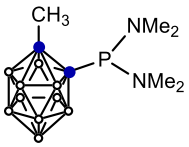

(5)

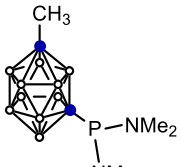

(6)

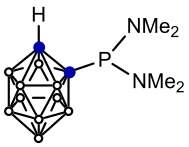

(7)

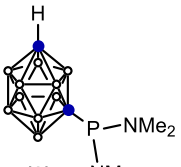

(8)

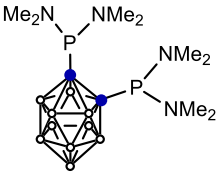

(9)

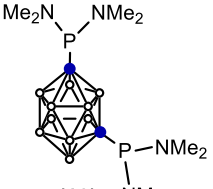

(10)

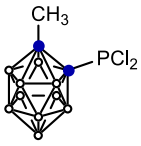

(11)

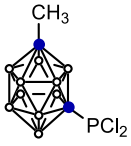

(12)

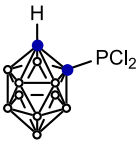

(13)

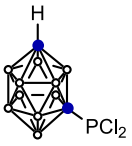

(14)

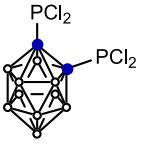

(15)

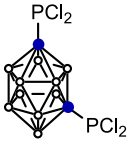

(16)

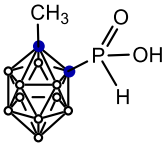

(17)

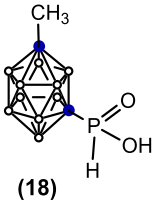

(18)

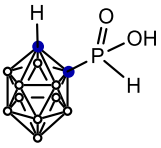

(19)

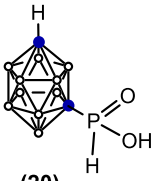

(20)

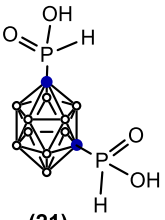

(21)

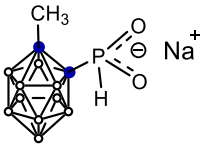

(22)

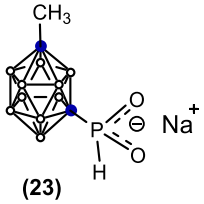

(23)

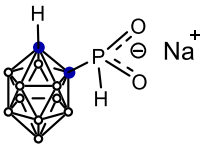

(24)

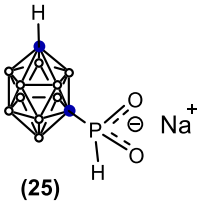

(25)

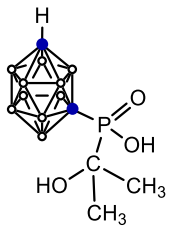

(26)

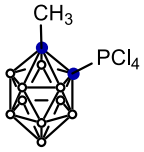

(27)

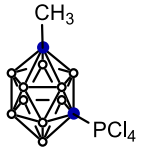

(28)

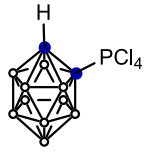

(29)

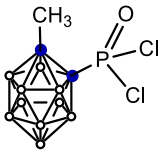

(30)

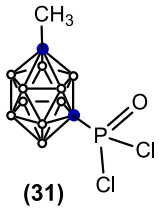

(31)

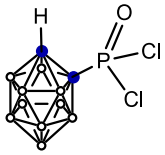

(32)

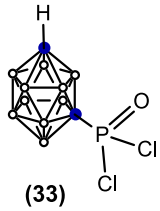

(33)

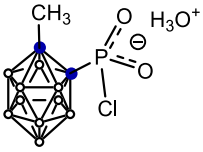

(34)

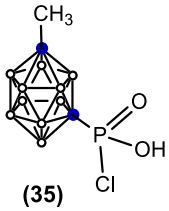

(35)

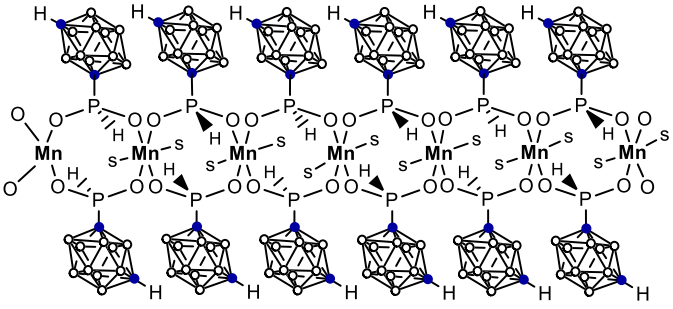

(36) s = MeOH

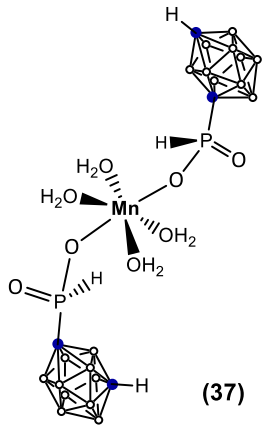

(37)

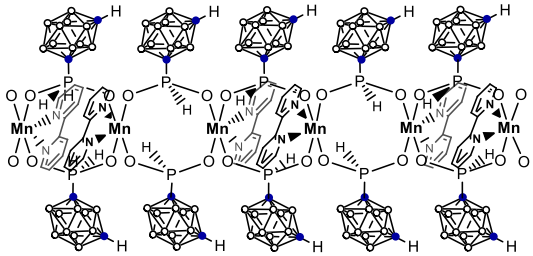

(38)

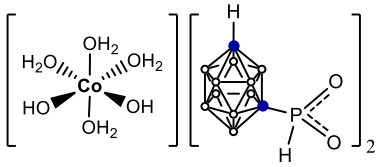

(39)

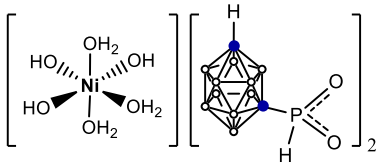

(40)

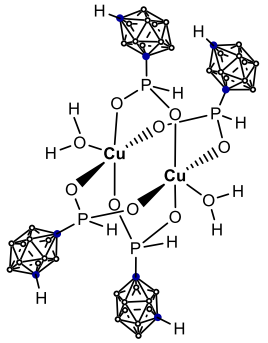

(41)

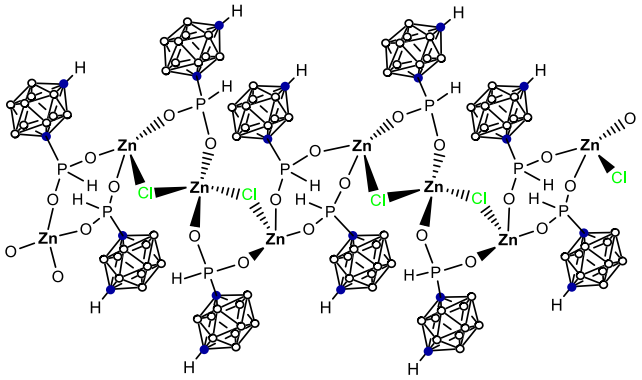

(42)

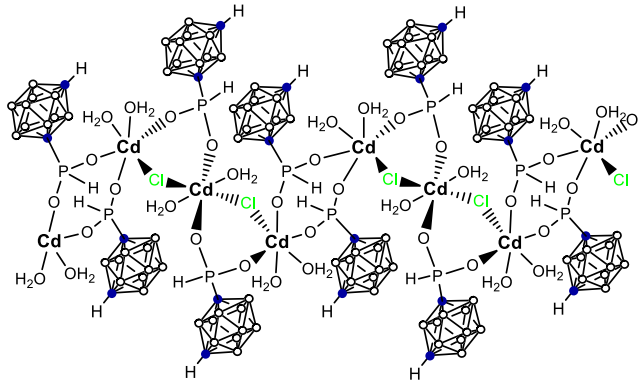

(43)

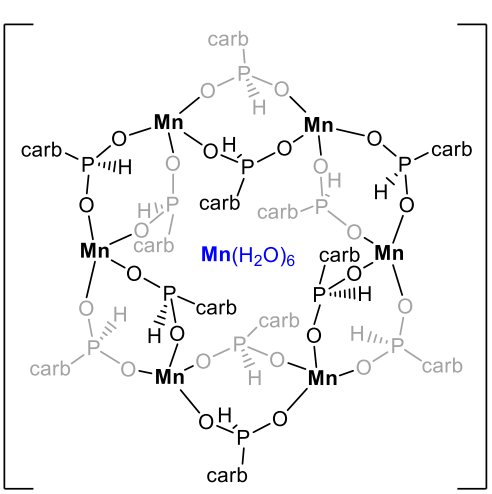

(44)

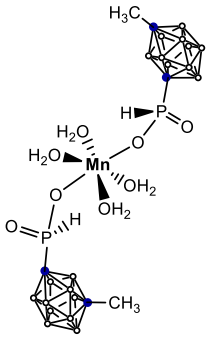

(45)

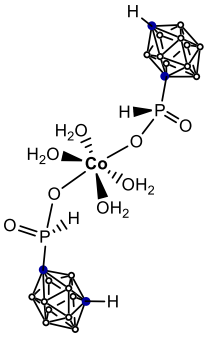

(46)

carb =

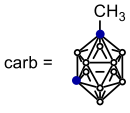

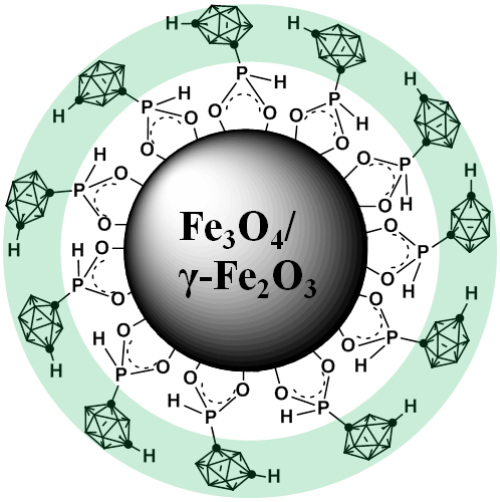

1-MNPs

Abbreviations

δ – NMR chemical shift

BNCT – Boron Neutron Capture Therapy

bipy – 4,4-bipyridine

C_c – carbon atom belonging to carborane cluster

C_{bpy} – carbon atom belonging to 2,2´-bipyridine

DSC – Differential Scanning Calometry

2,2´-bpm – 2,2´-bipyrimidine

2,2´-bpy – 2,2´-bipyridine

H_{CH3} – proton atom belonging to methyl group

IR – InfraRed

^{i}Pr – *iso*-propyl

MNPs – magnetic nanoparticles

1-MNPs – *meta*-carboranylphosphi-nate MNPs

Me – methyl

NCT – Neutron Capture Therapy O_w – oxigen atom belonging to water

NMR – Nuclear Magnetic Resonance

Ph – phenyl

n-BuLi – *normal*-butyl lithium

t-Bu – *tert*-buthyl

STEM-HAADF – High-angle annular dark-field (HAADF) scanning transmission electron microscopy (STEM)

TGA – ThermoGravimetric Analysis

TEM – Transmission Electron Spectroscopy

XPS – X-ray photoelectron Spectroscopy

$Ø_{carborane}$ – diameter of carborane cluster

Table of contents

Introduction

1.1 Carboranes

1.1.1 Boron chemistry and the nature of the B-B bonding

In the periodic table of elements, boron lines next to carbon. Both, boron and carbon have the property to catenate. Carbon forms cycles and polymers and is the base of organic chemistry. Boron forms clusters and induces a huge discipline of chemistry: Boron science. Boranes, boron clusters, and in particular, icosahedral dicarba-*closo*-dodecaboranes with impirical formula $C_2B_{10}H_{12}$ are of special interest. Boron clusters were considered as electron deficient compounds till Lipscomb´s discovery. William N. Lipscomb was awarded with the Nobel Prize in Chemistry 1976 "for his studies on the structure of boranes illuminating problems of chemical bonding". Lipscomb proposed the mechanism to understand the three-center two-electron (3c-2e) bond in boron clusters[1]. In 3c-2e a pair of electrons is shared between three atoms. The three atoms can be a boron atom at either end and a hydrogen atom in the middle as in the case of the diborane B-H-B bonds or the three atoms can be three boron atoms as in the polyhedral clusters. 3D aromaticity of boron or carborane clusters gives them unique properties that are not common in organic chemistry[2,3,4].

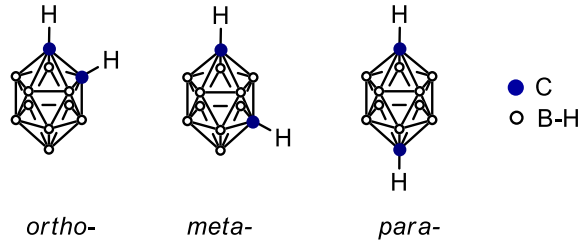

Figure 1.1 The three isomers of icosahedral dicarba-*closo*-dodecarboranes ($C_2B_{10}H_{12}$).

Relation between hydrocarbon and borohydride chemistries have been recently reported.[5,6] The idea is based on keeping the same number of valence electrons in a confined space. Thus “addition” of an extra electron to each boron atom in borohydrides yields molecular analogues of hydrocarbons. As a result, for any given hydrocarbon in organic chemistry can be find its borohydride analogue in

boron chemistry.[5] Following this direction, recently was reported the work that establishes a direct connection between Wade-Mingos rule of tridimensional aromatic *closo* boron hydride clusters and Hückel´s rule of planar aromatic annulenes, showing that they share a common origin regulated by the number of valence electrons in a electronic confined space[6].

1.1.2 Carboranes: Synthesis, properties and reactivity

Although *ortho*- and *meta*-carborane clusters are remarkable stable, in certain reaction conditions they exhibit high synthetic reactivity. From point of view of electrophilic substitution at the C_c-H vertices (C_c: carbon atom belonging to carborane cluster), both isomers display similar chemical reactivity. In both carborane isomers, the hydrogen atoms of the C_c-H units are more acidic than the ones bonded to B-H vertices, due to more electronegative character of carbon with respect to boron (2.5 and 2.0 respectively, according to Pauling scale). Thus, hydrogen atoms attached to carbon can be considered as acidic while those bonded to boron as hydride. The acidity of the C_c-H vertices decreases in the order of *ortho*-, *meta*- and *para*-carborane. In the same order decreases its vulnerability to get deprotonated.

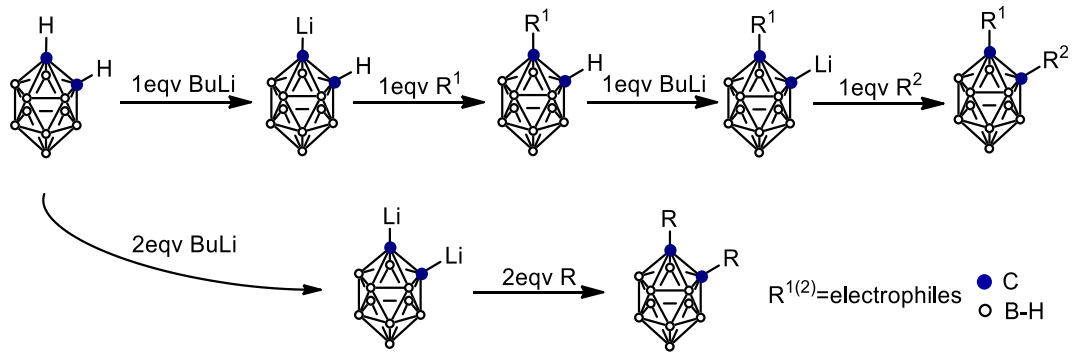

Scheme 1.1. Deprotonation reaction of C_c-H units followed by substitution with electrophilic agents.

This relatively acidic character of C_c-H units allows their deprotonation by strong alkali and alkaline earth metal bases, like for example *n*-butyllithium or Grignard reagents. The generated negative charge on the carbon atom of the

cluster, C_c, attracts electrophilic reagents, opening the way to the introduction of funcional groups at the C_c position of the cluster.

Scheme 1.1 shows the two possible pathways for substitutions at one or both of the C_c atoms. After dilithiation of the carborane cluster it is possible to introduce simultaneously twice the same substituent, which leads to symmetrically substituted carborane. The other pathway (top) demonstrates monosubstitution of the carborane cluster or the unsymmetrical disubstitution. The synthesis of monosubstituted carborane derivatives is more complicated compared to disubstituted. The reason is the disproportionation of Li[1,2-$C_2B_{10}H_{11}$] into Li_2[1,2-$C_2B_{10}H_{10}$] and 1,2-$C_2B_{10}H_{12}$ how it was found for *ortho*-carborane[7]. Several approaches have been developed to overcome this problem. Among them is using the way of protection/deprotection methodologies with dimethoxyethane as the solvent or by doing the reaction at high dilution[8,9,10]. Perhaps more simple method is carrying the monosubstitution reactions in ethereal solvents at low temperature and specific carborane concentration. It was suggested that depending on type of electrophile it is possible to find combination of conditions (ethereal sovent, temperature, carborane concentration) that facilitate the largest degree of monosubstitution[11].

The coupling to a boron atom of a carborane cluster can be performed through iodo-substituted carborane with following palladium-catalyzed cross-coupling reaction (Scheme 1.2).[7]

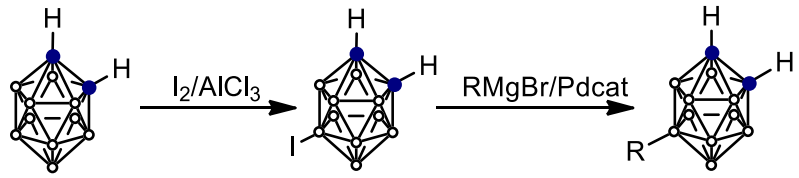

Scheme 1.2. *Ortho*-carborane substitution in the B(9) position through iodo-derivative.

1.2 *Closo* – Carboranylphosphorus compounds

1.2.1 General aspects on *closo*-carboranylphosphines

Since their discovery phosphines continue to be the most significant class of ligands in coordination chemistry and catalysis. Nowadays a big choice of different phosphine ligands[12] is commercially available from chemical products suppliers: monodentate, bidentate, Buchwald, cataCXium, Dalphos ligands.

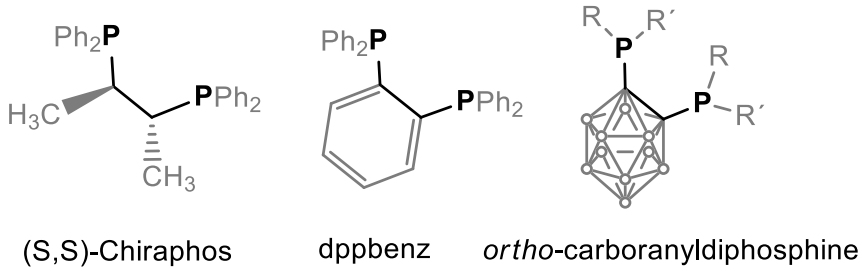

(S,S)-Chiraphos dppbenz *ortho*-carboranyldiphosphine

Figure 1.2 C_2-symmetric backbone of different phosphine ligands.

Bidentate phosphine ligands play an important role in catalysis. C_2-symmetric backbone of phosphine ligand is favored because it allows the formation of stable five-membered rings by coordination to transition metal through phosphorus atoms. Due to its C_2 symmetry 1,2-dicarba-*closo*-dodecaborane, or *ortho*-carborane, same way as ethylene and *ortho*-phenylene attracted lot of attention as a platform do produce chelating bidentate phosphine ligands (Figure 1.2).

Our group and others were interested in the exploration of the properties of phosphinate ligands synthesized on the *ortho*-carborane platform[13]. Among them P(III) and P(V) derivatives of *ortho*-carboranylphoshines[14]. Substituting conventional organic entities by boron clusters to produce new compounds could lead to remarkable properties as high rigidity, space occupancy and hydrophobicity of the cluster group. Carboranylphosphines is one of the examples[13]. By changing groups bonded to phosphorus, the steric and electronic effects can be modified, so it is possible to “tailor” properties of the phosphines as ligands. A representative drawing of the carboranyl phosphines, carboranyl phosphine oxides, carboranyl phosphinates and carboranyl phosphonates is shown in Figure 1.3.

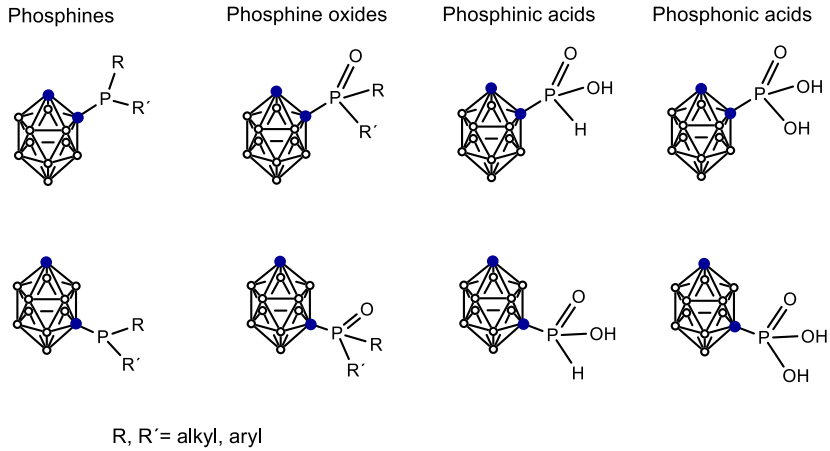

Figure 1.3 Phosphorus-substituted *closo*-carboranes.

1.2.2 *Closo* – Carboranylphosphines with P(III) moieties

The chemistry of *closo*-carboranylphosphines started in 1963[15], almost immediately after discover of *ortho*-carborane, when the first P(III) derivative, 1,2-$(PPh_2)_2$-1,2-*closo*-$C_2B_{10}H_{10}$, was synthesized by R. P. Alexander and H. Schroeder in a reaction between dilithio-*ortho*-carborane and two equivalents of diphenylchlorophosphine. This reaction became a fundamental for the synthesis of numerous symmetrical 1,2-bis(phosphino)-*closo*-carboranes.

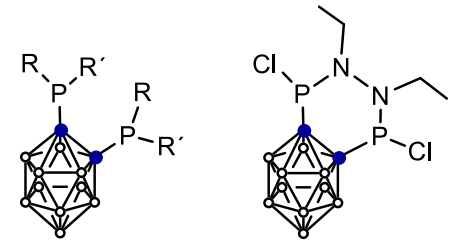

R= Ph; R´=Cl
R= t-Bu; R´=Cl
R= NEt_2; R´=Cl

Figure 1.4 1.2-bis(phosphino)-*closo*-carboranes.

P-chiral 1,2-bis(chlorophosphino)-*closo*-carboranes and cyclic compound showed on Figure 1.4 were obtained in the same reaction between dilithio-*ortho*-carborane and appropriate phosphine[16]. In many cases was possible to isolate each diastereomer.

Considering that chlorophosphines are good starting products for the synthesis of other organophosphorus compounds (phosphonate esthers and amides, phosphinic and phosphonic acids and their esters) it appeared of interest to synthesize *closo*-carboranylchloro-phosphine derivatives[15]. By the same scientists,

R. P. Alexander and H. Schroeder, it was found that equimolar quantities of dilithio-*ortho*-carborane and PCl_3 form a cyclic dimer [1,2-PCl-1,2-*closo*-$C_2B_{10}H_{10}]_2$. However, in the reaction of dilithio-*meta*-carborane with PCl_3 they found 1,7-bis(dichlorophosphino)-*closo*-carborane and *meta*-carborane containing polymer (Scheme 1.5). It can be explained by the fact that in *ortho*-carborane two carbon atoms of the cluster, C_c, are in adjacent position, while in *meta*-carborane they are separated by one B-H vertice.

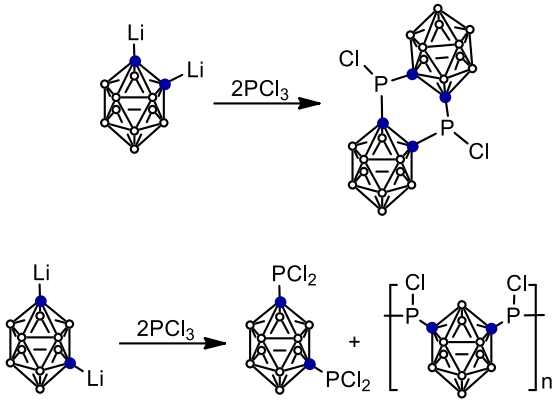

Scheme 1.5 Reaction of dilithiated *ortho*- and *meta*-carboranes and PCl_3.

In the same period of time Russian scientists also were investigating the chemistry of *closo*-carboranylchlorophosphines. They discovered that equimolar quantities of monolithio-*ortho*-carborane and PCl_3 gives a mixture of *closo*-carboranyldichlorophosphines and dicarboranylchlorophosphines[17] (Scheme 1.6). These results revealed that substitution of one chlorine atom in PCl_3 by carboranyl group increases reactivity of the other chlorine bonded to phosphorus. As a result, isolation of the dichlorophosphine in pure form was complicate, and the method mentioned above became not efficient for the synthesis of diclorophosphine derivative of carborane. Instead was developed the other method based on reaction

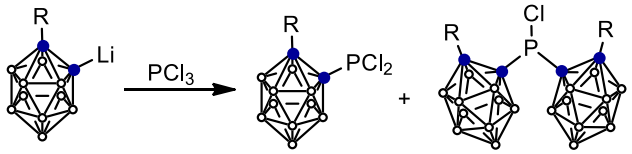

Scheme 1.6 Reaction of monolithio-*ortho*-carborane and PCl_3.

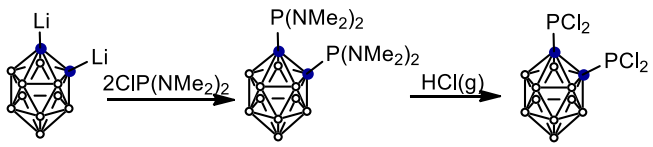

Scheme 1.7 Synthesis of 1,2-$(PCl_2)_2$-1,2-*closo*-$C_2B_{10}H_{10}$.

between dialkylaminophosphine derivative of carborane and dry HCl acid (Scheme 1.7).

Thus, diclorophosphine derivative, 1,2-$(PCl_2)_2$-1,2-*closo*-$C_2B_{10}H_{10}$, was obtained quantitatively from 1,2-$(P(NMe_2)_2$-1,2-*closo*-$C_2B_{10}H_{10}$ upon reaction with dry HCl in benzene solution.[18] 1,2-$(P(NMe_2)_2$-1,2-*closo*-$C_2B_{10}H_{10}$ was also synthesized in the reaction of dilithio-*ortho*-carborane with $ClP(NMe_2)_2$.

In contrast to organic dichlorophosphines, both alkyl- and aryl-, *closo*-carboranyldichlorophosphines were found to be stable in front of atmospheric oxygen at room temperature. Also they do not react with sulfur at temperatures below 200°C. However, they easily (exothermically) react with chlorine at ambient temperature producing *closo*-carboranyltetrachlorophosphines (Scheme 1.8).[19]

1.2.3 *Closo* – Carboranylphosphines with P(V) moieties

The first derivatives of carboranes that contain pentavalent phosphorus were synthesized by hydrolysis of diclorophosphine derivatives, 1-R-2-PCl_2-1,2-*closo*-$C_2B_{10}H_{10}$ (R=Me, Ph), producing phosphinic acids of *ortho*-carborane[18,20]. The same starting compounds in the reaction with chlorine gave tetrachlorophosphine derivative of carborane. Although tetrachlorophosphine derivatives were not isolated their existence was proved by the products of their hydrolysis, 1-R-2-$POCl_2$-1,2-*closo*-$C_2B_{10}H_{10}$ (R=Me, Ph) (Scheme 1.8).[21] Interestingly, that attempts to produce *closo*-

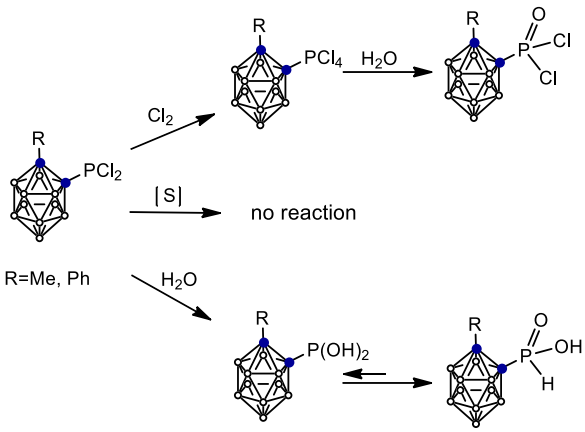

Scheme 1.8 Synthesis of the first *closo*–carboranylphosphines with P(V) moieties.

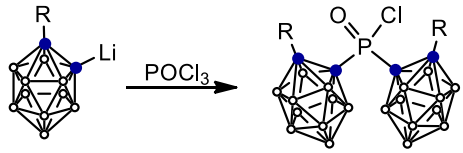

Scheme 1.9 Reaction of monolithio-*ortho*-carborane and $POCl_3$.

carboranyldichlorophosphonates by reaction of lithiated *ortho*-carborane and $POCl_3$ did not work how it was expected, giving a product of substitution of one chlorine atom by carboranyl group (Scheme 1.9). Even a big excess of $POCl_3$ gave products of substitution of two chlorine atoms producing dicarboranylchlorophosphonate, (1-R-1,2-*closo*-$C_2B_{10}H_{10})_2POCl$ (R=Me, Ph)[21].

Also P(V) derivatives can be achieved by oxidation of *closo*-carboranylchlorophosphines with chalcogens: oxygen (using H_2O_2), sulfur and selenium. The first product of oxidation by sulfur was produced upon reaction of 1-R-2-PPhCl-1,2-*closo*-$C_2B_{10}H_{10}$ (R = Me, Ph) with elemental sulfur in decane at 180ºC. The reaction of the same compound with chlorine followed by hydrolysis gives the P(V) derivative with oxygen[22] (Scheme 1.10).

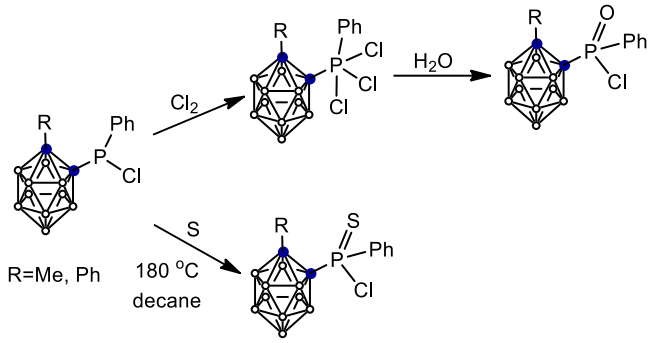

Scheme 1.10 Synthesis of oxidized carboranylphosphines.

Later in 2011 was reported a comprehensive study of the oxidation of *closo*-carboranylphosphines with H_2O_2, S and Se.[14] Oxidation of *closo*-carboranylmonophosphines with H_2O_2, S and Se yielded in all the cases the resulting oxidized monophosphine, whereas, for *closo*-carboranyldiphosphines different results were obtained. In the oxidation with H_2O_2 in acetone, both P atoms were oxidized, the reaction time depended on the organic groups bonded to the P atoms (e.g. longer time is needed for Ph than for ^{i}Pr) (Scheme 1.11). Different behavior was observed for dialkylcarboranyl and diarylcarboranyldiphosphines in oxidation with S and Se (Scheme 1.12). Oxidation of 1,2-$(PPh_2)_2$-1,2-*closo*-$C_2B_{10}H_{10}$ with sulfur produced three different species after purification: 1-$SPPh_2$-2-PPh_2-1,2-*closo*-

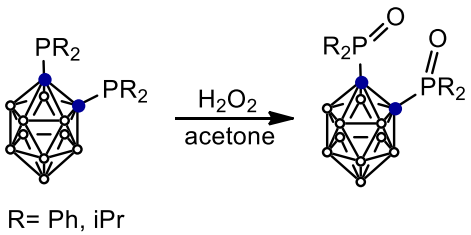

Scheme 1.11 Oxidation of *closo*-carboranyldiphosphines with H_2O_2.

$C_2B_{10}H_{10}$, 1,2-$(SPPh_2)_2$-1,2-*closo*-$C_2B_{10}H_{10}$ and 1-$SPPh_2$-2-$OPPh_2$-1,2-*closo*-$C_2B_{10}H_{10}$. Oxidation of 1,2-$(PiPr_2)_2$-1,2-*closo*-$C_2B_{10}H_{10}$ with S produced first the compound in which only one P atom is oxidized, respectively, 1-$SPiPr_2$-2-$PiPr_2$-1,2-*closo*-$C_2B_{10}H_{10}$ and if the reaction is prolonged, the C_c—P^iPr_2 bond cleavage takes place, yielding the monophosphine derivative, 1-SP^iPr_2-1,2-*closo*-$C_2B_{10}H_{11}$. Oxidation of 1,2-$(PPh_2)_2$-1,2-*closo*-$C_2B_{10}H_{10}$ with Se led only to 1-$SePPh_2$-2-PPh_2-1,2-*closo*-$C_2B_{10}H_{10}$ that remains intact even after refluxing in toluene for days. Oxidation of 1,2-$(P^iPr_2)_2$-1,2-*closo*-$C_2B_{10}H_{10}$ with selenium produces C_c— P bond cleavage, yielding the oxidized monophosphine 1-SeP^iPr_2-1,2-*closo*-$C_2B_{10}H_{11}$.

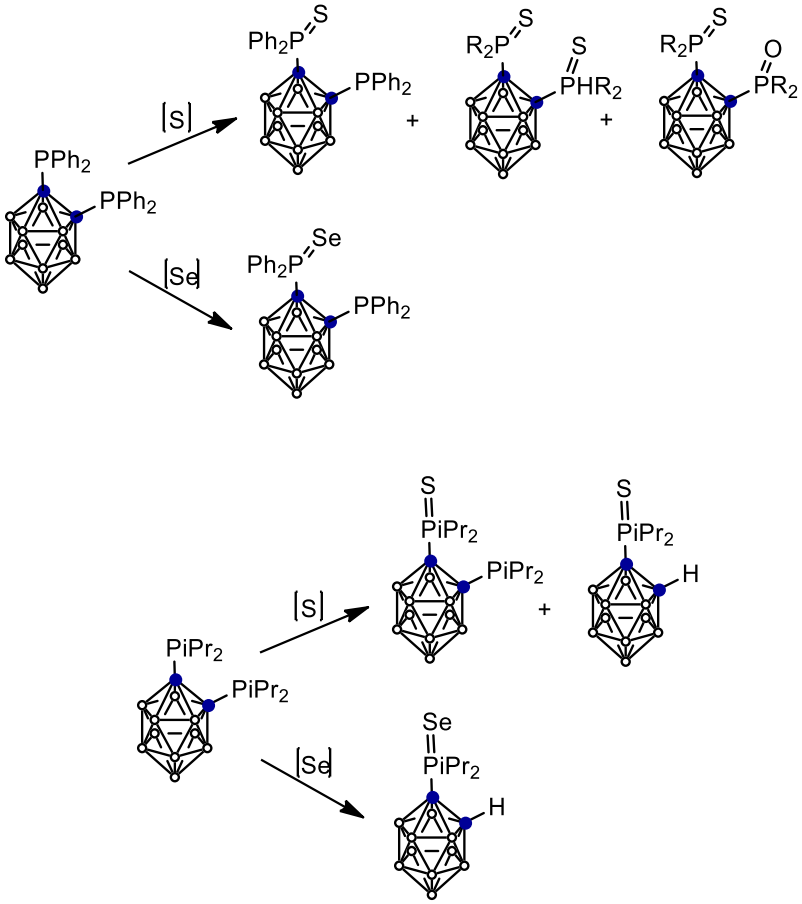

Scheme 1.12 Reaction of *closo*-carboranyldiphosphines with sulfur and selenium.

1.3 Coordination polymers incorporating icosahedral boron clusters

According to IUPAC Recommendations 2013 the definition of coordination polymer is: "*a coordination compound with repeating coordination entities extending in 1, 2, or 3 dimensions"*.[23] Coordination polymers are relevant to many fields such as organic and inorganic chemistry, biochemistry, material science, electrochemistry, pharmacology, being currently of great scientific interest and having many applications[24]. These structures are highly dependent on metal center and the nature of ligands.

Because carboranes exhibit an unusual combination of properties such as low nucleophilicity, chemical inertness, thermal stability,[25,26] electron-withdrawing via bonding at the carboranyl carbon atoms,[27,28] and electron-donating via bonding at the carborane boron atoms,[29,30] *closo*-carborane clusters can play a variety of roles in coordination polymers. They can be as guests that are accommodated by a coordination polymer. Anionic *closo*-carboranes can be incorporated into coordination polymers via B-H⋯M interactions directing a polymer chain.[31,32] Carboranes fuctionalized with the metal-binding group directly bonded to the cage (carboxylato, phosphino, thiolato) have been used to introduce C_2B_{10}-icosahedrons into the backbone of 1D coordination polymers. In this way, was found that carboranylcarboxilate ligands, 1-R-2-CO_2-1,2-*closo*-$C_2B_{10}H_{20}$ (R=CH_3, H) in the reaction with $MnCO_3$ in water produce air-stable water soluble polymeric compounds[33,34]. Depending on the substituent, -CH_3 or –H, on one of the C_c of the carboranylcarboxylate ligand, two different polymeric compounds were obtained: [Mn(μ-H_2O)(μ-1-CH_3-2-CO_2-1,2-*closo*-$C_2B_{10}H_{10})_2]_n{\cdot}(H_2O)_n$ and [Mn(H_2O)(μ-1-CO_2-1,2-*closo*-$C_2B_{10}H_{11})_2]_n{\cdot}2H_2O$ (Figure 1.5). To be noted that compound [Mn(μ-H_2O)(μ-1-CH_3-2-CO_2-1,2-*closo*-$C_2B_{10}H_{10})_2]_n{\cdot}(H_2O)_n$ was the first polynuclear Mn^{II} complex with carboxylate and aqua ligands bridging two Mn^{II} centers.

The polymeric nature of both polymers can be fragmented by coordination solvents, e.g. diethyl ether or Lewis bases, such as 2,2´-bipyridine, forming new compounds with low (mono-, di-, tri-) nuclearity, due to breakage of the corresponding polymer. The reactivity of [Mn(μ-H_2O)(μ-1-CH_3-2-CO_2-1,2-*closo*-

$C_2B_{10}H_{10})_2]_n\cdot(H_2O)_n$ with 2,2´-bipyrimidine leads to the formation of a new hybrid polymer $[Mn(1\text{-}CH_3\text{-}2\text{-}CO_2\text{-}1,2\text{-}closo\text{-}C_2B_{10}H_{10})_2(bpm)]_n$ (Figure 1.6).

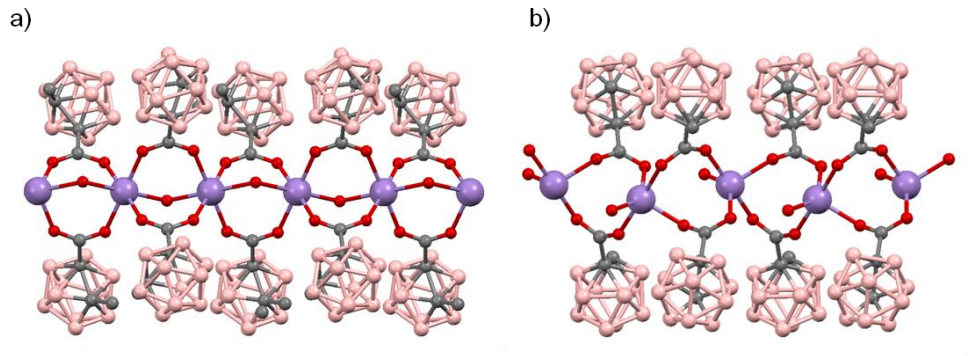

Figure 1.5 Structure of polymers $Mn(\mu\text{-}H_2O)(\mu\text{-}1\text{-}CH_3\text{-}2\text{-}CO_2\text{-}1,2\text{-}closo\text{-}C_2B_{10}H_{10})_2]_n\cdot(H_2O)_n$ (a) and $[Mn(H_2O)(\mu\text{-}1\text{-}CO_2\text{-}1,2\text{-}closo\text{-}C_2B_{10}H_{11})_2]_n\cdot 2H_2O$ (b) showing the monodimensional arrangement (H atoms are omitted for clarity).

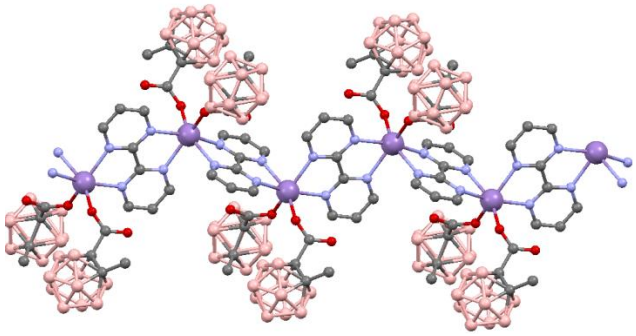

Figure 1.6 The polymer chain of the hybrid $[Mn(1\text{-}CH_3\text{-}2\text{-}CO_2\text{-}1,2\text{-}closo\text{-}C_2B_{10}H_{10})_2(bpm)]_n$ (H atoms are omitted for clarity).

Coordination properties of phosphino-functionalized carboranes $1,2\text{-}(PR_2)_2\text{-}1,2\text{-}C_2B_{10}H_{10}$ are well studied. And in the chemistry of coordination polymers, a few examples exist with this type of ligands. The synthesis of novel 1D chain was reported by Dou et al. in 2011 starting from $1,2\text{-}(PPh_2)_2\text{-}1,2\text{-}C_2B_{10}H_{10}$ and $HgCl_2$[35], $\{[Hg_5(1,2\text{-}(PPh_2)_2\text{-}1,2\text{-}C_2B_{10}H_{10})_2(\mu\text{-}Cl)_8]\cdot 2CH_2Cl_2\}_n$. The same year was reported other chain-like polymer, $[Ag_2(SCN)_2\{1,2\text{-}(PCy_2)_2\text{-}1,2\text{-}C_2B_{10}H_{10}\}_2]_n\cdot CH_2Cl_2$, prepared from $1,2\text{-}(PCy_2)_2\text{-}1,2\text{-}C_2B_{10}H_{10}$ (Cy = cyclohexyl) with silver salt AgSCN[36] (Figure 1.7).

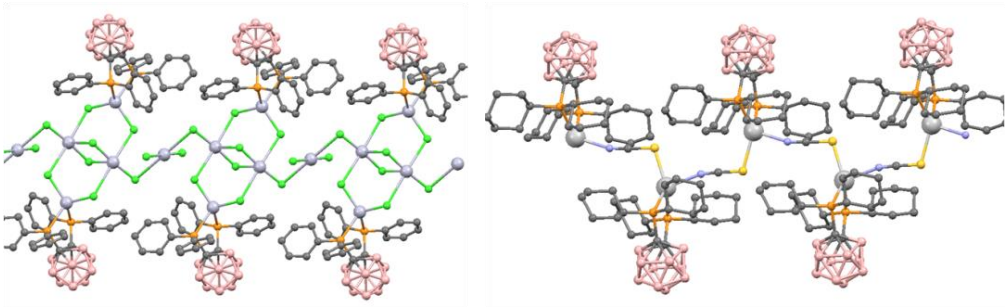

Figure 1.7 The 1D polymer chain structure of complexes $\{[Hg_5(1,2\text{-}(PPh_2)_2\text{-}1,2\text{-}C_2B_{10}H_{10})_2(\mu\text{-}Cl)_8]\cdot 2CH_2Cl_2\}_n$ and $[Ag_2(SCN)_2\{1,2\text{-}(PCy_2)_2\text{-}1,2\text{-}C_2B_{10}H_{10}\}_2]_n\cdot CH_2Cl_2$ (H atoms are omitted for clarity).

1.4 Characteristics and applications of phosphinate complexes

Phosphinic acids are of the general formula $R_2P(O)OH$ where R can be H, alkyl or aryl group or combination of any two. They are related to other P (V) compounds, such as phosphine oxides, phosphonic acids and phosphoric acid (Figure 1.8). Industrially, these types of phosphorus compounds and their esters are used for the separation and purification of different metals.[37]

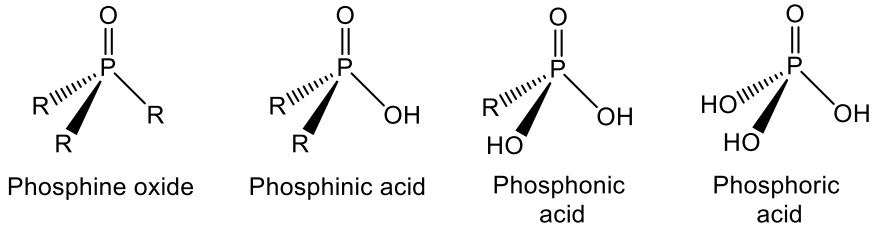

Figure 1.8 Schematic representation of P(V) compounds.

Mixtures of bis(2,4,4-trimethylpentyl)phosphinic acid and tri(2,4,4-trimethyloctyl)phosphine oxide are sold by Cytec Industries Inc. with the name *Cyanex 272* and are used for the extraction and purification of different metals. Notably, *Cyanex 272* is most commonly used in the separation of cobalt from nickel.[38] Despite their extensive use in the purification of different metals, the coordination chemistry of phosphinic acids is relatively unexplored.

Although phosphinic acids and related P (V) compounds are generally drawn with a phosphorus-oxygen double bond its nature has been the subject of intense studies for many years. Experimental and theoretical calculations clearly suggest the absence of conventional double bonding in the phosphorus-oxygen bond. The recent investigations emphasize that P=O unit is better described with the highly polar structure $P^{+}–O^{-}$.[39–41]

In some way phosphinic and carboxylic acids are structurally related (Figure 1.9). Both compounds are oxoacids in which the acidic moiety consists of an oxide and hydroxide bonded to a central atom that is electron deficient. Due to this deficiency, the hydroxyl group can ionize relatively easily to form either a phosphinate or carboxylate anion and a proton. Where carboxylic and phosphinic acids differ is in their geometry and nature of their bonding. Phosphinic acids are always tetrahedral in shape with four different moieties bonding to the central phosphorus atom. The identities of the two moieties that are not the oxide or hydroxide can have profound effects on the steric nature of the phosphinic acids, this could change how the phosphinic acid or phosphinate coordinates to metal atoms.

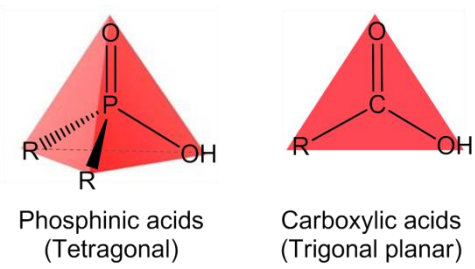

Figure 1.9 Geometry of phosphinic and carboxylic acids.

Carboxylic acids on the other hand, are trigonal planar compounds with only three moieties bonded to the central carbon atom. The identity of the one moiety that is not the hydroxide or oxide can also have similar steric effects on the coordination of the carboxylic acid or carboxylate to metal atoms. Unlike the O=P bond, the O=C double bond in carboxylic acids is in fact a true double bond consisting of one σ-bond and one π-bond. The carboxylate anion, when compared to the phosphinate anion, would have less electron density spread over its two oxygens due to its resonance structures. This would presumably decrease the

amount of electron density that can be donated to a metal center potentially lowering its effectiveness in stabilizing high oxidation state metals.

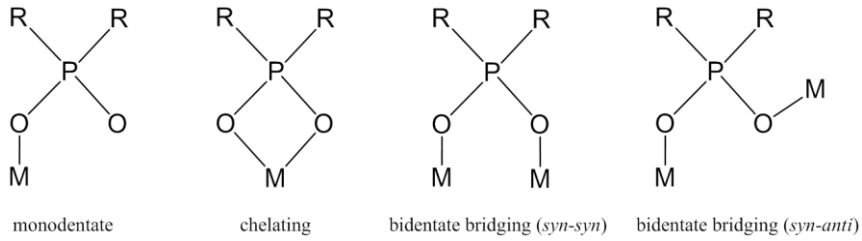

Figure 1.10 Examples of coordination modes of phosphinates.

Phosphinate anion exhibits a versatile coordination behavior displaying various bonding modes toward metal cations. Some of the more common modes are presented in Figure 1.10. Coordination chemistry of phosphinic acids type $R_2P(O)OH$ (R= alkyl, aryl) is more frequent then of type RPH(O)OH. A search at the Cambridge Structural Database (CSD), On February 9th 2017 shows 102 hits for phosphinic acid $R_2P(O)OH$ (R=alkyl, aryl) and 211 for its transition metal complexes, but only 20 hits for phosphinic acids R-P(H)O(OH) (R=alkyl, aryl) and 47 hits were found for its transition metal complexes. On the other hand, a search at the Cambridge Structural Database (CSD version 5.38) shows 375 hits for phosphonic acid $R\text{-}PO(OH)_2$ (R=alkyl, aryl) and >2200 hits for its transition metal complexes (Figure 1.11).

Figure 1.11 Relative percentage of hits of $R_2P(O)OH$, P(H)O(OH) and $R\text{-}PO(OH)_2$ and its corresponding complexes found at the Cambridge Structural Database (CSD), On February 9th 2017.

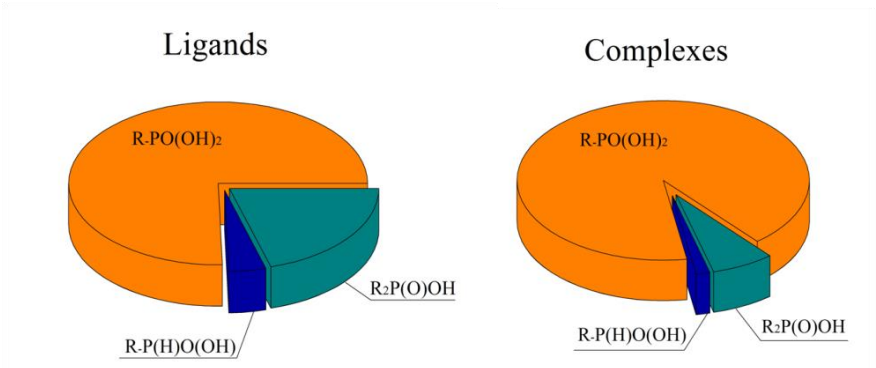

Most of a few complexes of phosphinic acids of the formula RPH(O)OH that have been found in the literature are formed with phenylphosphinate ligand, PhPH(O)OH and transition metals such as Mn^{II},[42,43,44,45] Sb^{II},[46,47] Co^{II},[48,49] Cu^{II},[48] Gd^{II},[50] Zn^{II},[51] Al^{III}.[52] In these metal phosphinate complexes, the phosphinate ligand is monodentate or bridging two metal centers.

Isotope	Cross section (barns)
^{10}B	3837
^{11}B	0.005
^{12}C	0.0035
^{1}H	0.33
^{14}N	1.7
^{35}Cl	43.6
^{23}Na	0.534
^{157}Gd	25400
^{153}Gd	0.02

Table 1.1 Thermal Neutron Cross Sections.

1.5 Boron Neutron Capture Therapy for tumor targeting

Neutron Capture Therapy (NCT) is a bimodal therapy that utilizes a neutron source to generate an internal destroying radiation in tumor cells that leads to their death. As opposed to conventional radiation therapy using X rays or γ rays where an external radiation source is required, a big advantage of NCT is that the surrounding healthy tissue is not exposed to the radiation that can be a big issue in treatment of tumors in deep parts of the body. Thus, NCT requires the use of an isotope with high neutron capture cross section. The “organic” elements such as C, H, O, N have very low neutron capture cross section (< 2 barn). In contrast, isotopes of other elements such as boron and gadolinium, ^{10}B and ^{157}Gd, are good at absorbing neutrons (capture cross section for ^{10}B is 3840 barn, for ^{157}Gd- 25400 barn). Also ^{10}B isotope was an attractive element due to its high

natural abundance of 20%. ^{157}Gd isotope also has a natural abundance of 15.7% that can be effective to capture neutrons. Up to now GdNCT has never been used clinically (i.e., in humans), the reason being the toxicity concern of gadolinium. On the other hand, over 900 patients have already undergone Boron Neutron Capture Therapie, BNCT, worldwide and effects of BNCT on malignant tumors and healthy surrounding tissue seemed to be established.

The history of BNCT started in 1932 since the discovery of the neutron by Chadwick,[53] followed by Locher´s proposal to use neutron capture reactions in cancer treatment (Figure 1.12).[54]

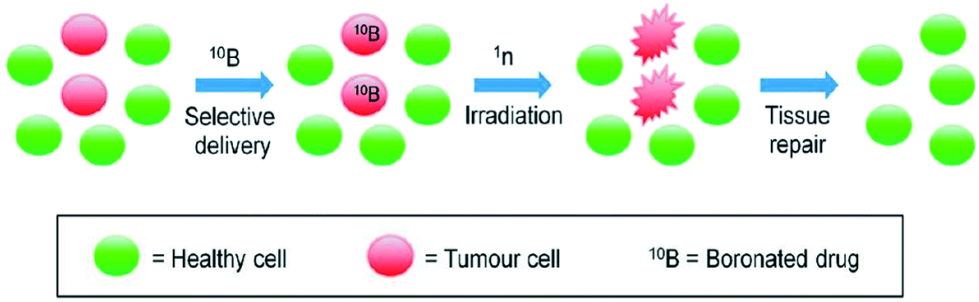

Figure 1.12 BNCT steps: the selective delivery of ^{10}B-containing drugs to tumor cells is followed by irradiation with thermal neutrons (^{1}n) to initiate the destruction of cancer cells and to allow tissue repair (figure from ref.[74]).

BNCT technique consists of two steps: the selective delivery of ^{10}B-containing agents to tumor cells followed by their irradiation with low-energy neutrons, which results into the prompt nuclear reaction. The predominant products of this reaction are ^{7}Li nuclei and high liner energy transfer (LET) α particles. LET particles are lethal but their effect is concentrated mostly inside of host cells due to their short path length in tissues (4.5-10μm).

Research in the area of development of boron-containing delivery agents for BNCT started ~ 60 years ago with the investigation of a large number of boron compounds, that were regarded as “first-generation” agents for BNCT.[55] The most important requirements for a BNCT delivery agent are: i) low toxicity, ii) water solubility, iii) good tumor-cell selectivity, with a tumor: normal tissue and tumor: blood rations higher than 3, iv) be deliverable at around 20 μg ^{10}B/g (tumor tissue),

v) persistence in tumor cells during the course of neutron irradiation, vi) capacity to penetrate biological barriers, such as the blood-brain barrier (BBB).

So far, clinically for the treatment of patients with malignant brain tumors and malignant melanoma has been used two main boron delivery agents: sodium borocaptate, $Na_2B_{12}H_{11}SH$ (BSH), and boronophenylalanine (BPA) which formulas are displayed in the Figure 1.13. And during the last 20 years a big number of boron delivery agents have appeared using different approaches. Among them are derivatives of biological molecules (aminoacids, nucleic acids, peptides, DNA-binding molecules), porphyrin derivatives, nanovehicles (liposomes), dendrimers. Also other delivery systems such as nanoparticles are currently under research. Hosmane et al. attempted to use magnetic nanoparticles for boron delivery into tumor cells.[56]

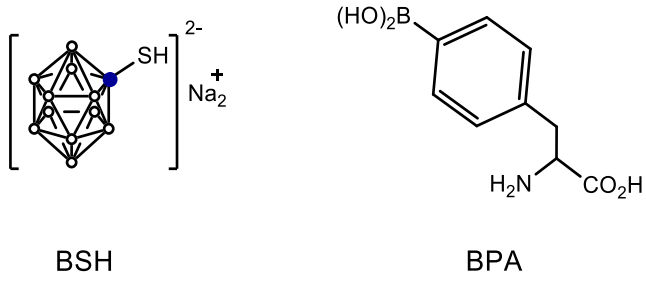

Figure 1.13 Chemical structures of boron compounds used in BNCT clinical trials.

1.6 Magnetic nanomaterials: properties and applications in biomedicine

Since the first synthesis of a magnetic fluid that was reported in 1965 in the pioneering work by Papell,[57] an increase of scientific production took place in this area (Figure 1.14).

The research field of magnetic nanoparticles is multi-disciplinary: chemists work on the synthetic part, physicists and engineers study their physical properties and their

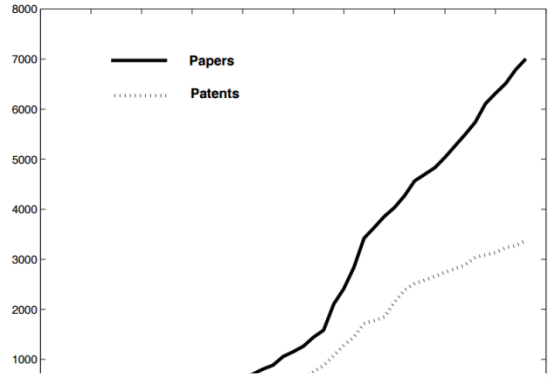

Figure 1.14 Increase in production of papers and patents on magnetic nanoparticles (figure from ref.[75]).

applicability, and biologists study their possibility in biomedical applications such as magnetic drug targeting, hyperthermia, Magnetic Resonance Imaging (MRI).[58–65]

What makes magnetic nanoparticles (MNPs) interesting for biomedical application? Most applications of MNPs are based on the following properties: i) their high surface/volume ratio; their size is at the scale of the important biomolecules such as proteins and DNA and 10^3 times smaller cells ii) MNPs follow the magnetic field; iii) MNPs absorb electromagnetic energy and heats up.

1.6.1 Magnetic property

The base of magnetism arises from two important characteristics of electrons: the orbital movement of the electron around the atomic nucleus and the movement of the electronic spin around its axis. This association of an orbital and a spin magnetic moments makes an electron to behave like a tiny magnet. Magnetization is the sum of all magnetic moments (m) of the atoms in a material per unit volume (V), $\mathrm{M} = \frac{\mathrm{m}}{\mathrm{V}}$ (emu/cm^3). For practical reasons, magnetization (M) is often referred to unit mass and expressed as emu/g.

All materials respond differently when they are exposed to an externally applied magnetic field, and according to this they can be classified into diamagnetic, paramagnetic, ferromagnetic, antiferromagnetic and ferromagnetic (Figure 1.15). In *diamagnetic* materials an applied magnetic field creates an induced magnetic field in the opposite direction, so they are repelled by a magnetic field. Materials whose atomic magnetic moments are uncoupled are *paramagnetic*. These materials are slightly attracted by a magnetic field and they do not retain the magnetic properties when the external field is removed. *Ferromagnetic* materials have aligned atomic magnetic moments of equal magnitude. In the presence of a magnetic field, they have a strong net magnetization that partially remains when the magnet is not longer applied. In *ferrimagnets* atomic magnetic moments align antiparallel but have different strength. *Antiferromagnetic* substances show zero net

magnetization even being under the influence of a magnetic field due to the antiparallel alignment of magnetic moments of equal magnitude.

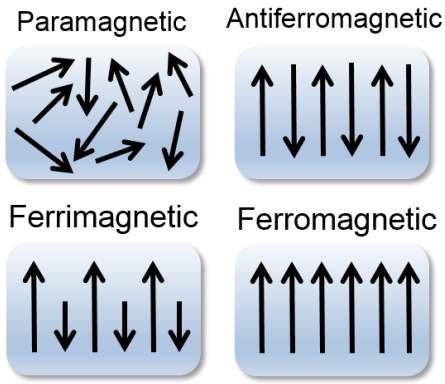

Figure 1.15 Types of magnetic materials (arrows represent the atomic magnetic moments orientation).

The domain structure of a ferromagnetic material determines the size dependence of its magnetic behavior (Figure 1.16). When the size of a ferromagnetic material is reduced below a critical value, it becomes a single domain. For single domain magnetic nanoparticles their magnetic energy becomes comparable to its thermal energy.

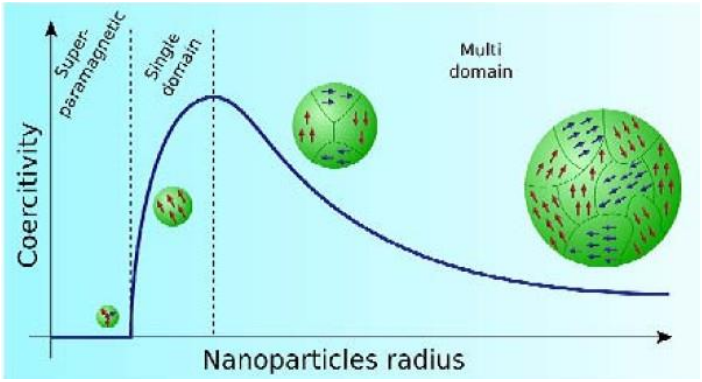

Figure 1.16 Schematic illustration of the coercivity-size relations of small particles (figure from ref.[76])

The respond of ferromagnetic materials on an applied magnetic field is described by hysteresis loop, which is characterized by two main parametrs: remanence (M_R) and coercivity (H_C). When the size of particles is below the size of

single-domain, its thermal energy overcomes its magnetic energy, so the magnetization vector of single-domain nanoparticles can be reversed spontaneously. As a result, the coercivity becomes zero, and particles become *superparamagnetic*. Superparamagnetism is a size effect of ferromagnetism. Superparamagnetic particles become magnetic in the presence of an external magnetic field, but demagnetize when the external magnetic field is removed, thus they have no hysteresis (Figure 1.17). This property makes superparamagnetic particles very attractive for applications in biological systems since they can be "activated" or "disactivated" depending on the applied external magnetic field.

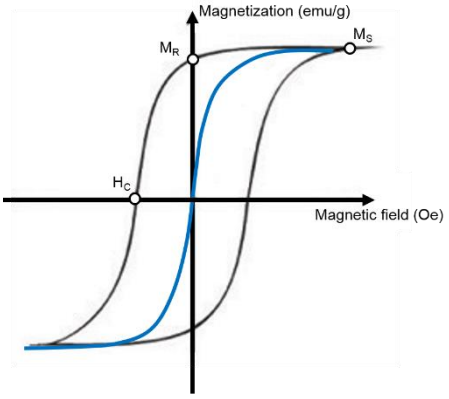

Figure 1.17 Magnetization *vs*. applied magnetic field for a ferromagnetic (black) and a superparamagnetic (blue) material.

The temperature plays an important role in defining the superparamagnetic state of magnetic nanoparticles. At some point at low temperatures in superparamagnetic materials, the thermal energy becomes smaller than its magnetic energy, and material is not superparamagnetic anymore. The temperature above which nanoparticles are in superparamagnetic state calls *blocking temperature*, T_B. The blocking temperature value in a superparamagnetic material can be found from zero-field cooling (ZFC) and field cooling (FC) measurements of

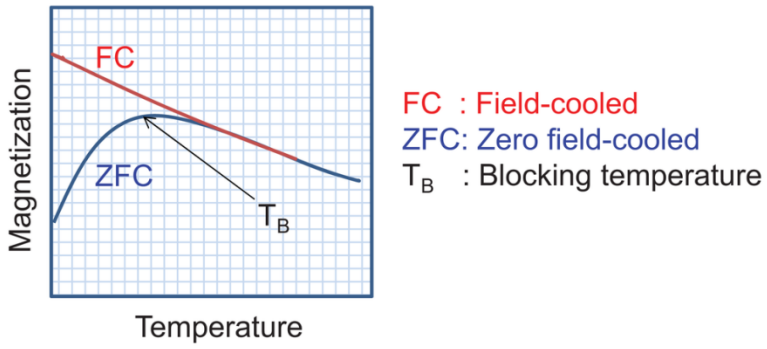

Figure 1.18 Zero-field cooling field cooling curves of superparamagnetic nanoparticles (figure from ref [77])

magnetization *vs* temperature (Figure 1.18), performed by heating the sample under a constant magnetic field in *Superconductive Quantum Interference Device* (SQUID). In ZFC curve, the magnetic moment increases with the temperature and then decreases, while the moment decreased in FC curve. The temperature at the peak point of ZFC curve is the Blocking temperature.

Magnetite, Fe_3O_4, is the most magnetic of all the naturally occurring minerals on earth, and it is widely being investigated in the form of superparamagnetic nanoparticles (SPIONs or MNPs) during the last 20 years for numerous *"in vivo"* and *"in vitro"* applications such as magnetic resonance imaging (MRI) contrast enhancement,[66,67] tissue repair, detoxification of biological fluids, hyperthermia, drug delivery, immunoassays and cell separation techniques.[68–70] Further developments in the synthesis and bioorthogonal chemistry of nanoparticles have broadened MNPs applications to the therapeutic areas.[71,72]

1.7 Objectives and justification of the thesis

From the brief introduction presented above it is clear that the chemistry of the carborane derivatives with phosphorus moieties have been well studied except carboranylphosphinic and carboranylphosphonic acids. This doctoral thesis symbolized the introduction a new research line to the existing ones in the research group and has been developed centered in the:

- Synthesis and characterization of carboranylphosphinic and carboranylphosphonic acids to use them as a versatile purely inorganic building blocks.

- Study of the coordination chemistry of *m*-carboranylphosphinate ligands with the first and the second raw transition metals, aiming to generate purely inorganic coordination polymers (CPs).

- Using possibilities offered by the phopshinate coordinating group, and properties bestowed by the *m*eta-carboranyl unit (spherical nature, hydrophobicity), we aimed to produce boron cluster-Magnetic Nanoparticles nanohybrids functionalized with *m*-carboranylphosphinate (**1**-MNPs), then learn on their structural and physicochemical properties. To illustrate their potential biomedical applications as drug carriers or in Boron Neutron Capture Therapy (BNCT) was planned to study the cytotoxicity and cellular uptake of these **1**-MNPs from culture media by different human cell lines.

(1) Eberhardt, W. H.; Crawford, B.; Lipscomb, W. N. *J. Chem. Phys.* **1954**, *22* (6), 989–985.

(2) Teixidor, F.; Viñas, C.; Demonceau, A.; Nuñez, R. *Pure Appl. Chem.* **2003**, *75* (9), 1305–1313.

(3) Scholz, M.; Hey-Hawkins, E. *Chem. Rev.* **2011**, *111* (11), 7035–7062.

(4) Poater, J.; Solà, M.; Viñas, C.; Teixidor, F. *Angew. Chemie Int. Ed.* **2014**, *53* (45), 12191–12195.

(5) Poater, J.; Solà, M.; Viñas, C.; Teixidor, F. *Chem. - A Eur. J.* **2013**, *19* (13), 4169–4175.

(6) Poater, J.; Solà, M.; Viñas, C.; Teixidor, F. *Chem. - A Eur. J.* **2016**, *22* (22), 7437–7443.

(7) Grimes, R. N. *«Carboranes» 2nd Edition, Academic Press: Burlington, MA*; Burlington, MA, 2011.

(8) Gomez, F. A.; Hawthorne, M. F. *J. Org. Chem.* **1992**, *57* (5), 1384–1390.

(9) Vinas, C.; Benakki, R.; Teixidor, F.; Casabo, J. *Inorg. Chem.* **1995**, *34* (14), 3844–3845.

(10) Valliant, J. F.; Guenther, K. J.; King, A. S.; Morel, P.; Schaffer, P.; Sogbein, O. O.; Stephenson, K. A. *Coord. Chem. Rev.* **2002**, *232* (1), 173–230.

(11) Popescu, A.-R.; Musteti, A. D.; Ferrer-Ugalde, A.; Viñas, C.; Núñez, R.; Teixidor, F. *Chem. - A Eur. J.* **2012**, *18* (11), 3174–3184.

(12) Aldrich.com. .

(13) Popescu, A. R.; Teixidor, F.; Viñas, C. *Coord. Chem. Rev.* **2014**, *269*, 54–84.

(14) Popescu, A.-R.; Laromaine, A.; Teixidor, F.; Sillanpää, R.; Kivekäs, R.; Llambias, J. I.; Viñas, C. *Chem. - A Eur. J.* **2011**, *17* (16), 4429–4443.

(15) Alexander, R. P.; Schroeder, H. *Inorg. Chem.* **1963**, *2* (6), 1107–1110.

(16) Sterzik, A.; Rys, E.; Blaurock, S.; Hey-hawkins, E. **2001**, *20*, 3007–3014.

(17) Zakharkin, L. I.; Bregadze, V. I.; Okhlobystin, O. Y. *J. Organomet. Chem.* **1965**, *4* (3), 211–216.

(18) L.I. Zakharkin, A.V. Kazantsev, M. N. Z. *Izv. Akad. Nauk SSSR, Ser. Khim.* **1969**, *9*, 2056–2057.

(19) Zakharkin, L. I.; Bregadze, V. I.; Okhlobystin, O. Y. *J. Organomet. Chem.*

1965, *4* (3), 211–216.

(20) A.V. Kazantsev, M.N. Zhubekova, L. I. Z. *Zh. Obs. Khim.* **1971**, *42*, 1570–1571.

(21) L.I. Zakharkin, M.N. Zhubekova, A. V. K. *Zh. Obs. Khim.* **1971**, *41*, 588–592.

(22) A.V. Kazantsev, M.N. Zhubekova, L. I. Z. *Zh. Obs. Khim.* **1971**, *41*, 2027.

(23) Batten, S. R.; Champness, N. R.; Chen, X.-M.; Garcia-Martinez, J.; Kitagawa, S.; Öhrström, L.; O'Keeffe, M.; Paik Suh, M.; Reedijk, J. *Pure Appl. Chem.* **2013**, *85* (8), 1715–1724.

(24) Fromm, K. M. *Coord. Chem. Rev.* **2008**, *252* (8), 856–885.

(25) Plesek, J. *Chem. Rev.* **1992**, *92* (2), 269–278.

(26) Grimes, R. N. *Carboranes. Third Edition*; Elsevier Inc.: New York/Oxford, 2016.

(27) Núñez, R.; Farràs, P.; Teixidor, F.; Viñas, C.; Sillanpää, R.; Kivekäs, R. *Angew. Chemie Int. Ed.* **2006**, *45* (8), 1270–1272.

(28) Teixidor, F.; Núñez, R.; Viñas, C.; Sillanpää, R.; Kivekäs, R. *Angew. Chemie* **2000**, *39* (23), 4290–4292.

(29) Teixidor, F.; Barberà, G.; Vaca, A.; Kivekäs, R.; Sillanpää, R.; Josep Oliva, A.; Viñas, C. *J. Am. Chem. Soc* **2005**, *127* (29), 10158–10159.

(30) Spokoyny, A. M.; Machan, C. W.; Clingerman, D. J.; Rosen, M. S.; Wiester, M. J.; Kennedy, R. D.; Stern, C. L.; Sarjeant, A. A.; Mirkin, C. A. *Nat. Chem.* **2011**, *3* (8), 590–596.

(31) Hardie, M. J. *J. Chem. Crystallogr.* **2006**, *37* (1), 69–80.

(32) Núñez, R.; Romero, I.; Teixidor, F.; Viñas, C.; Xie, Z.; Viñas, C.; Aliaga-Alcalde, N.; Matějíček, P.; Hosmane, N. S.; Beavis, P.; Heeney, M. *Chem. Soc. Rev.* **2016**, *45* (19), 5147–5173.

(33) Fontanet, M.; Rodríguez, M.; Romero, I.; Fontrodona, X.; Teixidor, F.; Viñas, C.; Aliaga-Alcalde, N.; Matějíček, P. *Dalt. Trans.* **2013**, *42* (22), 7838.

(34) Fontanet, M.; Rodríguez, M.; Fontrodona, X.; Romero, I.; Teixidor, F.; Viñas, C.; Aliaga-Alcalde, N.; Matějíček, P. *Chem. - A Eur. J.* **2014**, *20* (43), 13993–14003.

(35) Kong, L.; Zhang, D.; Su, F.; Lu, J.; Li, D.; Dou, J. *Inorganica Chim. Acta* **2011**, *370* (1), 1–6.

(36) Yang, L.-G.; Zhu, C.-C.; Zhang, D.-P.; Li, D.-C.; Wang, D.-Q.; Dou, J.-M. *Polyhedron* **2011**, *30* (9), 1469–1477.

(37) Kalina, D. G.; Horwitz, E. P.; Kaplan, L.; Muscatello, A. C. *Sep. Sci. Technol.* **1981**, *16* (9), 1127–1145.

(38) Tait, B. K. *Hydrometallurgy* **1993**, *32* (3), 365–372.

(39) Gilheany, D. G. *Chem. Rev.* **1994**, *94* (5), 1339–1374.

(40) D. B. Chesnut*, †; Savin‡, A. **1999**.

(41) Chesnut†, D. B. **2003**.

(42) Richeter, S.; Larionova, J.; Long, J.; van der Lee, A.; Leclercq, D. *Eur. J. Inorg. Chem.* **2013**, *2013* (18), 3206–3216.

(43) Kevin Bernot, †,‡; Javier Luzon, †; Roberta Sessoli, *,†; Alessandro Vindigni, §; Julien Thion, ǁ; Sébastien Richeter, ǁ; Dominique Leclercq, ǁ; Joulia Larionova, ǁ and; Lee⊥, A. van der. **2008**.

(44) Taylor, S. M.; McIntosh, R. D.; Beavers, C. M.; Teat, S. J.; Piligkos, S.; Dalgarno, S. J.; Brechin, E. K. *Chem. Commun. (Camb).* **2011**, *47* (5), 1440–1442.

(45) Inglis, R.; Dalgarno, S. J.; Brechin, E. K. *Dalt. Trans.* **2010**, *39* (20), 4826.

(46) Srungavruksham, N. K.; Baskar, V. *Eur. J. Inorg. Chem.* **2013**, *2013* (24), 4345–4352.

(47) Svoboda, T.; Jambor, R.; Růžička, A.; Padělková, Z.; Erben, M.; Dostál, L. *Eur. J. Inorg. Chem.* **2010**, *2010* (33), 5222–5230.

(48) Liu, M.-J.; Cao, D.-K.; Liu, B.; Li, Y.-Z.; Huang, J.; Zheng, L.-M. *CrystEngComm* **2012**, *14* (14), 4699.

(49) Lukeš, I.; Císařová, I.; Vojtíšek, P.; Bazakas, K. *Polyhedron* **1995**, *14* (20–21), 3163–3166.

(50) Kotková, Z.; Pereira, G. A.; Djanashvili, K.; Kotek, J.; Rudovský, J.; Hermann, P.; Vander Elst, L.; Muller, R. N.; Geraldes, C. F. G. C.; Lukeš, I.; Peters, J. A. *Eur. J. Inorg. Chem.* **2009**, *2009* (1), 119–136.

(51) Pothiraja, R.; Shanmugan, S.; Walawalkar, M. G.; Nethaji, M.; Butcher, R. J.; Murugavel, R. *Eur. J. Inorg. Chem.* **2008**, *2008* (11), 1834–1845.

(52) Y. Wang; S. Parkin, and; Atwood*, D. **2002**.

(53) Chadwick, J. *Proc. R. Soc. London A Math. Phys. Eng. Sci.* **1932**, *136* (830).

(54) G.L. Locher. *Am J Roentgenol Radium Ther. 1936* (36), 1–13.

(55) Hawthorne, M. F.; Maderna, A. **1999**.

(56) Zhu, Y.; Lin, Y.; Zhu, Y. Z.; Lu, J.; Maguire, J. A.; Hosmane, N. S. *J. Nanomater.* **2010**, *2010*, 1–8.

(57) Papell, S. S. Low Viscosity Magnetic Fluid Obtained by Colloidal Suspension of Magnetic Particles. U. S. Patent no. 3. 215, 1965.

(58) Feliu, N.; Docter, D.; Heine, M.; del Pino, P.; Ashraf, S.; Kolosnjaj-Tabi, J.; Macchiarini, P.; Nielsen, P.; Alloyeau, D.; Gazeau, F.; Stauber, R. H.; Parak, W. J.; Star, A.; Shvedova, A. A.; Ruiz-Lozano, P.; Serpooshan, V.; Shokrgozar, M. A.; Nienhaus, G. U.; Parak, W. J.; Star, A.; Shvedova, A. A. *Chem. Soc. Rev.* **2016**, *45* (9), 2440–2457.

(59) Lee, N.; Hyeon, T.; Park, Y. I.; Lee, N.; Li, F.; Song, C.; Choi, S. H.; Na, K.; Hyeon, T.; Kim, J.; Hyeon, T.; Beisiegel, U.; Adam, G.; Weller, H.; Choi, S. H.; Hyeon, T. *Chem. Soc. Rev.* **2012**, *41* (7), 2575–2589.

(60) Haun, J. B.; Yoon, T.-J.; Lee, H.; Weissleder, R. *Wiley Interdiscip. Rev. Nanomedicine Nanobiotechnology* **2010**, *2* (3), 291–304.

(61) Kaittanis, C.; Santra, S.; Santiesteban, O. J.; Henderson, T. J.; Perez, J. M. *J. Am. Chem. Soc.* **2011**, *133* (10), 3668–3676.

(62) Faivre, D.; Bennet, M. *Nature* **2016**, *535* (7611), 235–236.

(63) Ling, D.; Hyeon, T. *Small* **2013**, *9* (9–10), 1449–1449.

(64) Mahmoudi, M.; Sahraian, M. A.; Shokrgozar, M. A.; Laurent, S. *ACS Chem. Neurosci.* **2011**, *2* (3), 118–140.

(65) Lee, N.; Yoo, D.; Ling, D.; Cho, M. H.; Hyeon, T.; Cheon, J. *Chem. Rev.* **2015**, *115* (19), 10637–10689.

(66) Casula, M. F.; Floris, P.; Innocenti, C.; Lascialfari, A.; Marinone, M.; Corti, M.; Sperling, R. A.; Parak, W. J.; Sangregorio, C. *Chem. Mater.* **2010**, *22* (5), 1739–1748.

(67) Lee, N.; Hyeon, T. *Chem. Soc. Rev.* **2012**, *41* (7), 2575–2589.

(68) Ling, D.; Hyeon, T. *Small* **2013**, *9* (9–10), 1450–1466.

(69) Yoo, D.; Lee, J.-H.; Shin, T.-H.; Cheon, J. *Acc. Chem. Res.* **2011**, *44* (10), 863–874.

(70) Jun, Y.; Lee, J.; Cheon, J. *Angew. Chemie Int. Ed.* **2008**, *47* (28), 5122–5135.

(71) Mahmoudi, M.; Sahraian, M. A.; Shokrgozar, M. A.; Laurent, S. *ACS Chem. Neurosci.* **2011**, *2* (3), 118–140.

(72) Sosnovik, D. E.; Nahrendorf, M.; Weissleder, R. *Circulation* **2007**, *115* (15), 2076–2086.

(73) Weber, L.; Kahlert, J.; Brockhinke, R.; Böhling, L.; Halama, J.; Brockhinke, A.; Stammler, H.-G.; Neumann, B.; Nervi, C.; Harder, R. A.; Fox, M. A. *Dalt. Trans.* **2013**, *42* (30), 10982.

(74) Gianpiero, C.; Anis, D.; Aikaterini, R.; Eirini, T.; Ioannis, V. S.; Dimitrios, F. G.; John, T. *Med. Chem. Commun.* **2017**, *8* (1), 67–72.

(75) Scherer, C.; Figueiredo Neto, A. M. *Brazilian J. Phys.* **2005**, *35* (3A).

(76) Akbarzadeh, A.; Samiei, M.; Davaran, S. *Nanoscale Res. Lett.* **2012**, *7*, 144.

(77) Kolhatkar, A.; Jamison, A.; Litvinov, D.; Willson, R.; Lee, T. *Int. J. Mol. Sci.* **2013**, *14* (8), 15977–16009.

Results and Discussion

2. *Closo*- carboranylphosphinic acids

Our group and others are interested in carboranylphosphorus compounds mostly due to its properties as ligands for organometallic chemistry and enantioselective catalysis. In the group in which this thesis has been done, bidentate carboranyldiphosphines,[1,2] monodentate carboranylmonophosphines,[3] bidantate carboranylmonophosphinesmonothioethers,[4] bidantate carboranylmonophosphinesmonoamines[5] as well as oxides, sulphides and selenides of carboranyldiphosphines and carboranylmonophosphines[6] have been synthesized and their reactivity through metals investigated with the objective to isolated the corresponding complexes that were tested as catalysts in hydrogenation reaction of terminal[7–12] and internal olefins,[13] cyclopropanation,[14,15] radical polymerisation of vinyl monomers[16,17] as well as in Kharasch-type reaction, namely the "atom transfer radical addition" (ATRA).[18–20]

Although carboranylphosphinic, R-OPH(OH), and carboranylphosphonic, R-P(O)$(OH)_2$, acids were reported years ago[21,22] neither their characterization nor reproducible procedures of synthesis were available. Therefore, the initial goal of this thesis was to attempt the preparation and characterization of carboranylphosphonic acids, R-P(O)$(OH)_2$, aiming towards the designing of purely inorganic ligands that are capable to coordinate to metals producing stable water-soluble coordination polymers (CPs). Unexpectedly, was found that carboranylphosphinic acids of *ortho*- and *meta*-carborane, R-OPH(OH), and its sodium salts were easy to obtain in a good yield. Then, the influence of the boron cluster (*ortho*- and *meta*-) on the reactivity of the phosphinate group was studied as well.

2.1 Synthetic pathway of the *ortho*- and *meta*-carboranylphosphinic acids and its sodium salts

From the literature it was known that diclorophosphine derivatives of *ortho*- and *meta*-carborane are readily hydrolysed to corresponding phosphonous acids that immediately undergo tautomeric isomerization to phosphinic acid form (Scheme 2.1). For the synthesis of diclorophosphines of carboranes we used the

method based on reaction between dialkylaminophosphine derivative of carborane and dry HCl acid. Mono- and disphosphinic acids of *ortho*- and *meta*-carborane and its sodium salts have been synthesized by this method and fully characterized.

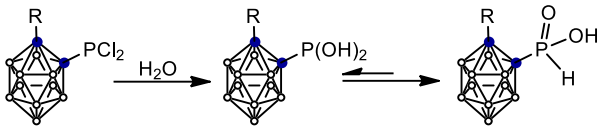

Scheme 2.1 Hydrolysis of diclorophosphine derivatives of *closo*-carboranes (on the example of *ortho*-carborane derivatives)

Althought the synthetic procedure for the synthesis of some monophosphinic acids like 1-CH_3-2-OPH(OH)-1,2-*closo*-$C_2B_{10}H_{10}$ and 1-CH_3-7-OPH(OH)-1,2-*closo*-$C_2B_{10}H_{10}$ had been previously established[21,22], their full characterization remained unpublished and have been reported in this thesis.

Our first attempt in this PhD thesis was to achieve an efficient synthetic procedure for the isolation of these carboranylphosphinic acids as well as monophosphinic acids, 1-OPH(OH)-1,2-$C_2B_{10}H_{11}$, and 1-OPH(OH)-1,7-$C_2B_{10}H_{11}$, and diphosphinic acids of *ortho*- and *meta*-carborane, 1,2-(OPH(OH))2-1,2-$C_2B_{10}H_{10}$, and 1,7-$(OPH(OH))_2$-1,7-$C_2B_{10}H_{10}$. This goal was carried out by slight modifications in procedures that previously reported.

2.1.1 Synthesis of monophosphinic acids of *ortho*- and *meta*-carborane

The synthesis of monophosphinic acids starting from 1-CH_3-1,2-*closo*-$C_2B_{10}H_{10}$ or 1-CH_3-1,7-*closo*-$C_2B_{10}H_{10}$ was achieved by deprotonation of C_c-H vertex with *n*-BuLi followed by electrophilic reaction with $ClP(NMe_2)_2$ at 0 °C (Scheme 2.2). After working up bis(dymethylaminophosphine)-*closo*-carborane derivatives were isolated in high yield (95 and 90 %, for compounds **5** and **6**, respectively).

As shown in Scheme 2.3, dichlorophosphine derivatives **11** and **12** were obtained by passing a stream of dry HCl through benzene solutions of **5** and **6**. Corresponding phosphinic acids, **17** and **18**, were isolated by hydrolysis of **11** and **12** in 70 % and 90 % yield, respectively. Addition of 10 % NaOH solution to water suspensions of **17** and **18** till pH neutral gave the corresponding sodium salts, **22** and **23**

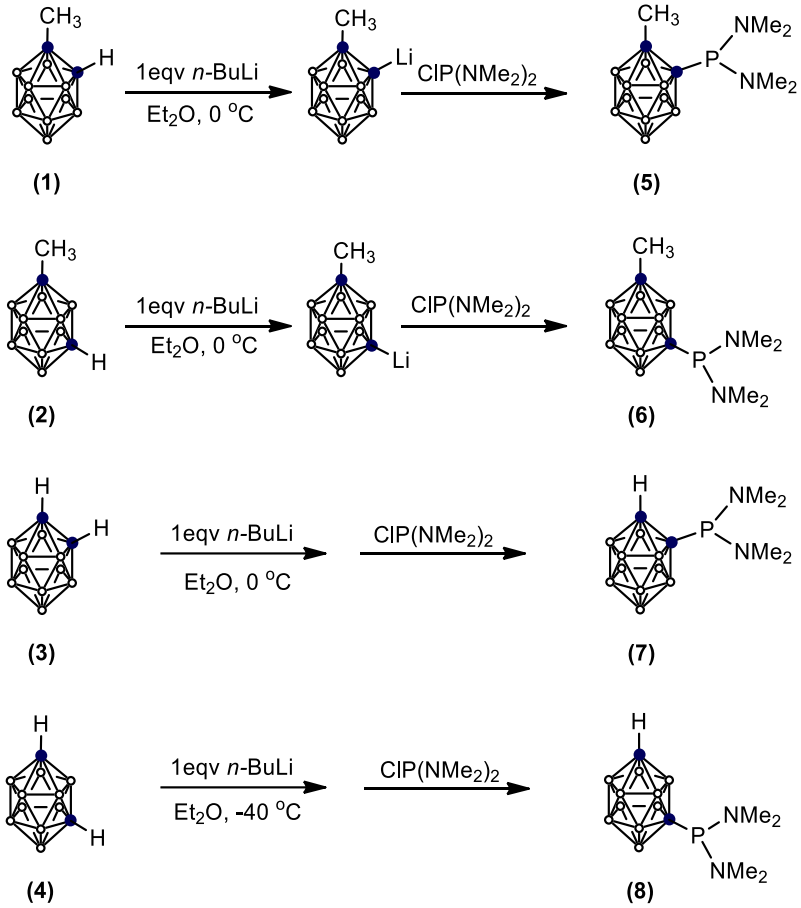

Scheme 2.2. Synthesis of bis(dymethylaminophosphine)-*closo*-carborane derivatives **5** – **8**.

The preparation of monophosphinic acids starting from 1,2-*closo*-$C_2B_{10}H_{12}$ and 1,7-*closo*-$C_2B_{10}H_{12}$ was not so trivial due to the tendency of the monolithiated carborane disproportionate to unreacted and dilithiated species[23]. For *meta*-carborane it was found that the best conditions that give around 90 % of 1-$P(NMe_2)_2$-1,7-*closo*-$C_2B_{10}H_{11}$ were in abs. Et_2O at -40 °C or at -20 °C and initial *meta*-carborane concentration 0.23 $molL^{-1}$. Lowering the temperature to -60 °C lead to significant increase of unreacted *meta*-carborane up to 28 %. For *ortho*-carborane over 90 % of 1-$P(NMe_2)_2$-1,2-*closo*-$C_2B_{10}H_{10}$, **7**, was obtained in abs.

Et_2O at 0 ºC and concentration 0.23 $molL^{-1}$, reaching up to 93 %. Table 2.1 summarizes this monosubstitution reaction at different temperatures.

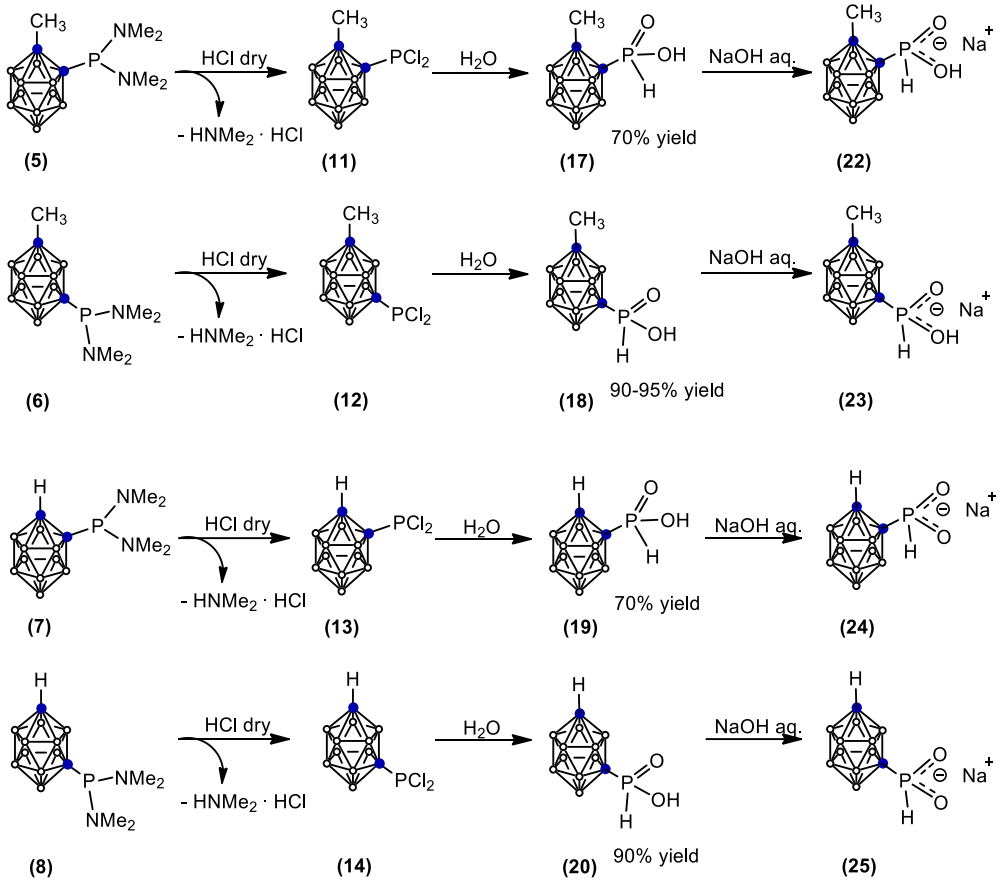

Scheme 2.3. Synthesis of *ortho*- and *meta*-carboranylphosphinic acids (**17**-**20**) and corresponding sodium salts (**22**-**25**).

Table 2.1. Percentage of unreacted carborane (*ortho*- or *meta*-) in the synthesis of 1-$P(NMe_2)_2$-*closo*-$C_2B_{10}H_{11}$.

C_{carb} [mol L^{-1}]	T [ºC]	*m*-carborane unreacted [%]	*o*-carborane unreacted [%]
0.23	-60ºC	28	no tested
0.23	-40ºC	10-12	no tested
0.23	-20ºC	10-12	6-7
0.23	0ºC	24	6-7

As shown in Scheme 2.3, dichlorophosphine derivatives **11** - **14** were obtained by passing a stream of dry HCl through benzene solutions of **5** - **8**. The corresponding phosphinic acids, **17** - **20**, were isolated by hydrolysis of **11** – **14** in 70 % (for *ortho*-carborane derivatives) and 90-95 % yield (for *meta*-carborane derivatives). Addition of 10 % NaOH solution to water suspensions of **17** - **20** till pH neutral gave the corresponding sodium salts, **22** - **25**.

2.1.2 Synthesis of diphosphinic acids of *ortho*- and *meta*-carborane

The synthesis of **9** was reported by Hill et al. in 1978 starting from dilithiated *ortho*-carborane and bis(dimethylamino)chlorophosphine with 58 % yield[24]. The synthesis of **10** was already reported by Alexander and Schroeder[25] in 1966 starting from 1,7-$(PCl_2)_2$-1,7-*closo*-$C_2B_{10}H_{10}$, that after reaction with dimethylamine gas, $HNMe_2$, gave **10** in about 30 % total yield. In 2009 Hey-Hawkins et al. also obtained **10** in 60 % yield following the same procedure as Hill, which was an improved yield and easier access than the synthesis of Alexander and Schroeder[26]. In this PhD thesis, disubstitution of *ortho*- and *meta*-carborane by phosphinate group have been performed by a similar synthetic procedure to that of the monophosphinic acids (Scheme 2.4). Compounds **9** and **10** were obtained in 95 % and 97 % respectively, following the same procedure described by Hill et al.

Surprisingly, the final product of the synthesis of *ortho*- carboranyl diphosphinic acid was not the expected one. During hydrolysis C_c – P bond cleavage took place, yielding the monophosphinic acid 1-OPH(OH)-1,2-*closo*-$C_2B_{10}H_{11}$. In the case of *meta*-carborane the final product resulted in 1,7-$(OPH(OH))_2$-1,7-*closo*-$C_2B_{10}H_{10}$ as it was expected.

The similar process that leads to C_c– P cleavage was observed for diisopropylcarboranyldiphosphines after going to oxidation with Se[27] as it was mentioned in the introduction.

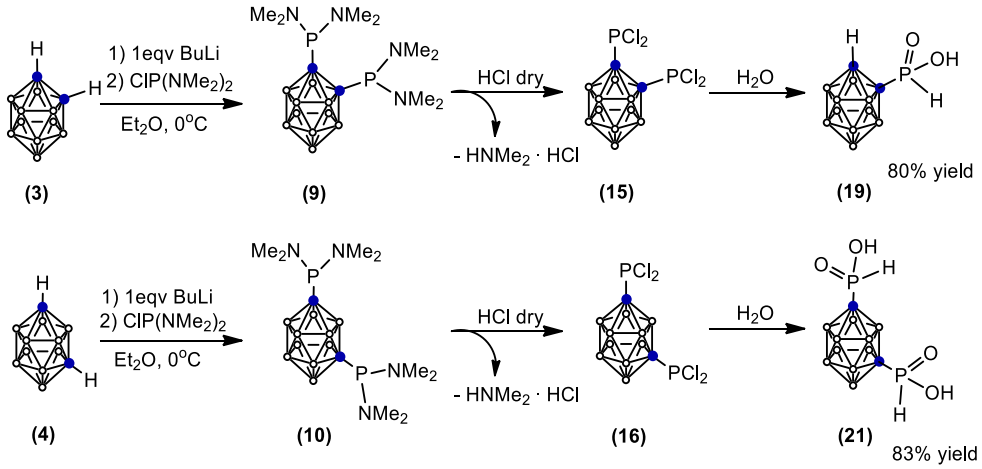

Scheme 2.4. Synthesis of diphosphinic acid derivatives of *closo*-$C_2B_{10}H_{10}$ (*ortho*- and *meta*-).

2.2 Characterization and structural aspects on the *ortho*- and *meta*-carboranylphosphinic acids and its sodium salts

2.2.1 Spectroscopic measurements

Compounds **5 - 25** were characterized by multinuclear NMR spectroscopy (^1H, $^1H\{^{11}B\}$, $^1H\{^{31}P\}$, ^{11}B, $^{11}B\{^1H\}$, $^{13}C\{^1H\}$, ^{31}P, $^{31}P\{^1H\}$), infrared spectroscopy (ATR-FTIR), elemental analysis, and some of them by mass spectroscopy (MALDI-TOF-MS), thermal gravimetric analysis (TGA) and X-ray diffraction. On the FTIR spectrum of selected example phosphinic acid **20** (Figure 2.1) showed B-H absorptions in the range at 2655-2593 cm^{-1} that supports the *closo* cluster structure, at 3059 cm^{-1} characteristic stretching vibrations of C_c-H.

The presence of phosphinic acid group in the molecule is observed by the presence of P-H absorption at 2419 cm^{-1} and P=O at 1211 cm^{-1}. In general on infrared spectra the fundamental stretching vibrations of the P-H bonds appear at 2327 and 2421 cm^{-1}, and those at 991 and 1121 cm^{-1} may be assigned to bending motions of P-H bonds[28]. Interestingly, in the present work no evidence of a free hydroxyl group in carboranylphosphinic acids **17** - **21** has been found. Such groups must have characteristic absorption due to the stretching vibration of the O-H bond at about 3620 cm^{-1}. The hydrogen bonding effect in phosphinic acids could lower stretching frequency of O-H bond. It was possible to observe on the infrared

spectrum of phenylphosphinic acid that showed a broad band at approximately 2588 cm^{-1} (Figure 2.2). Absorption of O-H bond in this region at about 2550 and 2680 cm^{-1} was found in the literature for several other organic phosphinic acids[28].

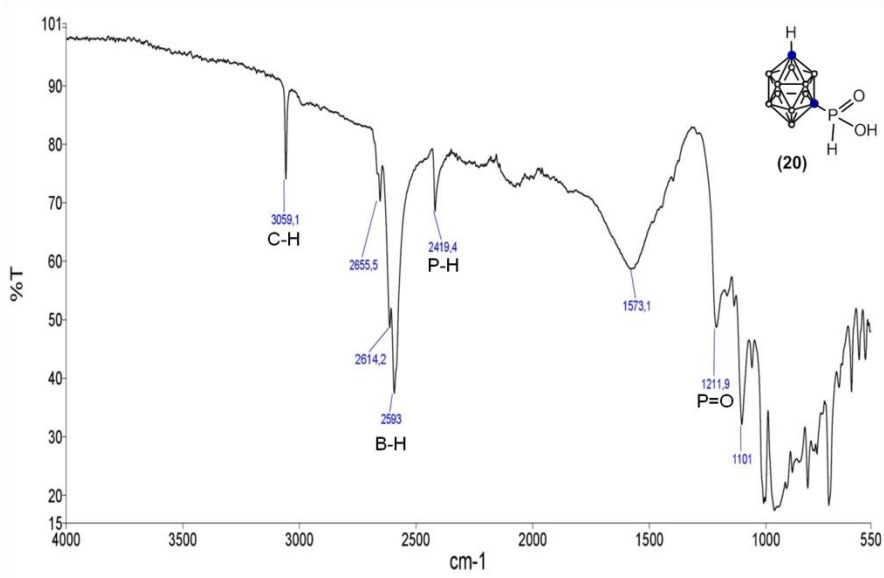

Figure 2.1 FTIR spectrum of phosphinic acid **20**

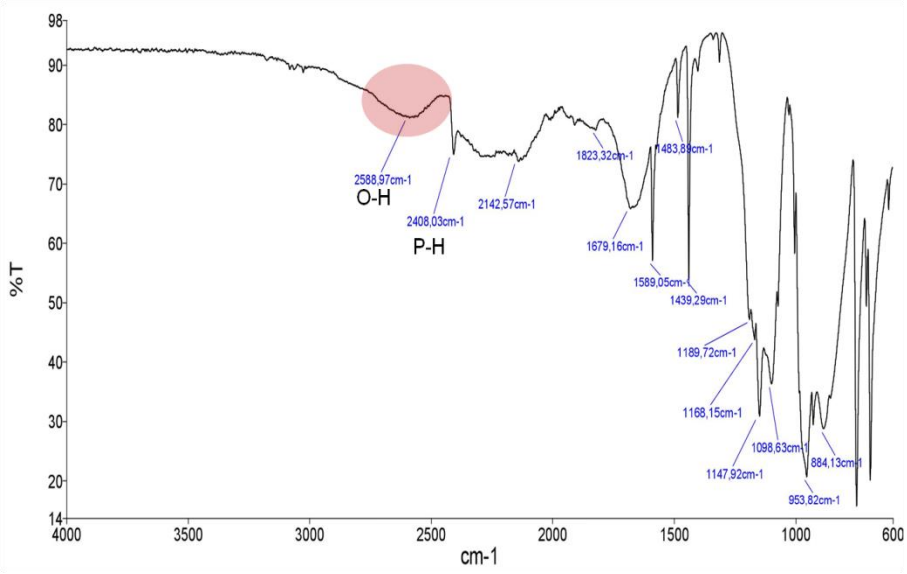

Figure 2.2 FTIR spectrum of phenylphosphinic acid

In the case of carborane derivatives in the same region at about 2593 - 2655 cm^{-1} B-H absorptions appear. It could explain why it was impossible to observe hydroxyl group vibrations for carboranylphosphinic acids **17** - **21**. Infrared spectra of these compounds have been studied, and results are summarized in Table 2.2.

Table 2.2. Infrared characteristics of phosphinic acids

Frequency (cm^{-1})	Remarks
2550-2680	Characteristic broad hydrogen-bonded O-H stretch.
~1211	P=O stretch
2327 – 2421	P-H stretch

Closo-carboranylphosphinic acids, compounds **17-20**, displayed a singlet around 17 ppm (for *ortho*-isomer) and 21 ppm (for *meta*-isomer) on $^{31}P\{^{1}H\}$ NMR spectrum that turns to a doublet in the ^{31}P NMR spectrum with coupling constant in the range of $^{1}J(P,H)$= 635 Hz indicating the presence of a P-H bond in the compounds (Figure 2.3). Chemical shifts on $^{31}P\{^{1}H\}$ NMR for sodium salt of *closo*-carboranylphosphinic acids, **22** - **25**, are shielded upfield compare to corresponding acid forms, being the difference of 6.15- 7.87 ppm.

Table 2.3 shows the ^{31}P chemical shifts of these phosphorus compounds derivated from *ortho*- and *meta*-carborane, which appear in the region between δ +162.20/ +9.21 ppm. The ^{31}P resonances in all *ortho*-carborane derivatives appear at higher frequency compared with those of the *meta*-carborane derivatives. From Table 2.3, it is clear when comparing the two cluster isomers, *ortho*- and *meta*-, of the different carboranylphosphorus derivatives that the $^{31}P\{^{1}H\}$-NMR chemical shift has

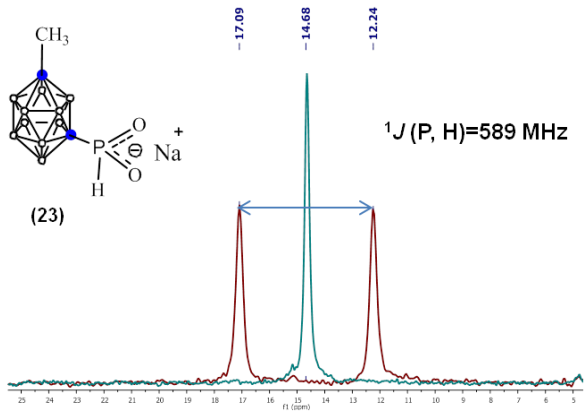

Figure 2.3 ^{31}P NMR (red) and $^{31}P\{^{1}H\}$ NMR (blue) in H_2O of compound **23.**

Table 2.3. $^{31}P\{^{1}H\}$ NMR chemical shifts for the *closo*-carboranyl phophines (**5**-**14)**, phosphinic acids (**17**-**20**) and corresponding phosphinates **(22-25).**

Entries	Compound	Solvent	δ (^{31}P), ppm (J, MHz)	Δδ(^{31}P), ppm
5	1-CH_3-2-$P(NMe_2)_2$-1,2-*closo*-$C_2B_{10}H_{10}$	$CDCl_3$	99.32	+6.45
6	1-CH_3-7-$P(NMe_2)_2$-1,7-*closo*-$C_2B_{10}H_{10}$	$CDCl_3$	105.77	
7	1-$P(NMe_2)_2$-1,2-*closo*-$C_2B_{10}H_{11}$	$CDCl_3$	108.10	-2.18
8	1-$P(NMe_2)_2$-1,7-*closo*-$C_2B_{10}H_{11}$	$CDCl_3$	105.65	
11	1-CH_3-2-PCl_2-1,2-*closo*-$C_2B_{10}H_{10}$	$CDCl_3$	155.38	+6.82
12	1-CH_3-7-PCl_2-1,7-*closo*-$C_2B_{10}H_{10}$	$CDCl_3$	162.20	
13	1-PCl_2-1,2-*closo*-$C_2B_{10}H_{11}$	$CDCl_3$	156.94	+5.15
14	1-PCl_2-1,7-*closo*-$C_2B_{10}H_{11}$	$CDCl_3$	162.09	
17	1-CH_3-2-OPH(OH)-1,2-*closo*-$C_2B_{10}H_{10}$	$CDCl_3$	17.08 (640)	+3.70
18	1-CH_3-7-OPH(OH)-1,7-*closo*-$C_2B_{10}H_{10}$	$CDCl_3$	20.78 (633)	
19	1-OPH(OH)-1,2-*closo*-$C_2B_{10}H_{11}$	$CDCl_3$	17.22 (652)	+3.84
20	1-OPH(OH)-1,7-*closo*-$C_2B_{10}H_{11}$	$CDCl_3$	21.06 (635)	
22	$[Na\cdot(H_2O)_4][1\text{-}CH_3\text{-}2\text{-}OPH(O)\text{-}1,2\text{-}closo\text{-}C_2B_{10}H_{10}]$	D_2O	9.21 (449)	+5.42
23	[Na][1-CH_3-7-OPH(O)-1,7-*closo*-$C_2B_{10}H_{10}$]	D_2O	14.63 (t, (^1J(P, D)=89)	
		H_2O	14.65 (d, ^1J(P, H)=589)	
24	[Na][1-OPH(O)-1,2-*closo*-$C_2B_{10}H_{11}$]	D_2O	9.53 (d, ^1J(P, H)=602)	+5.13
		H_2O		
25	[Na][1-OPH(O)-1,7-*closo*-$C_2B_{10}H_{11}$]	D_2O	14.66 (d, ^1J(P, H)=583)	

the same trend to deshield going from *ortho*- to *meta*-isomer: +6.45 ppm between entries **5** and **6**, +6.82 ppm between **11** and **12**, +3.70 pmm between **17** and **18**, +5.42 ppm between **22** and **23**. It is also important to notice when comparing

entries **5** and **7**, entries **6** and **8**, entries **11** and **13**, entries **12** and **14** on Table 2.3 that there is no influence on the nature of the R group (R= Me, H) bonded to the second C_c, being the difference 0.11 ppm in all cases. There is almost no difference on the chemical shifts for the phosphinic acids **17** and **19**, **18** and **20**, and corresponding sodium salts, entries **22** and **24**, **23** and **25**. To emphasize that the $^{1}J(P, H)$ of the salts **23** and **25** indicates that for each isomer the substituent on the other C_c has no influence on the coupling constant, 589 and 583 Hz, respectively. However, the $^{1}J(P, H)$ is more influenced by the isomer as observed for **22** and **23** (449 and 589 Hz) or for **24** and **25** (602 and 583 Hz).

Figure 2.4 shows ^{31}P NMR shifts overview among derivatives of 1-CH_3-2-OPH(OH)-1,2-$C_2B_{10}H_{10}$. The order of shielding the ^{31}P NMR chemical shift follows OPH(O) > OPH(OH) > $P(NMe_2)_2$ > PCl_2.

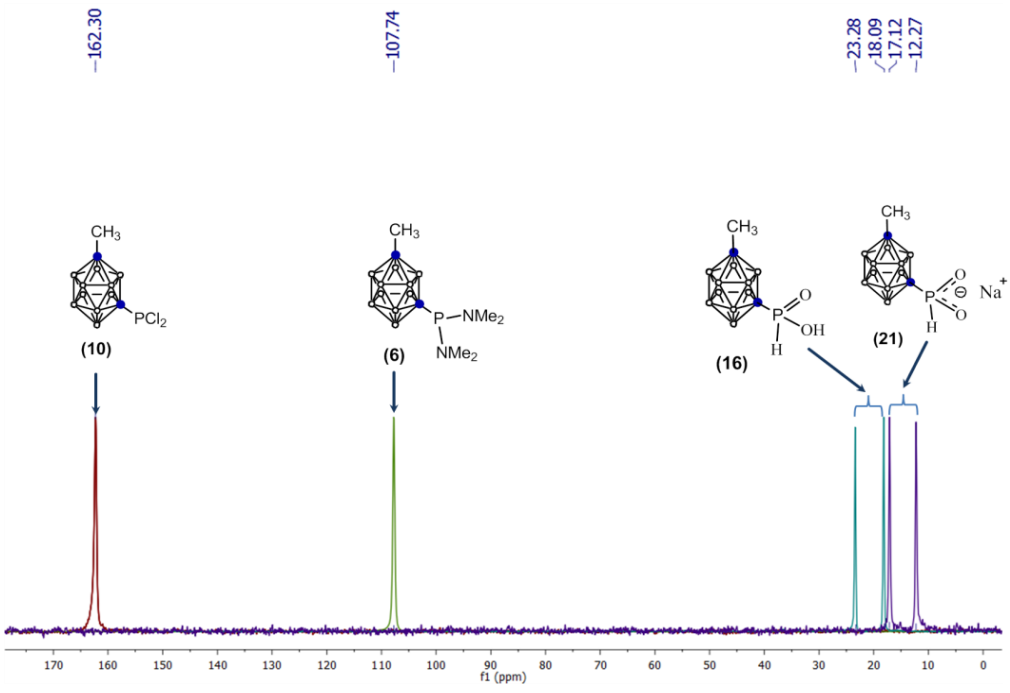

Figure 2.4 ^{31}P NMR of derivatives of 1-CH_3-2-OPH(OH)-1,2-$C_2B_{10}H_{10}$: **10**, **6**, **16**, **21**

It is known that phosphinic acids form strong hydrogen bonds of the type P–O–H···O=P, producing dimers (Figure 2.5). Thus, hydrogen bonding lengthens the O-H bond and reduces the valence electron density around the proton. As a result, the chemical shift of OH in the ^{1}H NMR spectrum is deshielded in the dimeric form compared to free OH group.

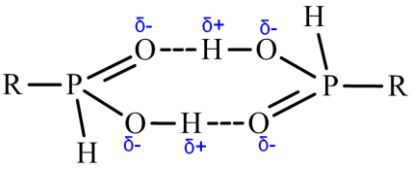

Figure 2.5 Cyclic dimer of phosphinic acid RP(O)H(OH).

The process of dimerization can be promoted by cooling. Thus, on cooling **20** in $CDCl_3$, the resonance at 5.45 ppm in the room temperature ^{1}H NMR spectrum that corresponds to free OH shifts to 11.41 ppm at -60 ºC (lots of H bonding) (Figure 2.6).

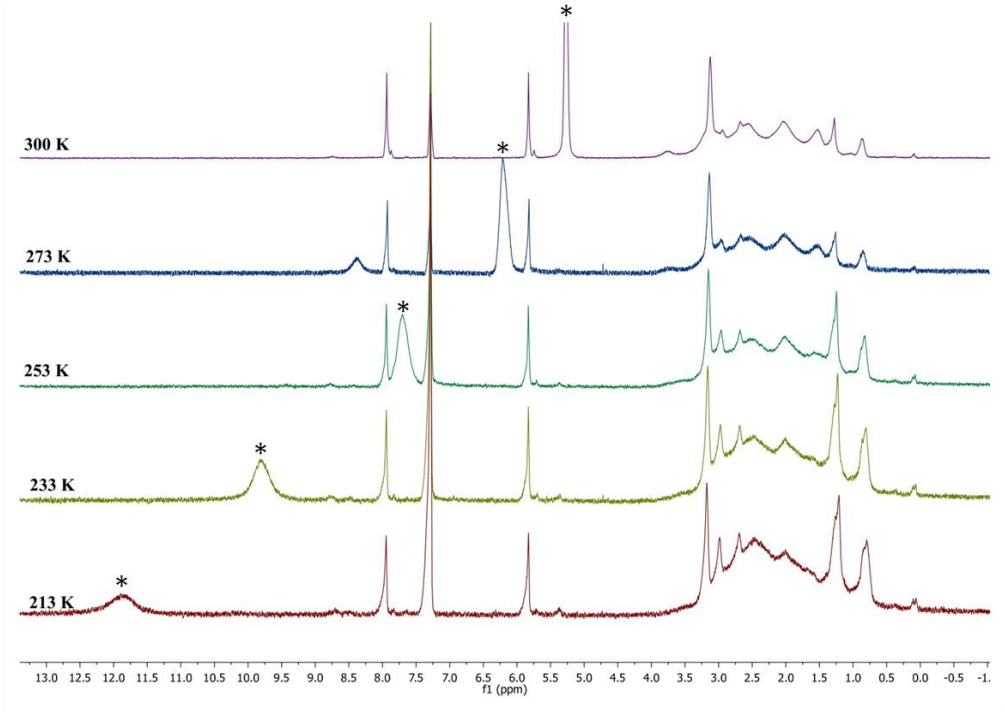

Figure 2.6 Variable temperature ^{1}H NMR spectra of 1-OPH(OH)-1,7-$C_2B_{10}H_{11}$ (**20**) in $CDCl_3$

Also Raman spectroscopy of 1-OPH(OH)-1,7-*closo*-$C_2B_{10}H_{11}$ (**20**) in KBr pellet (10, 50 and 100 %) were run. Spectra clearly indicate the presence of C_c-H,

B-H and P-H resonances (Figure 2.7) and confirm that this carboranylphosphinic acid is detected in all range of the studied concentrations. This is very important because Raman spectroscopy is an optical technique that is used for medical diagnostics; from *in vitro* to *in vivo* cancer detection.[29]

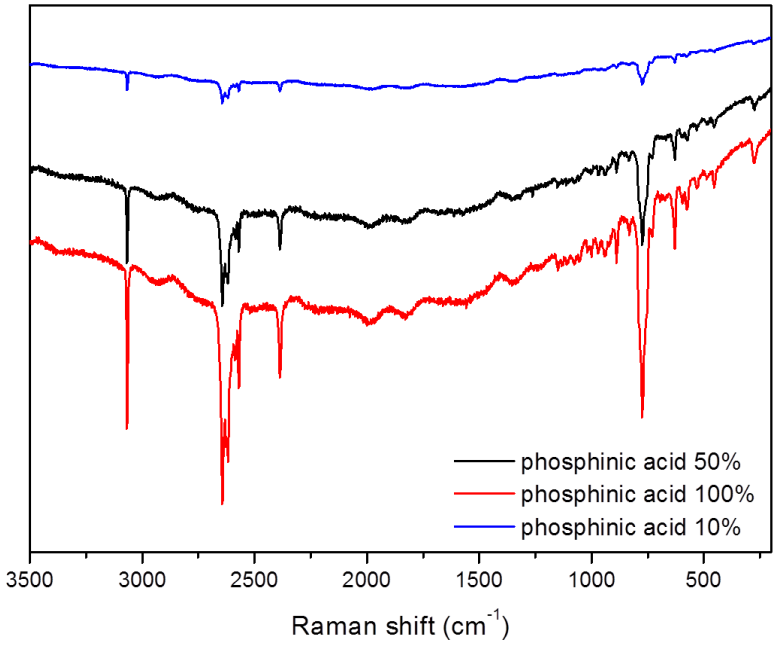

Figure 2.7 Comparison of Raman spectra of samples with different concentrations of 1-OPH(OH)-1,7-*closo*-$C_2B_{10}H_{11}$ (**20**)

2.2.2 Structural characterization

The molecular structures of *ortho*-carboranyl bisdimethylaminophosphines (compounds **5**, **7** and **9**) were unambiguously elucidated by X-ray diffraction of suitable crystals grown from diethyl ether solutions (Figure 2.8). Compound **5** crystallizes in triclinic space group P1, compounds **7** and **9** in the monoclinic space group P2**1**/n. In all three molecular structures C_c-C_c bond length lies in the range of common C-C bonds and the C_c–P bonds are similar (Table 2.4).

Good crystals of the sodium salt of the *ortho*-carboranyl phosphinic acid, **22**, (Figure 2.9) suitable for X-ray diffraction were grown from water that fully confirmed its molecular structure. For **22** the P–C_c bond length (1.844(2) and 1.856(2) Å) is

similar to those in the *ortho*-carboranylmonophosphines (1.884(4) - 1.871 Å),[30–32] while the C_c–C_c bond (1.664(3) and 1.676(3) Å) is slightly shorter (1.702(6) and 1.731(9) Å). The P–H bond length (1.29(2) and 1.32(2) Å) compares well with similar bonds found in secondary phosphinocarbaboranes (1.31(2) and 1.372(1) Å)[33,34] or phosphonium salts (1.30(2) and 1.38(4)).[35,36] The crystal structure of **22** is composed of alternating (001) layers of carboranyl clusters and hydrated Na^+ ions, Figure 2.10 displays its packing. Hydrogen bonding interactions link layers together involving coordinated water molecules and phosphonate groups.

Table 2.4 Selected bond lenghts (Å) for compounds **5**, **7**, **9**

	5	**7**	**9**
C1-C2	1.681	1.663	1.711
P1-C1	1.906	1.905	1.921
P2-C2	-	-	1.907
P1-N1	1.679	1.669	1.679
P1-N2	1.668	1.664	1.670
P2-N3	-	-	1.670
P2-N4	-	-	1.687

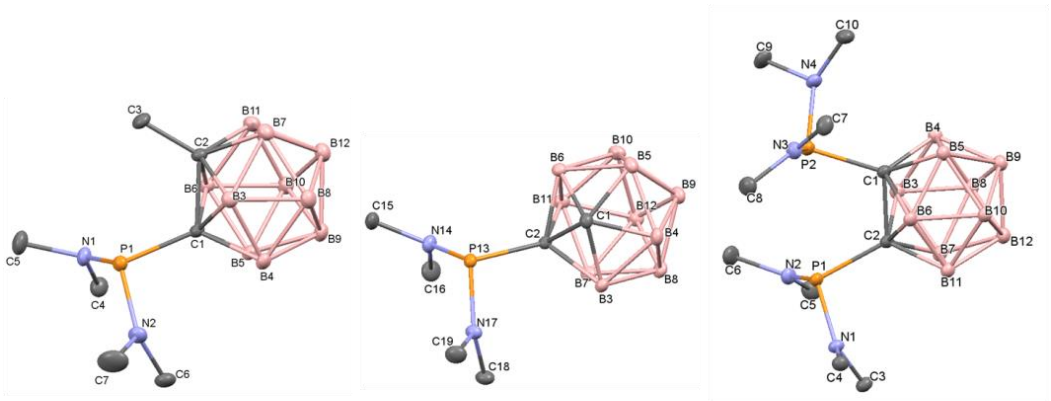

Figure 2.8 Molecular structures of *ortho*-carboranyl bisdimethylaminophosphines **5**, **7** and **9** (H atoms are omitted for clarity).

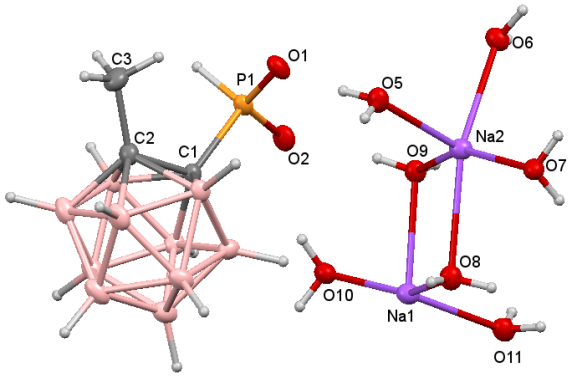

Figure 2.9 Molecular structure of the compound **22**.

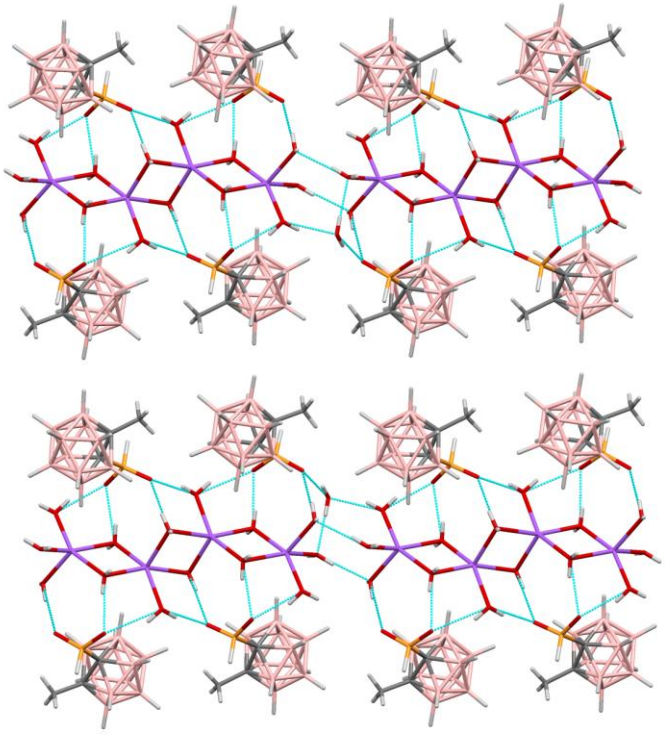

Figure 2.10 Packing of the compounds **22**.

For *meta*-carboranyl bisdimethylamino-phosphine, **8**, X-ray analysis confirmed the substitution of one C_c with a phosphorus moiety (Figure 2.11).

Compound **8** crystallizes in orthorhombic space group Pna21. Selected bond lengths and angels are presented in Table 2.4.

Table 2.4 Selected bond lenghts (Å) and bond angles (º) for compound **8**

Bond lengths		Bond angles	
C1-P13	1.893(2)	N14-P13-C1	104.30(9)
P13-N14	1.673 (19)	N14-P13-N17	110.81(10)
P13-N17	1.683 (19)	N17-P13-C1	100.92(10)

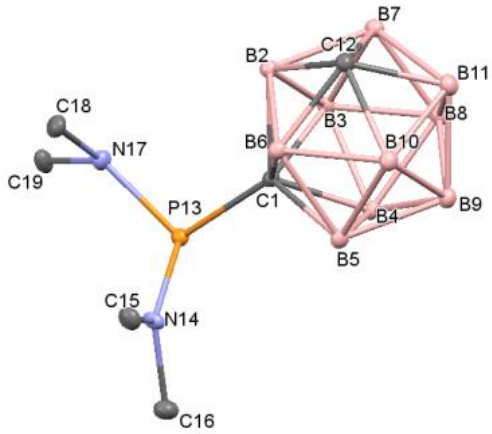

Figure 2.11 Molecular structure of compound **8** (H atoms are omitted for clarity).

Good crystals of the sodium salt of the *m*-carboranylphosphinic acid **24** were grown from an *i*-PrOH/water solution. Figure 2.12 displays the asymmetric unit cell that contains two ligands with different P-H bond lengths (1.30(2) and 1.34(2) Å) and two sodium atoms that corresponds to $[Na_2][1\text{-}OPH(O)\text{-}1,7\text{-}closo\text{-}C_2B_{10}H_{11}]_2 CH(OH)(CH_3)_2$, **24**. A sodium atom coordinates to two oxygen atoms one from each ligand being the Na-O bond distances 2.263 and 2.290 Å while, the other sodium (Na1) coordinates to three oxygen atoms, one also from each ligand (2.1602(17) and 2.3570(16) Å) and the third one to one *i*-PrOH molecule (2.3108(18) Å). Sodium atoms complete their coordination sphere with O donor atoms from adjacent asymmetric units, generating 2D chains running along the *a* axis.

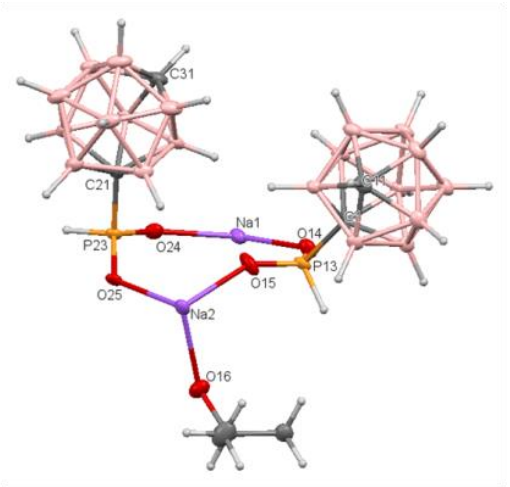

Figure 2.12 Molecular structure of compound **24**.

Good crystals of the *o*-carboranylphosphinic acid, 1-OPH(OH)-1,2-*closo*-$C_2B_{10}H_{11}$, **18**, *m*-carboranylphosphinic acid 1-OPH(OH)-7-CH_3-1,7-*closo*-$C_2B_{10}H_{10}$, **19**, and *m*-carboranyldiphosphinic acid, 1,7-$(OPH(OH))_2$-1,7-*closo*-$C_2B_{10}H_{10}$, **21**, were grown from water solution. Figure 2.13 displays their X-ray structures that unambiguously prove their chemical structure.

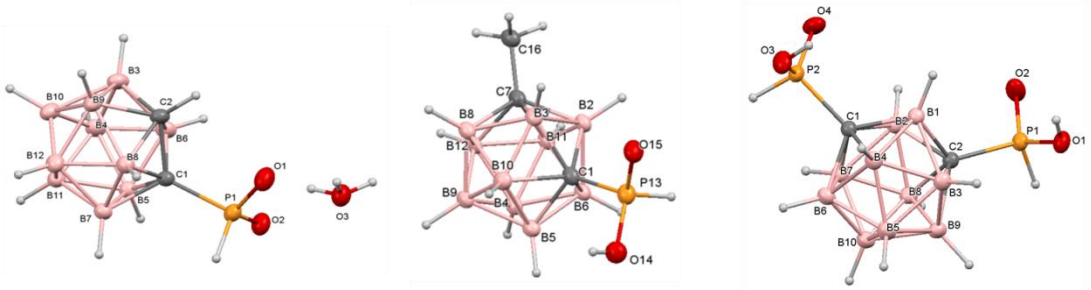

Figure 2.13 Molecular structures of closo-carboranylphosphinic acids **18**, **19**, **21**.

TGA/DSC of acids **19**-**20** and its corresponding sodium salts, **24**-**25,** was run under an argon atmosphere in the range from room temperature to 700ºC. Data obtained by TGA/DCS are displayed in Table 2.5 and TGA/DSC graphs of **20** and

25 in Figure 2.14. For the acid 1-OPH(OH)-1,7-*closo*-$C_2B_{10}H_{11}$, **20**, the weight loss of 31.30 % at 280 ^oC is due to the removal of phosphinate functional group, OPH(OH). For its sodium salt, **25**, the weight loss of 24.58 % at 380 ^oC corresponds to the phosphinate group except phosphorus, O(H)(OH)Na.

Table 2.5 Thermal gravimetric analysis (TGA) data for compounds **19-20** and **24-25**.

Compound	% Weight loss (T[^oC])
19	7.96 (200), 28.76(300)
20	31.30 (280)
21	2.06 (224)
24	3.63 (230), 9.27 (300)
25	24.58 (380)
OPH(OH)-C_6H_5	30.91 (230)

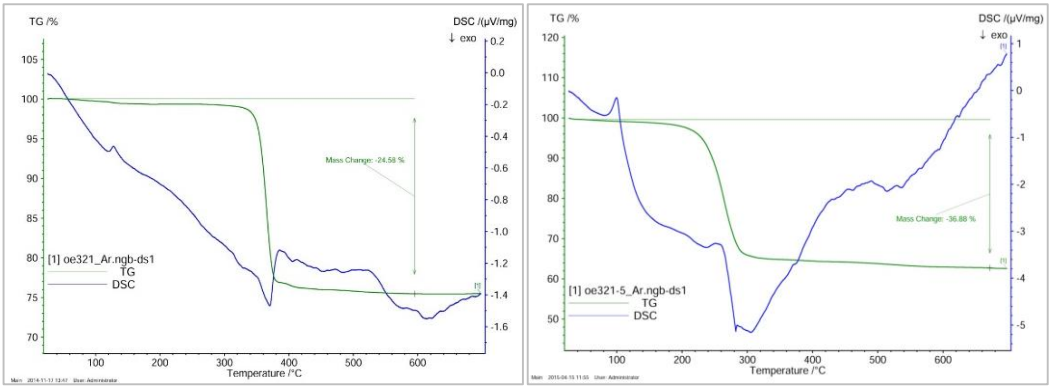

Figure 2.14 TGA/DSC curves for compounds **20** and **25**.

TGA results and $^{11}B\{^1H\}$ NMR spectroscopy demonstrate that *ortho*-carboranylphosphinic acids and its sodium salts are much less stable than their *meta*-carborane analogues. It was found that the sodium salt of *ortho*-carboranylphosphinic acid, **22**, undergoes a partial deboronation in aqueous medium (Figure 2.15). It can be explained by the fact that phosphinic acids are involved in tautomeric equilibrium between phosphinic and phosphonous acid isomers (see the section 2.3) where phosphonous acid, carrying an electron pair on the phosphorus atom, can act as a nucleophilic agent producing “decapitation” or

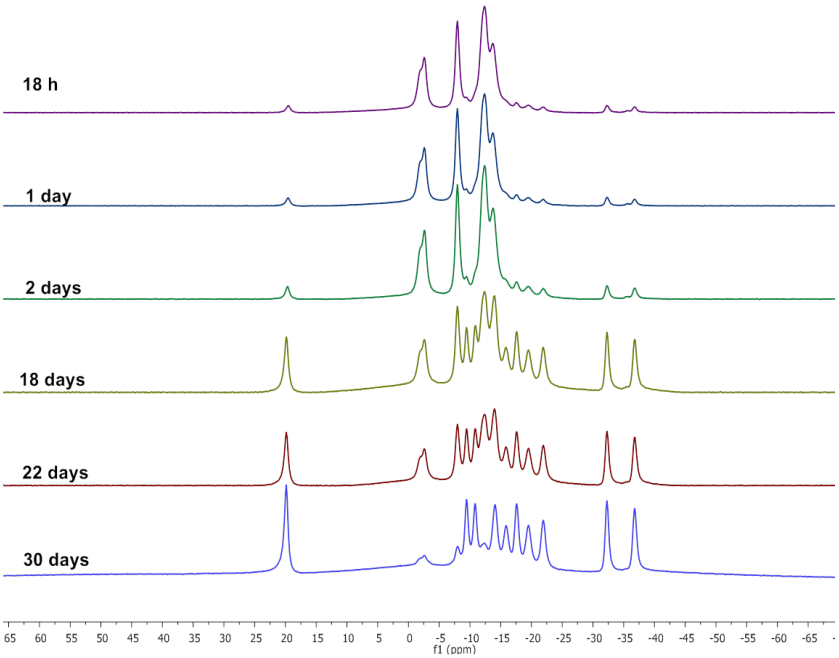

Figure 2.15 $^{11}B\{^{1}H\}$ NMR spectra of **22** in H_2O showing the partial degradation of the *ortho*-cluster.

partial deboronation of *ortho*-carborane cluster. Another explanation can be the nature of the P-O bond in phosphinic acids that can be described as a short σ-bond in which the oxygen carriers a negative charge and the phosphorus contains a positive charge a displayed in the Figure 2.16.[37] Thus, phosphinic acids may act as a nucleophile and produce partial deboronation of the *ortho*-carborane cluster.

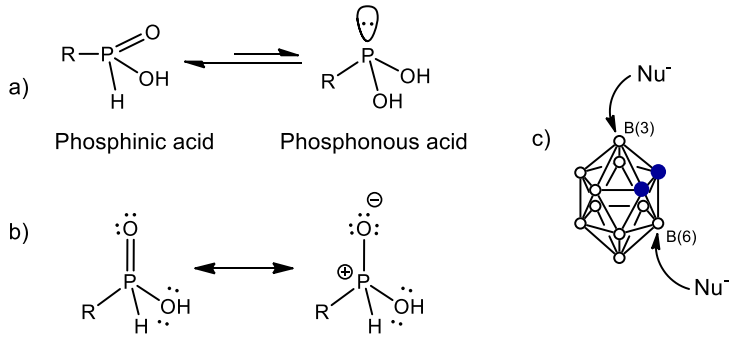

Figure 2.16 Phosphonous acid tautomeric forms (a), the Lewis structure of phosphinic acid (b), and drawing of the ortho-carborane cluster showing the reactivity of the boron vertices in front of nucleophilic agents (c).

Having enough information on the different phosphinic acids of *ortho*- and *meta*-carborane, for further use we put our attention on the *meta*-carborane derivatives due to its enhanced stability compare to *ortho*-isomer derivatives.

2.3 Tautomerism and isotopic exchange P-H/P-D in D_2O

It is reported that the phosphorous-bonded hydrogen of phenylphosphinic acid undergoes isotopic exchange with deuterium from the solvent[38]. It was suggested that this exchange is due to the tautomerism between the pentacoordinated phosphorous ROPH(OH) in organophosphinic acids and the tricoordinated one in $RP(OH)_2$ in organophosphonous acids[39]. This tautomeric equilibrium (Figure 2.17) is completely shifted to P(V) tautomer, so free phosphonous acid normally can not be detected by spectroscopic methods. In contrast to other known phosphinic acids, was found that phosphinic acid $(CF_3)_2POH$ is the prevalent tautomeric form over $(CF_3)_2P(O)H$[40,41].

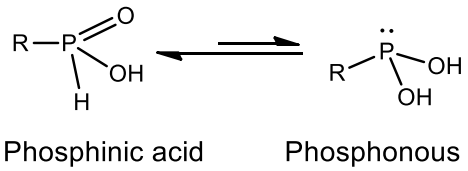

Figure 2.17 Tautomeric equilibrium between phosphinic and phosphonous acid isomers.

To know the influence of the *meta*-carboranyl ligand, the kinetics of this acid- and base-isotopic exchange, between the hydrogen atom bound to phosphorous with deuterium from the D_2O solvent, was studied by means of $^{31}P\{^1H\}$ and ^{31}P NMR spectra for compounds 1-OPH(OH)-1,7-$C_2B_{10}H_{11}$, **20**, Na[1-Me-7-OPH(O)-1,7-$C_2B_{10}H_{10}$], **23** (Figure 2.18), and Na[1- OPH(O)-1,7-$C_2B_{10}H_{11}$], **22**.

A point to note is that the ^{31}P and $^{31}P\{^1H\}$ NMR spectra of **22** in D_2O exhibits after 3.5h a triplet (1:1:1) at 14.63 ppm with a $^1J(P,D)$ of 86 Hz as a result of the completed isotopic exchange while, no exchange was observed for **8** after 2 days in D_2O. The phosphinic acid form of 1-OPH(OH)-1,7-$C_2B_{10}H_{11}$ goes under isotopic exchange but the reaction is not as fast as in the case of Na[1-Me-7-OPH(O)-1,7-$C_2B_{10}H_{11}$]. After 48 hours in D_2O, a triplet (1:1:1) at 12.96 ppm with a $^1J(P,D)$ of 87

Hz was observed. ^{1}H NMR spectrum provided information on the deuterated conversion that was 90%.

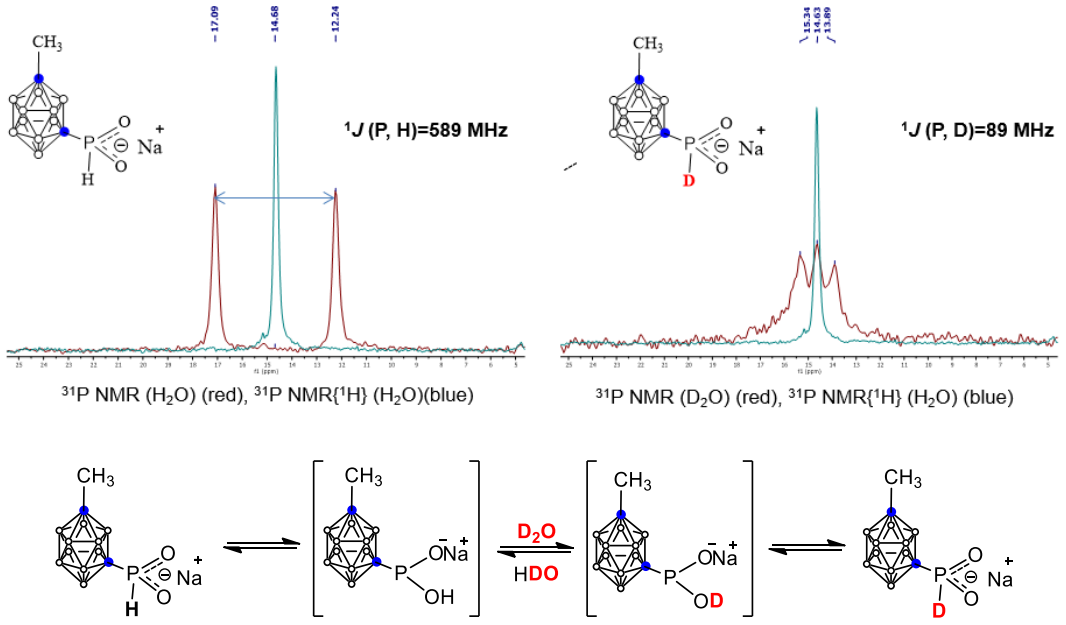

Figure 2.18 P-H/P-D exchange in D_2O observed by ^{31}P and ^{31}P{^{1}H} NMR spectra for Na[1-Me-7-OPH(O)-1,7-*closo*-$C_2B_{10}H_{10}$], **23**.

2.4 P-H bond reactivity: reaction with acetone. Pudovik reaction

Phosphinic acids add to aldehydes or ketones when the reactants are heated together for prolonged period of time, forming α-hydroxyalkylphosphinic acids (Scheme 2.5).[42] For instance, the phosphinic acid $(C_6H_5)_2P(O)H$ in solution with acetone produces the adduct $(C_6H_5)_2P(O)C(OH)Me_2$, which is however not retained in the solid state on evaporation of the reaction mixture to dryness giving the starting compound $(C_6H_5)_2P(O)H$.[43] On the other hand, the same phosphinic acid $(C_6H_5)_2P(O)H$ adds irreversibly at ambient temperature to the double bond of benzaldehyde[43].

Replacement of hydrogen, bonded to phosphorus, we also observed for *meta*-carboranylphospinic acid, **20**, forming α-hydroxyalkylphosphinic acid **26**. Thus, care must be taken to prevent reaction with aldehydes or ketones. On the

other hand, α-hydroxyalkylphosphinic acids together with α-hydroxyalkylphosphonic acids are compounds with wide ranging biological activities. The addition of compounds containing a P-H bond to aldehydes or ketones, the Pudovik reaction, is the most versatile pathway to these compounds[44].

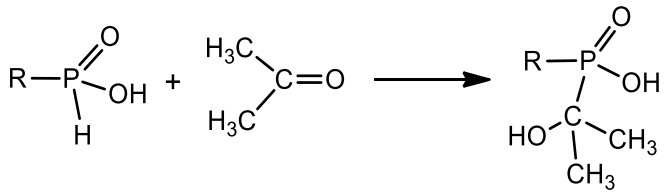

Scheme 2.5 Reaction between phosphinic acid and acetone.

We observed that stirring **20** with acetone during 10 days leads to the full transformation of *meta*-carboranylphosphinic acid into compound **26**. Figure 2.19 shows the ^{31}P NMR spectrum evolution of **20** in acetone with time. Compound **26** was fully characterized by NMR and IR spectroscopy and elemental analysis.

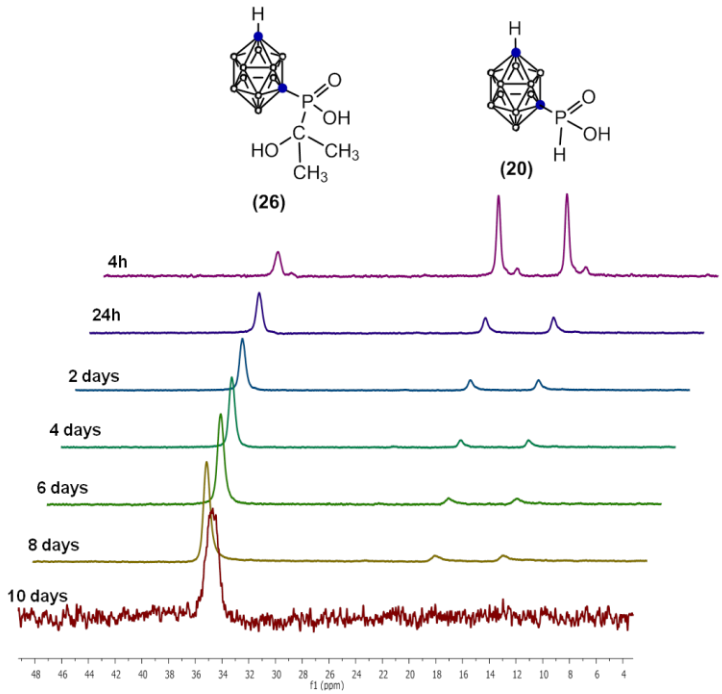

Figure 2.19 ^{31}P NMR spectra (in acetone) showing the reaction progress of **20** with acetone

For the reaction of **20** with acetone the following mechanism pathway via phosphonous tautomer of **20** has been proposed (Figure 2.20).

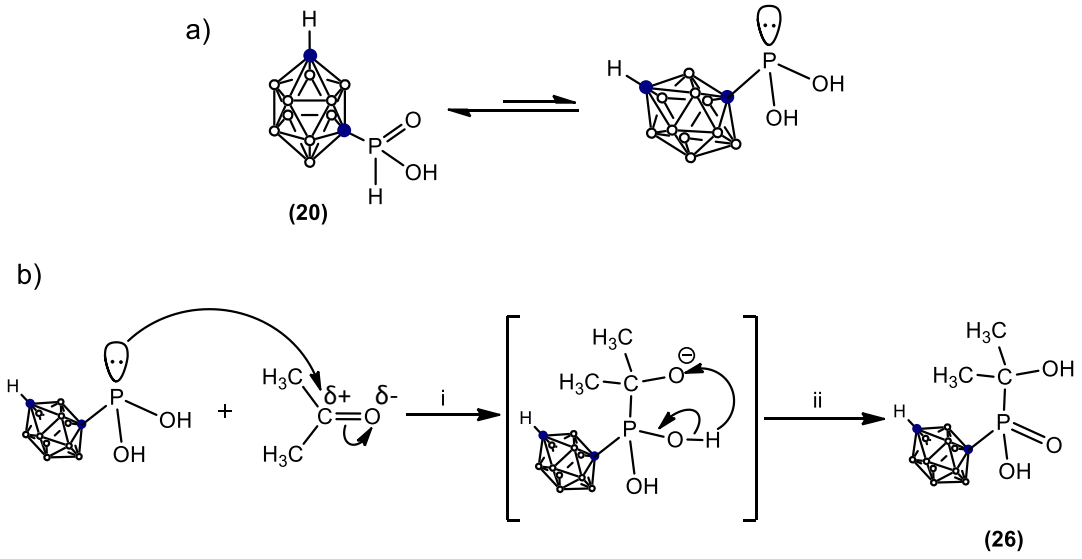

Scheme 2.20 Tautomeric equilibrium between phosphinic and phosphonous acid isomers of **20** (a), proposed pathway of the reaction of **20** with acetone (b).

The infrared spectrum of the compound **26** showed the absence of P-H absorption around 2419 cm^{-1} (Figure 2.21). In the same time new absorptions in the range of 2879-2997 cm^{-1} appeared that supports the presence of CH_3 groups that come from acetone precursor. Characteristic broad O-H stretching vibrations appear at 3100-3500 cm^{-1}.

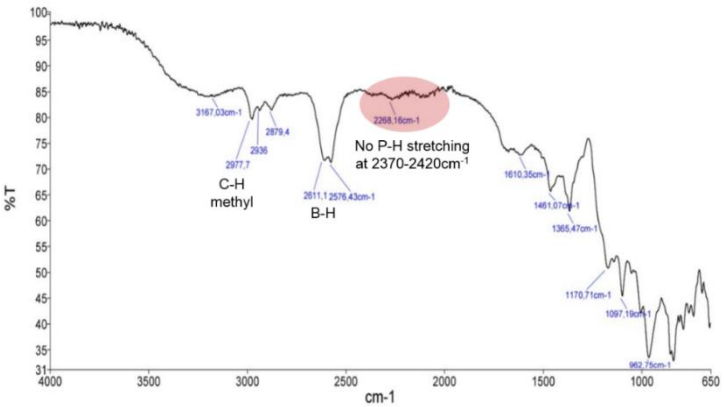

Figure 2.21 FTIR spectrum of compound **26**.

The ^{1}H NMR analysis revealed four resonances at 3.71 ppm, 2.68 ppm, 1.46 ppm and 1.41 ppm (Figure 2.22). First one at 3.71 pmm corresponds to the acidic H of P-OH, the second at 2.68 ppm to alcoholic H of OH bonded to tertiary carbon atom, and the last two resonances at 1.46 and 1.41 ppm are from CH_3 moieties. Finally elemental analysis revealed that the chemical composition of the reaction product is **26**·1/2H_2O.

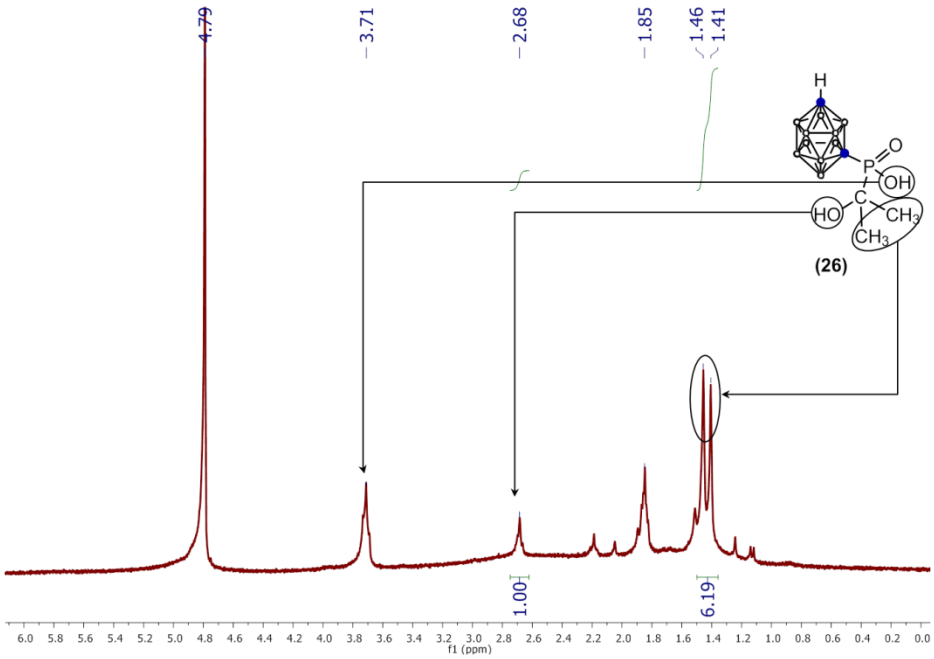

Figure 2.22 ^{1}H NMR spectrum in D_2O of compound **26**

2.5 Acidity of *ortho- and meta*-carboranylphosphinic acids

Phosphinic acids possess one acidic P-OH group (Figure 2.23); the acidity of organophosphinic acids varies in the range of 1.3-2.5 pK_a. The similar way as carboxylic acids, pK_a values of phosphinic acids depend on backbone molecule and the presence of other functional groups.

Most of the carboxylic acids have pKa value around 4.8, and any substituent on its backbone molecule which tends to stabilize the carboxylate anion by electron withdrawal increases the acidity and lowers the pKa. Surprisingly, it works

differently for carboranylphosphinic acids. We compared acid strengths of different carboranylphosphinic acids and its organic analogue phenylphosphinic acid. To our surprise, *meta*-carborane enhances acidity of corresponding phosphinic acid comparing to *ortho*-carborane and phenyl group. Representative values for dissociation constants, pKa values, in water are presented in Figure 2.24. But the presence of electron donating group such as CH_3 on the second $C_{cluster}$ decreases acidity of the corresponding carboranylphosphinic acid increasing pKa on 0.2.

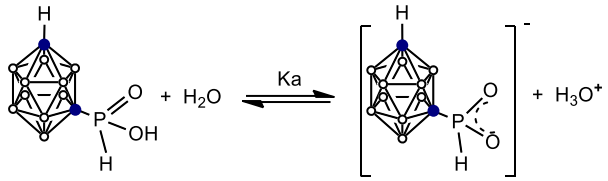

Figure 2.23 *Meta*-carboranylphosphinic acid and the corresponding conjugate base (phosphinate).

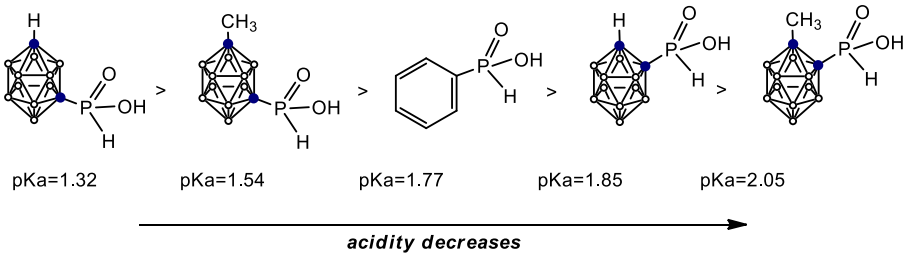

Figure 2.24 pKa values of *ortho*-, *meta*-carboranylphosphinic acids and phenylphosphinic acid.

2.6 Stability under oxidation

The reducing power of phosphinic acids is characteristic of these compounds containing the P-H group. However, *meta*-carboranylphosphinic acids are more stable in front of oxidation then it´s organic analogue phenylphosphinic acid. Thus, kinetics of oxidation of phenylphosphinic acid and *meta*-carboranylphosphinic acid, **20**, by sodium (meta)periodate, $NaIO_4$, in aqueous solution was investigated. Important to note that we studied the oxidation of phenylphosphinic acid and compound **20** with hydrogen peroxide in water, and none of them was oxidized even during 14 days.

Oxidation of phenylphosphinic acid with sodium (meta)periodate, $NaIO_4$, in aqueous medium leads to phenylphosphonic acid. The ^{31}P NMR spectroscopy brought the clear information on the reaction progress (Figure 2.25). The doublet at δ 19.97 ppm that corresponds to P-H coupling in the phenylphosphinic acid molecule starts to decrease after 1h, while a new resonance at δ 14.71 ppm that corresponds to phenylphosphonic acid appears. In 48h there is almost no starting compound left.

The hydrolysis (oxidation) of *meta*-carboranylphosphinic acid, **20**, with sodium (meta)periodate, $NaIO_4$, in water implies two processes: the partial deboronation of the *closo*-cluster (Figure 2.26) and oxidation of the P-H bond (Figure 2.27) possibly with the C_c-P bond splitting.

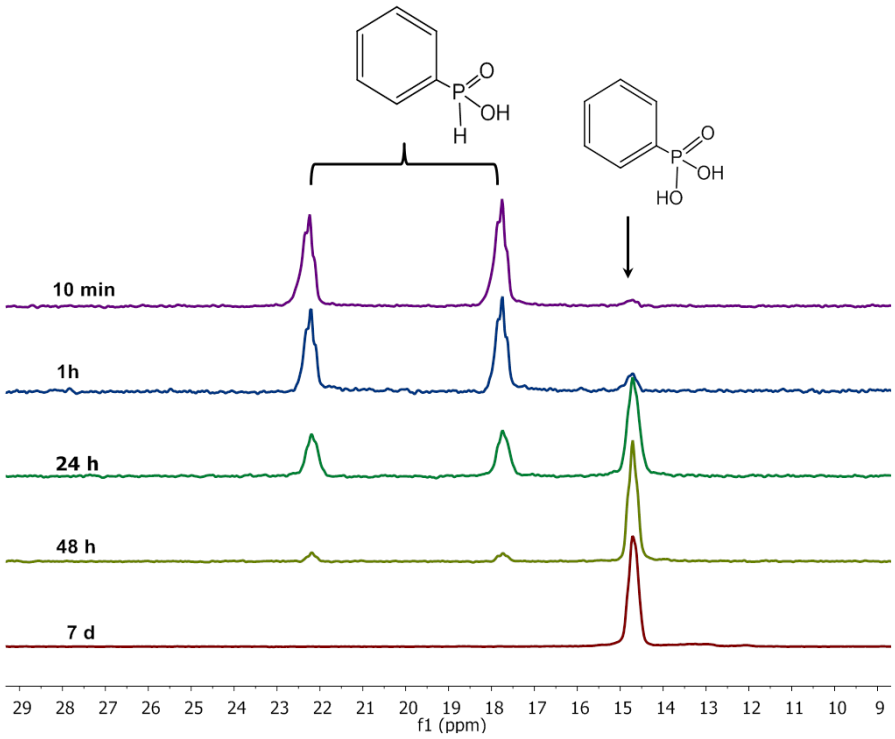

Figure 2.25 Reaction progression measured by ^{31}P NMR spectra for the reaction of phenylphosphinic acid with $NaIO_4$ in H_2O.

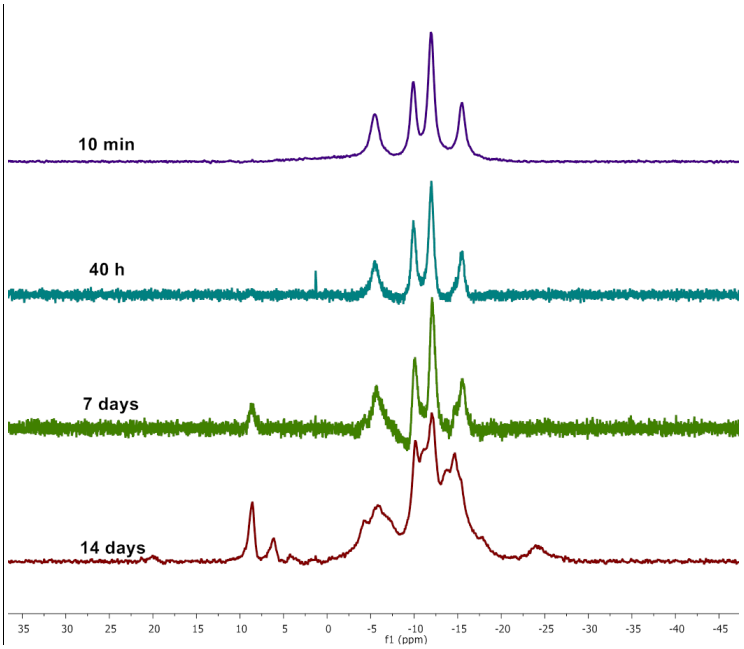

Figure 2.26 Reaction progression measured by $^{11}B\{^{1}H\}$ NMR spectra for the reaction of **20** with $NaIO_4$ in H_2O.

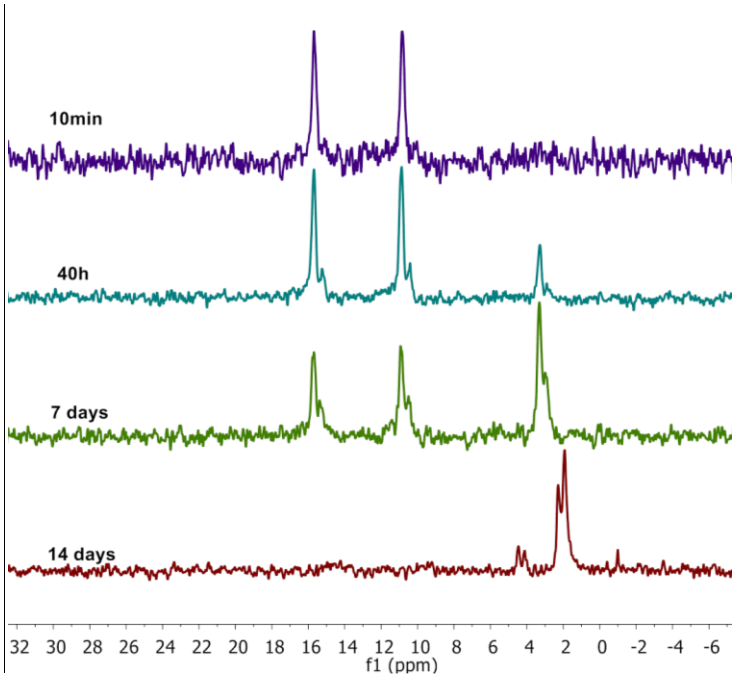

Figure 2.27 Reaction progression measured by ^{31}P NMR spectra for the reaction of **20** with $NaIO_4$ in H_2O.

(1) Paavola, S. Thesis (http://ethesis.helsinki.fi/julkaisut/mat/kemia/vk/paavola/).

(2) Mar Abar. Thesis (https://www.educacion.es/teseo/mostrarRef.do?ref=150021).

(3) Núñez, R. Thesis (https://www.educacion.es/teseo/mostrarRef.do?ref=167364).

(4) Rajae Benakki. Thesis (https://www.educacion.es/teseo/mostrarRef.do?ref=201486).

(5) Anna Laromaine. Thesis (https://www.educacion.es/teseo/mostrarRef.do?ref=381420).

(6) Adrian Radu Popescu. Thesis (http://www.tdx.cat/handle/10803/117472).

(7) Teixidor, F.; Flores, M. A.; Viñas, C.; Kivekäs, R.; Sillanpää, R. *Angew. Chemie Int. Ed. English* **1996**, *35* (19), 2251–2253.

(8) Teixidor, F.; Flores, M. A.; Viñas, C.; Kivekäas, R.; Sillanpää, R. *Angew. Chemie* **1996**, *108* (19), 2388–2391.

(9) Teixidor, F.; Flores, M. A.; Viñas, C.; Raikko Kivekäs; Sillanpää, R. **1998**.

(10) C.Viñas; Núñez, R.; Teixidor, F.; R. Kivekäs; Sillanpää, R. **1998**.

(11) Viñas, C.; Flores, M. A.; Núñez, R.; Teixidor, F.; Raikko Kivekäs; Sillanpää, R. **1998**.

(12) Viñas, C.; Nuñez, R.; Teixidor, F.; Raikko Kivekäs; Sillanpää, R. **1996**.

(13) Teixidor, F.; Flores, M. A.; Vinas, C.; Sillanpää, R.; Kivekäs, R. *J. Am. Chem. Soc.* **2000**, *122* (9), 1963–1973.

(14) Demonceau, A.; Simal, F.; Noels, A. F.; Viñas, C.; Nuñez, R.; Teixidor, F. *Tetrahedron Lett.* **1997**, *38* (23), 4079–4082.

(15) Demonceau, A.; Simal, F.; Noels A. F. *Tetrahedron Lett.* **1997**, *38* (45), 7879–7882.

(16) Delfosse, S.; Richel, A.; Simal, F.; Demonceau, A.; Noels, A. F.; Tutusaus, O.; Núñez, R.; Viñas, C.; Teixidor, F. In *Advances in Controlled/Living Radical Polymerization*; 2003; pp 116–129.

(17) Tutusaus, O.; Delfosse, S.; Simal, F.; Demonceau, A.; Noels, A. F.; Núñez, R.; Viñas, C.; Teixidor, F. In *Inorganic Chemistry Communications*; 2002; Vol. 5, pp 941–945.

(18) Tutusaus, O.; Delfosse, S.; Demonceau, A.; Noels, A. F.; Núñez, R.; Viñas, C.; Teixidor, F. *Olefin cyclopropanation catalysed by half-sandwich ruthenium complexes*; 2002; Vol. 43.

(19) Tutusaus, O.; Viñas, C.; Núñez, R.; Teixidor, F.; Demonceau, A.; Delfosse, S.; Noels,

A. F.; Ignasi Mata; Molins. *J. Am. Chem. Soc* **2003**, *125* (39), 11830–11831.

(20) Tutusaus, O.; Delfosse, S.; Demonceau, A.; Noels, A. F.; Viñas, C.; Teixidor, F. *Kharasch addition catalysed by half-sandwich ruthenium complexes. Enhanced activity of ruthenacarboranes*; 2003; Vol. 44.

(21) L.I. Zakharkin, A.V. Kazantsev, M. N. Z. *Izv. Akad. Nauk SSSR, Ser. Khim.* **1969**, *9*, 2056–2057.

(22) A.V. Kazantsev, M.N. Zhubekova, L. I. Z. *Zh. Obs. Khim.* **1971**, *42*, 1570–1571.

(23) Popescu, A.-R.; Musteti, A. D.; Ferrer-Ugalde, A.; Viñas, C.; Núñez, R.; Teixidor, F. *Chem. - A Eur. J.* **2012**, *18* (11), 3174–3184.

(24) Hill, W. E.; Silva-Trivino, L. M. *Inorg. Chem.* **1978**, *17* (9), 2495–2498.

(25) Alexander, R. P.; Schroeder, H. *Inorg. Chem.* **1966**, *5* (3), 493–495.

(26) Stadlbauer, S.; LÃ¶nnecke, P.; Welzel, P.; Hey-Hawkins, E. *European J. Org. Chem.* **2009**, *2009* (36), 6301–6310.

(27) Popescu, A.-R.; Laromaine, A.; Teixidor, F.; Sillanpää, R.; Kivekäs, R.; Llambias, J. I.; Viñas, C. *Chem. - A Eur. J.* **2011**, *17* (16), 4429–4443.

(28) Daasch, L.; Smith, D. *Anal. Chem.* **1951**, *23* (6), 853–868.

(29) Kong, K.; Kendall, C.; Stone, N.; Notingher, I. *Adv. Drug Deliv. Rev.* **2015**, *89*, 121–134.

(30) Núñez, R.; Viñas, C.; Teixidor, F.; Sillanpää, R.; Kivekäs, R. *J. Organomet. Chem.* **1999**, *592* (1), 22–28.

(31) Kivekäs, R.; Sillanpää, R.; Teixidor, F.; Viñas, C.; Nunez, R.; IUCr. *Acta Crystallogr. Sect. C Cryst. Struct. Commun.* **1994**, *50* (12), 2027–2030.

(32) Kivekäs, R.; Teixidor, F.; Viñas, C.; Nuñez, R.; IUCr. *Acta Crystallogr. Sect. C Cryst. Struct. Commun.* **1995**, *51* (9), 1868–1870.

(33) Kreienbrink, A.; Lönnecke, P.; Findeisen, M.; Hey-Hawkins, E. *Chem. Commun.* **2012**, *48* (75), 9385.

(34) Balema, V. P.; Pink, M.; Sieler, J.; Hey-Hawkins, E.; Hennig, L. *Polyhedron* **1998**, *17* (11), 2087–2093.

(35) Charmant, J. P. H.; Haddow, M. F.; Mistry, R.; Norman, N. C.; Orpen, A. G.; Pringle, P. G.; Welch, A. J.; Macgregor, S. A.; Ormsby, D. L.; Rosair, G. M.; Schmidt, F.; Wilson, N. M.; Welch, A. J. *Dalt. Trans.* **2008**, *127* (11), 1409.

(36) Teixidor, F.; Núñez, R.; Viñas, C.; Sillanpää, R.; Kivekäs, R. *Inorganic* **2001**, *40* (11), 2587–2594.

(37) Lyssenko, K. A.; Grintselev-Knyazev, G. V.; Antipin, M. Y. *Mendeleev Commun.* **2002**, *12* (4), 128–130.

(38) Reuben, J.; Samuel, D.; Silver, B. L. *J. Am. Chem. Soc.* **1963**, *85* (20), 3093–3096.

(39) Martin, R. B. *J. Am. Chem. Soc.* **1959**, *81* (7), 1574–1576.

(40) Griffiths, J. E.; Burg, A. B. *J. Am. Chem. Soc.* **1960**, *82* (6), 1507–1508.

(41) Dobbie, R. C.; Straughan, B. P. *Spectrochim. Acta Part A Mol. Spectrosc.* **1971**, *27* (2), 255–260.

(42) Orthaber, A.; Albering, J. H.; Belaj, F.; Pietschnig, R. *J. Fluor. Chem.* **2010**, *131* (10), 1025–1031.

(43) Hoge, B.; Neufeind, S.; Hettel, S.; Wiebe, W.; Thösen, C. *J. Organomet. Chem.* **2005**, *690* (10), 2382–2387.

(44) Cai, J.; Zhou, Z.; Zhao, G.; Tang, C. *Heteroat. Chem.* **2003**, *14* (4), 312–315.

3. *Closo*- carboranylphosphonic acids

In organic chemistry with phosphinic acids in hand, ready access to the corresponding phosphonic acids is assured, since many oxidizing agents can accomplish this conversion in excellent yield. However, there are ways to bypass the phosphinic acid intermediate in phosphonic acid synthesis. Thus, the phosphonous dichlorides can be oxidized directly to give the phosphonic dichlorides (phosphonyl dichlorides) that can be hydrolyzed easily to the phosphonic acids. Another common procedure is addition of halogen, usually chlorine, to phosphonous dichlorides to form the corresponding tetrachloride species. These compounds are rapidly hydrolyzed with complete loss of halogen forming phosphonic acids. This process is generally restricted to the synthesis of arylphosphonic acids (Scheme 3.1).

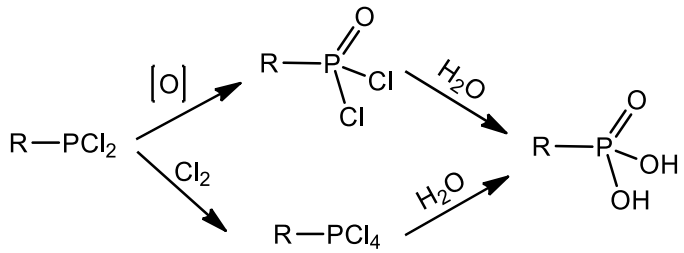

Scheme 3.1 General synthetic pathway to obtain organic phosphonic acids.

In this chapter we attempted to synthesize and characterize carboranylphosphonic acids using the approaches described above. In these studies clear differences between *ortho*- and *meta*-isomers of carborane have been noted.

3.1 Synthetic pathway of the *ortho*- and *meta*-carboranylphosphonic acids

The first attempt in this PhD thesis to produce *closo*-carboranylphosphonic acid, R-P(O)$(OH)_2$, was done starting from the reaction between lithiated 1-Me-1,2-*closo*-$C_2B_{10}H_{10}$ and $POCl_3$. It was known that even a big excess of $POCl_3$ leads to the product of substitution of two chlorine atoms in $POCl_3$ producing dicarboranylchlorophosphonate, (1-R-1,2-*closo*-$C_2B_{10}H_{10})_2$POCl (R=Me, Ph).[1] Our

attempts to reproduce the reaction unexpectedly gave the product of reduction of phosphorus, (1-Me-1,2-*closo*-$C_2B_{10}H_{10})_2PCl$. The X-ray structure confirmed that the phosphorus atom was in P(III) oxidation state (Scheme 3.1 and Figure 3.1).

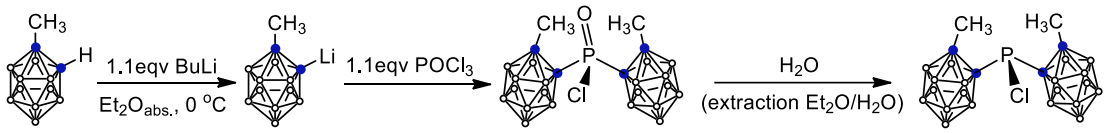

Scheme 3.1 Deprotonation of 1-Me-1,2-*closo*-$C_2B_{10}H_{10}$ followed by reaction with $POCl_3$.

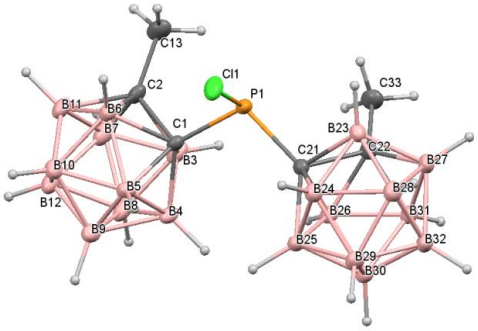

Figure 3.1 Molecular structure of (1-Me-1,2-*closo*-$C_2B_{10}H_{10})_2PCl$

Generally, the corresponding reduction of phosphoryl chlorides to halophosphines is not common. Only one case was found in the literature where cyclic phosphinic chloride was reduced with trichlorosilane to a phosphinous chloride.[2] $^{31}P\{^1H\}$ NMR revealed that the reduction of P(V) to P(III) occurred after the contact with H_2O during the extraction with the mixture H_2O/Et_2O, where water played the role of reducing agent producing H_2O_2 (Scheme 3.2).

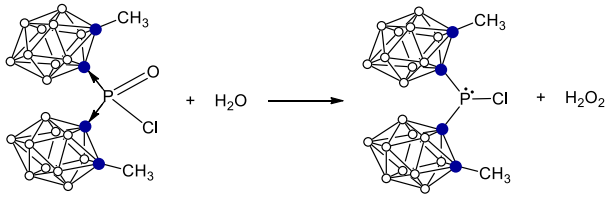

δ (^{31}P) = 24.22 ppm δ (^{31}P) = 99.99 ppm

Scheme 3.2 Reduction of (1-Me-1,2-*closo*-$C_2B_{10}H_{10}$)$_2$POCl to (1-Me-1,2-*closo*-$C_2B_{10}H_{10}$)$_2$PCl and corresponding ^{31}P NMR chemical shifts.

Other attempt to produce *closo*-carboranylphosphonic acids, was done by the oxidation of corresponding *closo*-carboranylphosphinic acids by hydrogen peroxide, H_2O_2, using it as an oxidizing agent. It turned that when forcing the reaction conditions leading to *ortho*-carboranylphosphonic acid, by oxidation of the sodium salt of the *ortho*-carboranylphosphinic acid, **22**, with H_2O_2, only 1-Me-1,2-*closo*-$C_2B_{10}H_{11}$ was recovered due to the cleavage of the C_c-P bond as it happened in the deboronation process of *ortho*-carboranylphoshines with alkoxide.[3]

With *meta*-carboranylphosphinic acids hydrogen peroxide did not produce any reaction. Using sodium (meta)periodate, $NaIO_4$, as an oxidizing agent, instead of the oxidation of P-H bond to P-OH it started to deboronate the cluster together with cleavage of C_c-P bond forming phosphorous acid H_3PO_3 as a second product of reaction. Thereby, by these methods mentioned above was impossible to obtain carboranylphosphonic acids.

Although carboranylphosphonic acids were reported years ago, neither their characterization nor reproducible procedures of their synthesis are available.[4,5] The synthetic pathway used by authors is shown in Scheme 3.1 on the example of 1-Me-1,2-*closo*-$C_2B_{10}H_{11}$. As a consequence, in this PhD thesis an attempt to reproduce the reported synthesis with slight modifications was done. With the goal to produce *ortho*-carboranylphosphonic acid, 1-Me-2-OP(OH)$_2$-1,2-*closo*-$C_2B_{10}H_{10}$, a stream of Cl_2 was passed through a benzene solution of 1-Me-2-PCl$_2$-1,2-*closo*-$C_2B_{10}H_{10}$, **11**, during 15 minutes. It was expected to get 1-Me-2-PCl$_4$-1,2-*closo*-$C_2B_{10}H_{10}$, **27**, that generates 1-Me-2-OPCl$_2$-1,2-*closo*-$C_2B_{10}H_{10}$, **30**, by hydrolysis, and from which the target compound 1-Me-2-OP(OH)$_2$-1,2-*closo*-$C_2B_{10}H_{10}$ would be obtained (Scheme 3.3). A white solid (in 76% yield) was isolated that produced good crystals from aqueous water solution. Unexpectedly, X-ray diffraction studies showed that the solid corresponds to [H_3O][1-Me-2-OPCl(O)-1,2-*closo*-$C_2B_{10}H_{10}$]·H_2O, **34**. Figure 3.2 displays its molecular structure. The P–C_c distance, 1.828(2) Å, is the same compared with **19** while, C_c–C_c bond length 1.672(2) Å is a little longer. The crystal packing is driven by hydrogen bonding interactions between

water molecules and chlorophosphonic groups building a 2D sheet structure. Hydronium molecules reinforced the above referred structure by additional hydrogen bonds.

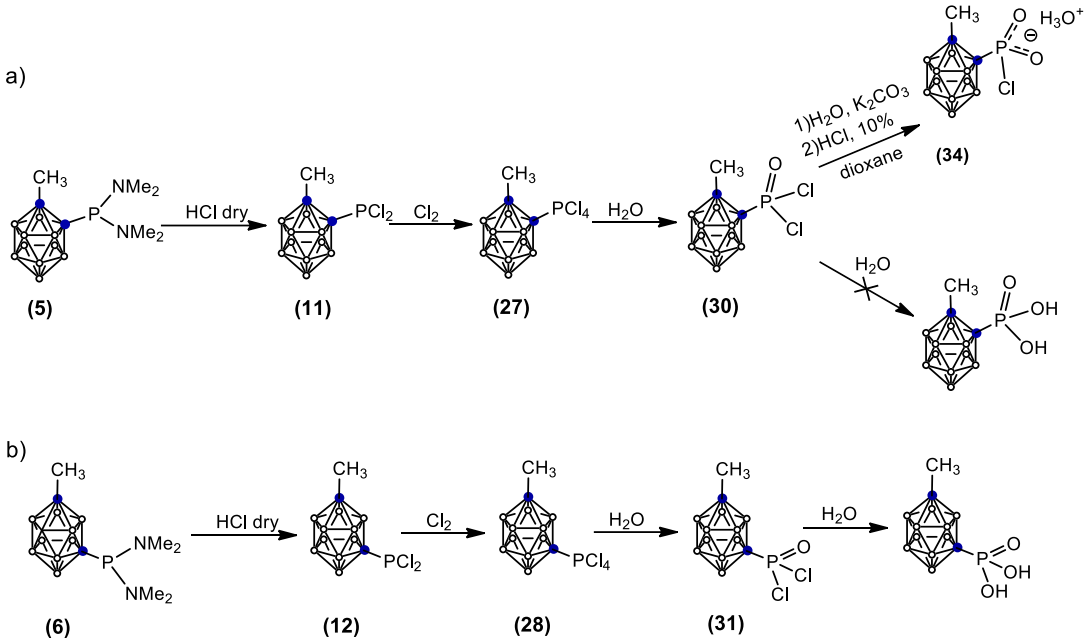

Scheme 3.3 Synthesis of *closo*-carboranylphosphonic acid derivatives ((a) *ortho*- and (b) *meta*-).

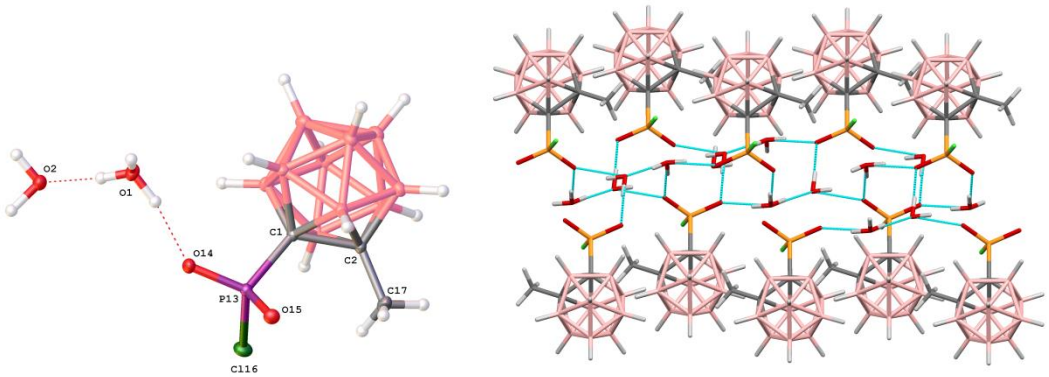

Figure 3.2 Molecular structure and crystal packing of $[H_3O][1\text{-Me-2-OPCl(O)-1,2-}C_2B_{10}H_{10}]$, **34**.

Table 3.1 Selected bond lenghts (Å) and bond angles (º) for compound **34**.

Bond lengths		Bond angles	
Cl16-P13	2.0167(7)	O15-P13-Cl16	106.64(6)
P13-O15	1.4927(13)	O15-P13-C1	109.51(8)
P13-O14	1.4897(14)	O14-P13-Cl16	107.55(6)
P13-C1	1.8380(18)	O14-P13-O15	117.80(8)
		O14-P13-C1	108.21(8)
		C1-P13-Cl16	106.57(6)

Other attempt to hydrolyze **30** to phosphonic acid was done in water/dioxane solution. In this conditions already after 24 hours the 1-CH_3-2-$POCl_2$-1,2-*closo*-$C_2B_{10}H_{10}$, **30**, suffers the full cluster decomposition to $B(OH)_3$. Figure 3.3 displays the differences in the ^{11}B NMR during the degradation of the cluster.

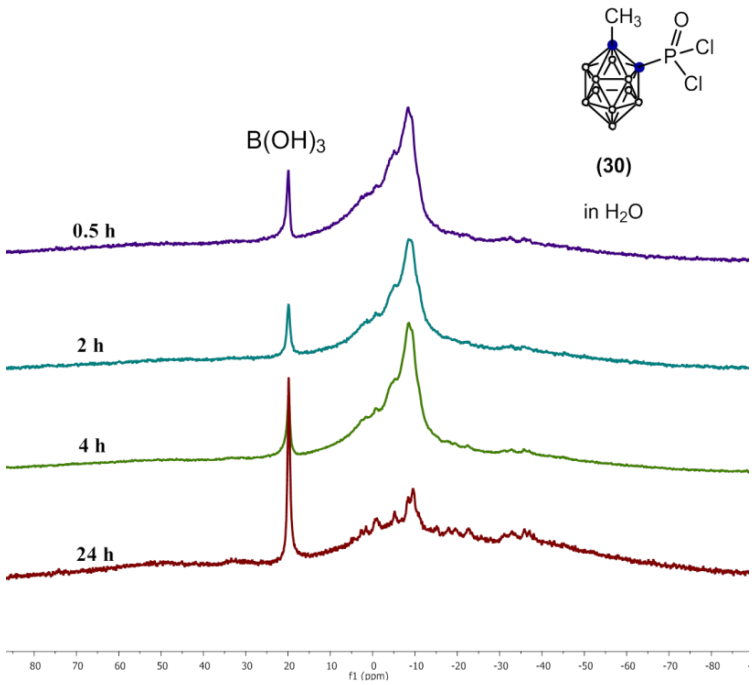

Figure 3.3 $^{11}B\{^1H\}$ NMR spectra of **30** in H_2O showing the full decomposition of the *ortho*-cluster to $B(OH)_3$.

In the case of *meta*-carborane the attempt to produce *meta*-carboranylphosphonic acid 1-Me-7-OP(OH)$_2$-1,7-*closo*-$C_2B_{10}H_{10}$ resulted in a like manner. However, *meta*-carboranyl cage demonstrated a higher stability during hydrolysis because almost no boric acid was produced. The synthesis pathway was the same as it was done previously with 1-Me-2-OP(OH)$_2$-1,2-*closo*-$C_2B_{10}H_{10}$, a stream of Cl_2 was passed through a benzene solution of 1-Me-7-PCl$_2$-1,7-*closo*-$C_2B_{10}H_{10}$, **12**, during 15 minutes. It was expected to get 1-Me-7-PCl$_4$-1,7-*closo*-$C_2B_{10}H_{10}$, **28**, that generates 1-Me-7-OPCl$_2$-1,7-*closo*-$C_2B_{10}H_{10}$, **31**, by hydrolysis. Compound **31** was fully characterized by multinuclear NMR analysis, ^{1}H, ^{1}H{^{11}B}, ^{11}B, ^{11}B{^{1}H}, ^{13}C{^{1}H}, ^{31}P, infrared spectroscopy, elemental analysis. The hydrolysis of **31** was studied in two different conditions: in aqueous media and in dioxane/water mixture in the presence of Na_2CO_3 (basic hydrolysis). In both cases was found that the most favourable product of hydrolysis of **31** was 1-Me-7-OPCl(OH)-1,7-*closo*-$C_2B_{10}H_{10}$, **35**.

The progress of the reaction of hydrolysis of **31** in aqueous solution has been studied as a function of time to determine intermediates and final product. In this sense, the progress of the reaction was monitored by ^{31}P-NMR and ^{11}B{^{1}H}-NMR spectroscopies (Figures 3.4 and 3.5). This study provides useful information about the stepwise character of hydrolysis of **31** in water. The resonance at δ 24.61 ppm in the ^{31}P-NMR spectrum that corresponds to non-altered 1-Me-7-OPCl$_2$-1,7-*closo*-$C_2B_{10}H_{10}$, **31**, decreases with time while a new peak at δ 13.69 ppm from 1-Me-7-OPCl(OH)-1,7-*closo*-$C_2B_{10}H_{10}$, **35**, increases. In 5 days there is almost no starting compound left while only the peak at δ 13.69 ppm is observed and a new small peak from 1-Me-7-OP(OH)$_2$-1,7-*closo*-$C_2B_{10}H_{10}$ at δ 3.52 ppm started to appear. Then, the resonance at 13.69 ppm also decreases with time and the latter one at δ 3.52 ppm grows. After 32 days the ratio between resonances δ 13.69 ppm and 3.52 ppm was about 1:1. The ^{11}B{^{1}H}-NMR spectra (Figure 3.5) also shows changes with the time but was not so informative as the ^{31}P-NMR. To be noted here, that during hydrolysis almost no boric acid formation was observed.

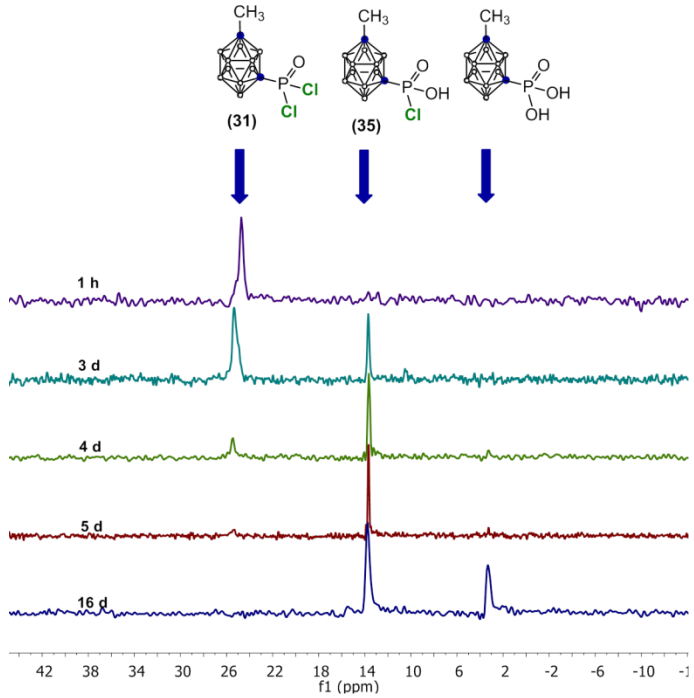

Figure 3.4 ^{31}P NMR spectra of **31** in H_2O

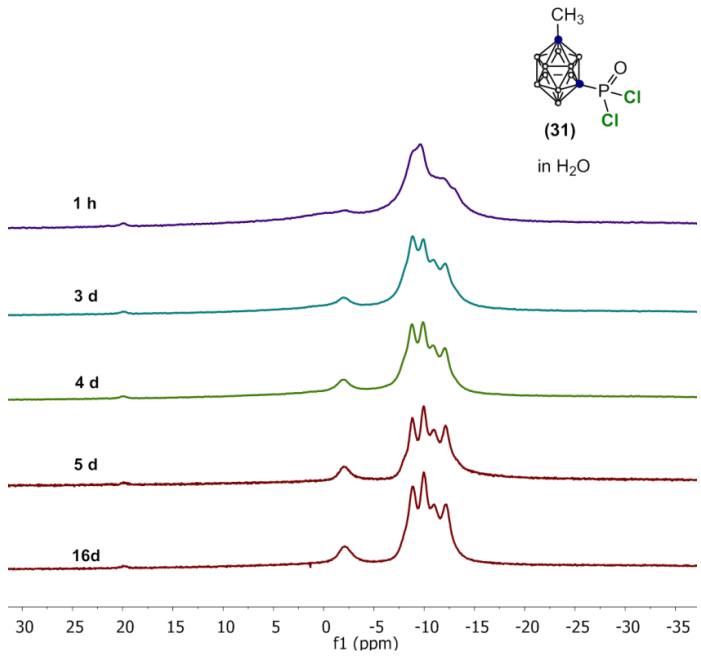

Figure 3.5 $^{11}B\{^1H\}$ NMR spectra of **31** in H_2O

The basic hydrolysis of **31** in dioxane/water solution in the presence of Na_2CO_3 also resulted in 1-Me-7-OPCl(OH)-1,7-$C_2B_{10}H_{10}$, **35,** according to ^{31}P-NMR that gave only the resonance at δ 13.69 ppm.

Laying emphasis here that in the organic chemistry the arylphosphonic dichlorides (phosphonyl dichlorides) can be hydrolyzed easily to the phosphonic acids with the substitution of both chlorine atoms in the same time, while in carborane chemistry *ortho*-carboranylphosphonic acids are not stable or in the case of *meta*-carborane the substitution of the second chlorine atom by OH group in carboranylphosphonyl dichlorides is much more complicated. Thus, the hydrolysis of carboranylphosphonyl dichlorides in the case of *meta*-carborane practically stops after substitution of the first chlorine atom (Scheme 3.6). It can be explained by the enhanced electron-withdrawing properties via bonding at the carboranyl carbon atoms compared to phenyl group, which makes the phosphorus atom pull electron density stronger toward itself. As a result chlorine atoms are less labile.

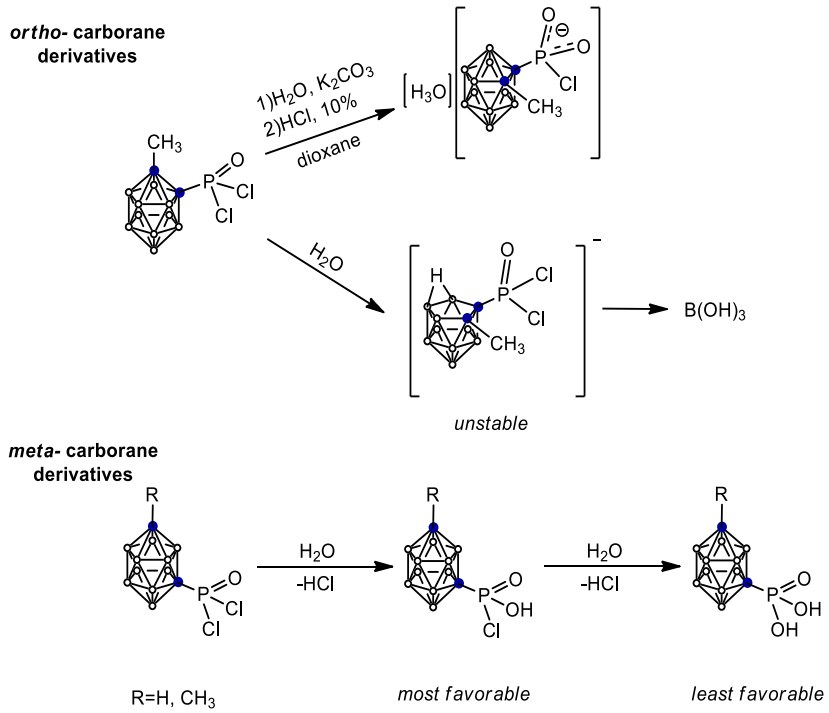

Scheme 3.6 Hydrolysis of carboranylphosphonic dichlorides (*ortho*- and *meta*-).

(1) L.I. Zakharkin, M.N. Zhubekova, A. V. K. *Zh. Obs. Khim.* **1971**, *41*, 588–592.

(2) Quin, L. D.; Szewczyk, J. *Phosphorus Sulfur Relat. Elem.* **1984**, *21* (2), 161–170.

(3) Teixidor, F.; Viñas, C.; Mar Abad, M.; Nuñez, R.; Kivekäs, R.; Sillanpää, R. *J. Organomet. Chem.* **1995**, *503* (2), 193–203.

(4) L.I. Zakharkin, A.V. Kazantsev, M. N. Z. *Izv. Akad. Nauk SSSR, Ser. Khim.* **1969**, *9*, 2056–2057.

(5) A.V. Kazantsev, M.N. Zhubekova, L. I. Z. *Zh. Obs. Khim.* **1971**, *42*, 1570–1571.

5. *Meta*-carboranylphosphinate Magnetic Nanoparticles

In this chapter, magnetic nanoparticles (MNPs) coated with *meta*-carboranylphosphinate, [1-OPH(O)-1,7-*closo*-$C_2B_{10}H_{11}$] [**1**], have been prepared (**1**-MNPs) by classic co-preciitation synthesis and have been characterized by different techniques (transmission electron microscopy images, electron diffraction, X-ray powder diffraction, infrared spectroscopy, energy dispersive X-ray analysis, high resolution X-ray photoelectron spectroscopy, magnetometry measurements) that have provided information on structural and physicochemical distinctive properties of these **1**-MNPs. The stability of prepared MNPs was studied before and after sterilization under autoclave conditions (steam heated under pressure at 121 ºC during 1 h).

To illustrate their potential biomedical applications, the cellular uptake of these **1**-MNPs from culture media was studied by a human cell line of capillary-derived human brain endothelial cells (hCMEC/D3). Additionally, to explore its potential ability to penetrate into malignant tumors as drug carriers or in Neutron Capture Therapy for treating cancer locally, we will show that these **1**-MNPs are taken up from culture media by the glioblastoma multiforme cell line A172. Finally, will be demonstrated that the systemic administration of **1**-MNPs in adult mice is well tolerated at mid-term with no major signs of toxicity.

5.1 Preparation and characterization of *meta*-carboranylphosphinate MNPs

The preparation of magnetite nanoparticles coated with *meta*-carboranylphosphinate (**1**-MNPs) was performed in two steps as follows: i) the preparation of the core of MNPs was carried out under inert (nitrogen) atmosphere using the aqueous co-precipitation method. This method, which is the concomitant precipitation from ferrous and ferric iron in alkaline aqueous solution, is the most widely applied synthesis route for the MNPs formation (Figure 5.1a). $FeCl_2$ and $FeCl_3 \cdot 6H_2O$ in a 1:2 ratio were dissolved in deionized and degassed water at room temperature. After stirring for 20 minutes $[NH_4]OH$ aqueous solution (30 wt.%) was added at once to the above mixture under vigorous stirring. Immediately a black

suspension was formed, which suggested the formation of magnetic nanoparticles. The reaction mixture was then stirred vigor-ously for 2 h. The precipitate was isolated from the aqueous solution by magnetic decantation, and washed with distilled water three times. ii) The second step was the fictionalization of the MNPs with the *meta*-carboranylphosphinate (Figure 5.1b). A saturated solution of 1-OPH(OH)-1,7-closo-$C_2B_{10}H_{11}$, H[**1**], in H_2O was added. Next, the mixture was sonicated for 2 h. The **1**-MNPs were separated from the aqueous solution by magnetic decantation, washed with distilled water three times and dried at 50 ^oC for 2 h in vacuum.

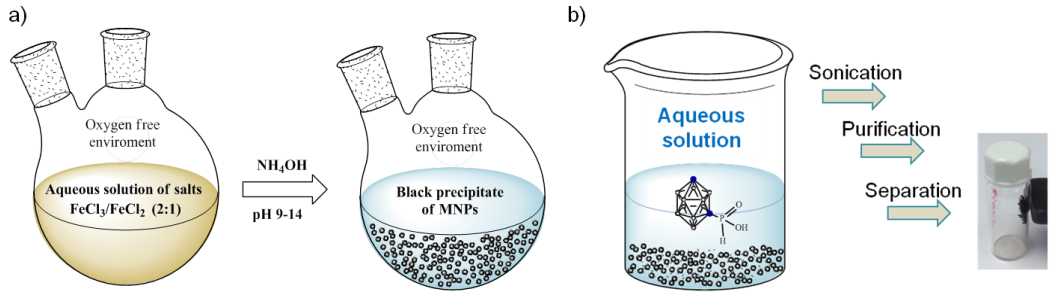

Figure 5.1 a) Synthesis of MNPs by co-precipitation method. b) funtionalization of the MNPs with the *meta*-carboranylphosphinate

5.1.1 Chemical characterization of *meta*-carboranylphosphinate MNPs.

The prepared solid **1**-MNPs were subjected to a number of analytical techniques such as FTIR Spectroscopy, EDX analysis, high resolution XPS, and $Fe^{2+/3+}$ chemical titration. Figure 5.2 shows the FTIR spectra of H[**1**] (green), its sodium salt Na[**1**] (red), **1**-MNPs (black) and non functionalized MNPs (blue). Strong absorptions at 2594 cm^{-1} in all three the pure *m*-carboranylphosphinate ligand [**1**], Na[**1**] and **1**-MNPs, due to B–H stretches, dominate the IR spectra and support the presence of a *closo*-carboranyl cluster structure onto the surface of **1**-MNPs.[1]

It is worth noting that the P=O stretching band of the phosphinate group, which was present at 1210 cm^{-1} in the spectrum of H[**1**], is absent in the spectrum of **1**-MNPs, but two new bands at 1189 and 1068 cm-1 appeared, which were

ascribed to asymmetric $\nu_{as(POO^-)}$ and symmetric $\nu_{s(POO^-)}$ stretch of coordinated phosphinate group.[2,3]

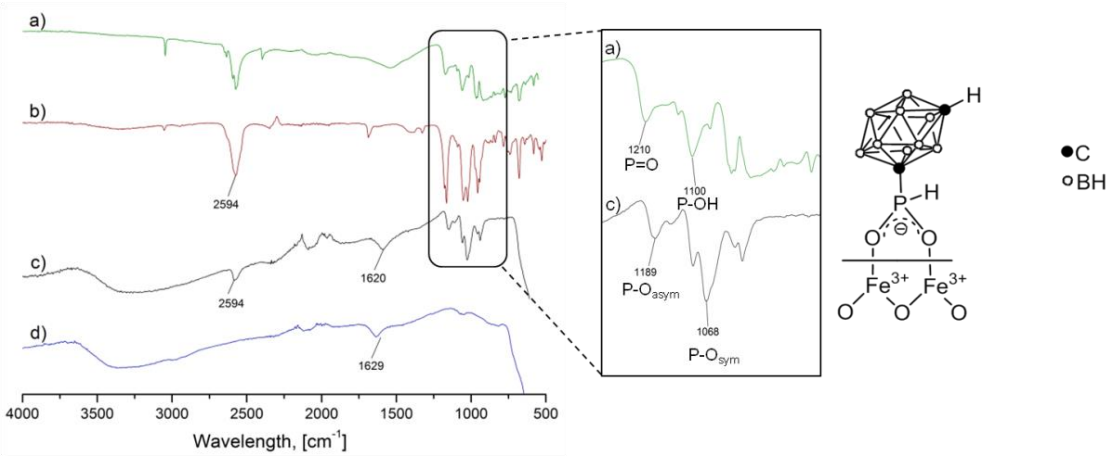

Figure 5.2 Comparison between the IR spectra of the *m*-carboranylphosphinic acid (H[**1**] in green), its sodium salt (Na[**1**] in red), **1**-MNPs (in black) and none functionalized MNPs (in blue)

This result revealed that [**1**] was chemisorbed onto the surface of magnetite nanoparticles as a phosphinate bidentated bridging ligand coordinated to the iron atoms of the iron oxide super paramagnetic nanoparticles (Figure 5.2). In addition, the IR spectrum of pristine MNPs shows a peak at 1629 cm^{-1} that remains in the **1**-MNPs spectrum and is associated to coordinated water to the Fe center of the core.

To further verify that **1** is attached onto the surface of **1**-MNPs, Energy Dispersive X-ray (EDX) analysis of **1**-MNPs was performed. Phosphorus was detected by EDX analysis (Figure 5.3)

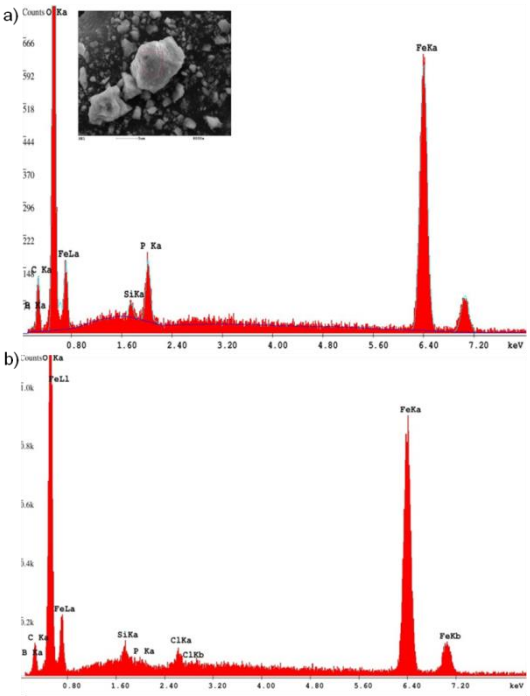

Figure 5.3 EDX analysis of **1**-MNPs (up) and non functionalized MNPs (down)

proving that *meta*-carboranylphosphinate was coating MNPs surface with an atomic composition for **1**-MNPs of 92.89 and 7.13 % for Fe and P, respectively. This corresponds to a ratio 13:1 (Fe:P), indicating that the composition of the **1**-MNPs can be referred to as (1-OPH(O)-1,7-*closo*-$C_2B_{10}H_{11})_8(2Fe_3O_4{\cdot}Fe_2O_3)_{13}$.

The high resolution X-ray photoelectron spectroscopy (XPS) analysis performed on **1**-MNPs (Figure 5.4) displays peaks at 189 and 133 eV, which are characteristic of a B-B[4] and P-O bonds (Figure 5.4b, 5.4c), confirming the presence of *meta*-carboranylphosphinate as well as the peaks at 711.2 and 724.9 eV indicating Fe in the Fe_3O_4 phase at the MNP core (Figure 5.4d).[5]

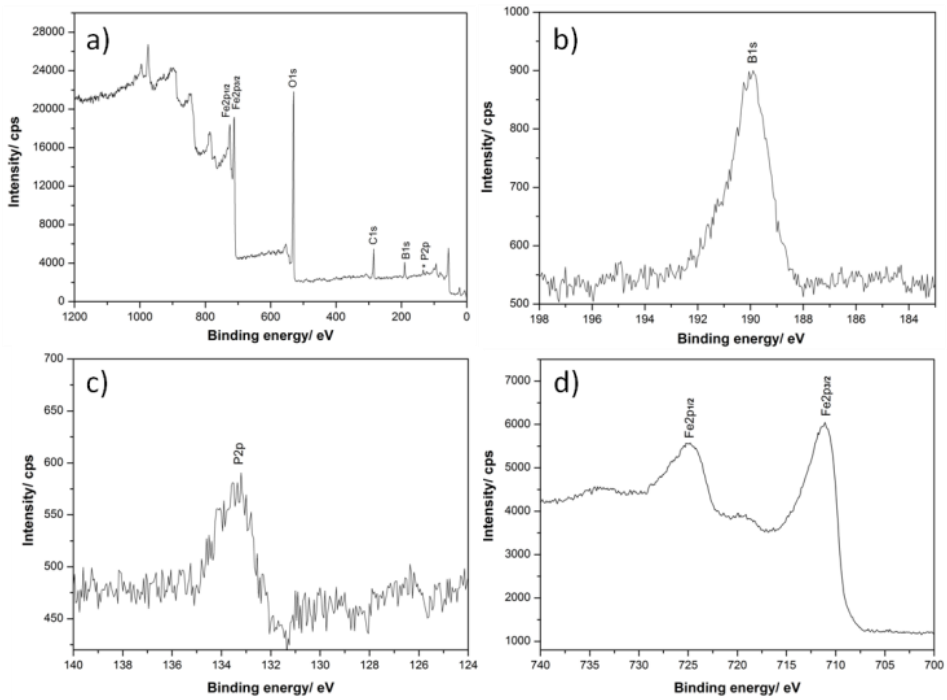

Figure 5.4 XPS of **1**-MNPs, (a). High resolution spectra XPS of **1**-MNPs in the B 1s, P 2p and Fe 2p regions, (b), (c) and (d) respectively

Chemical titration. The iron oxide nanoparticles, the most explored magnetic nanoparticles up to date, are composed of Fe^{2+} and Fe^{3+} oxides. In order to evaluate the amount of Fe^{2+} and Fe^{3+} ions forming the core of the **1**-MNPs nanoparticles, redox titrations were performed. The chemical titration indicated an amount of 25.08 % of Fe^{2+} to the total amount of $Fe^{2+/3+}$; while for pure magnetite

(Fe_3O_4 = $FeO{\cdot}Fe_2O_3$) it is expected a 33% (Table 5.1). This result revealed that the iron oxide core of the synthesized **1**-MNPs consists of a mixture of both magnetite and maghemite phases, with a composition $2Fe_3O_4{\cdot}Fe_2O_3$.

Table 5.1. Redox titration analysis results of **1**-MNPs before autoclave sterilization.

n	$W_{1\text{-MNPs}}$, µg	Fe^{2+} content, wt.%$_{Fe2+/totFe}$	Fe^{3+} content, wt.%$_{Fe3+/totFe}$
1	540	23.57	76.43
2	528	26.67	73.33
3	546	25.00	75.00
MEAN	538	25.08	74.92

5.1.2 Morphological, structural and physicochemical characterization of the **1**-MNPs

The magnetic properties of nanoparticles depend upon their physical structure: the size and the shape of the particles, their microstructure, and the chemical phases in which they are present. Moreover, the biological behaviour of magnetic nanoparticles also strongly depends upon their size and shape as well as their polydispersity, charge, and nature of the coating. Several physicochemical techniques are used to determine these parameters.

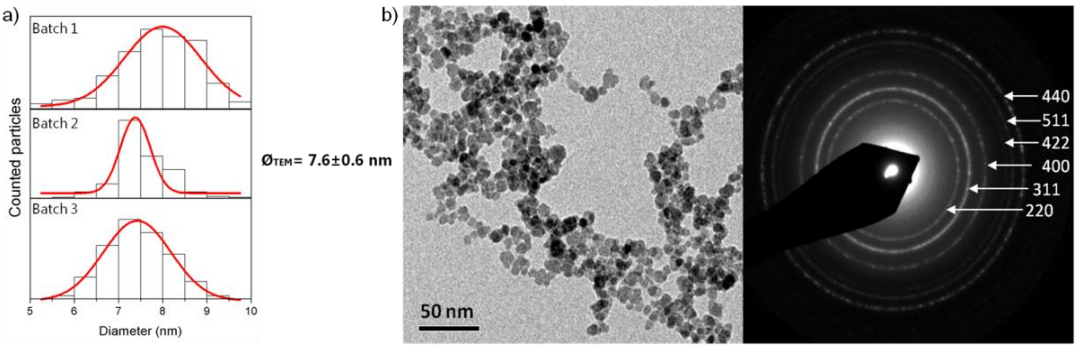

Figure 5.5 a) Particle size distribution histograms from three batches of freshly prepared **1**-MNPs, prepared following the same synthesis, and mean particle size diameter. b) TEM micrograph with particle size distribution histogram and electron diffraction pattern of synthesized **1**-MNPs.

The morphological and structural characterization of **1**-MNPs was performed using transmission electron microscopy (TEM) and powder X-ray diffraction (XRD). Particle imaging and sizing of synthesized **1**-MNPs was investigated by TEM analysis. **1**-MNPs nanoparticles are observed to have spherical shape (Figure

5.5b). Mean particle diameters ($Ø_{TEM}$) were statistically calculated for each sample by counting 200 particles and fitting the particle size histogram from three different batches, prepared following by the same way of synthesis, to a Gaussian function, producing a mean particle diameter of 7.6 ± 0.6 nm (Figure 5.5a). The 8 % polydispersity indicates the narrow particle size distribution, although **1**-MNPs were prepared by the aqueous co-precipitation method. The electron diffraction of **1**-MNPs shows well defined diffraction rings confirming that the particle core composition is made of magnetite/maghemite spinel structure. The line profile was fitted for observed six peaks with the following Miller indices: (220), (311), (400), (422), (511), and (440). The XRD pattern of **1**-MNPs revealed the average crystallite size, D, calculated from the peak broadening refinements, and resulted as 9.0 ± 0.6 nm (Figure 5.6). This result is in a good agreement with the mean particle diameter from TEM of 7.6 ± 0.6 nm.

The magnetic property of iron oxide (Fe_3O_4) nanoparticles is affected by the distribution of iron ions in octahedral and tetrahedral sites of spinel structure.[6] The magnetic spins of the ions in the octahedral sites are ferromagnetically coupled to each other and antiferromagnetically coupled with tetrahedral sites. Because the numbers of Fe^{3+} ions in the octahedral sites and the tetrahedral sites are the same, their magnetic spins cancel each other. Consequently, the magnetic spins of only Fe^{2+} ions in the octahedral sites contribute to the net magnetic moment. Ferromagnetic iron, that is 100 % composed by Fe^{2+}, has the highest saturation magnetization (218 emu g^{-1}) because of the absence of cancelled magnetic spins.[7]

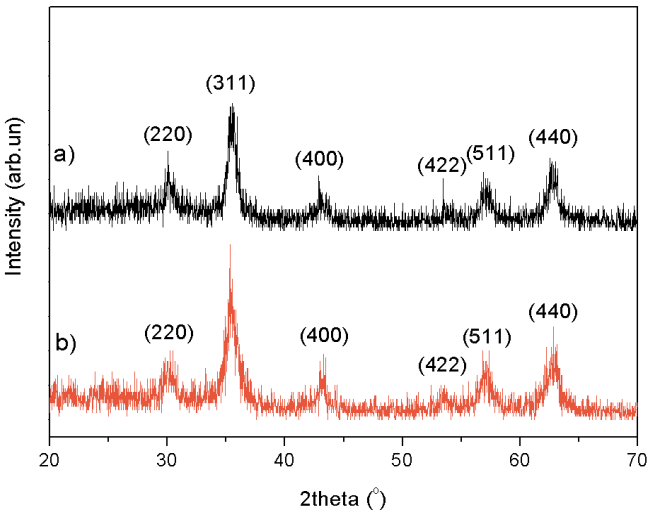

Figure 5.6 X-ray diffraction patterns corresponding to **1**-MNPs (black) and the typical magnetite/maghemite spinel structure (red).

However, Fe^{2+} is oxidized upon harsh conditions of temperature, moisture and oxygen as these that can be found in an autoclave for sterilization. Thus one

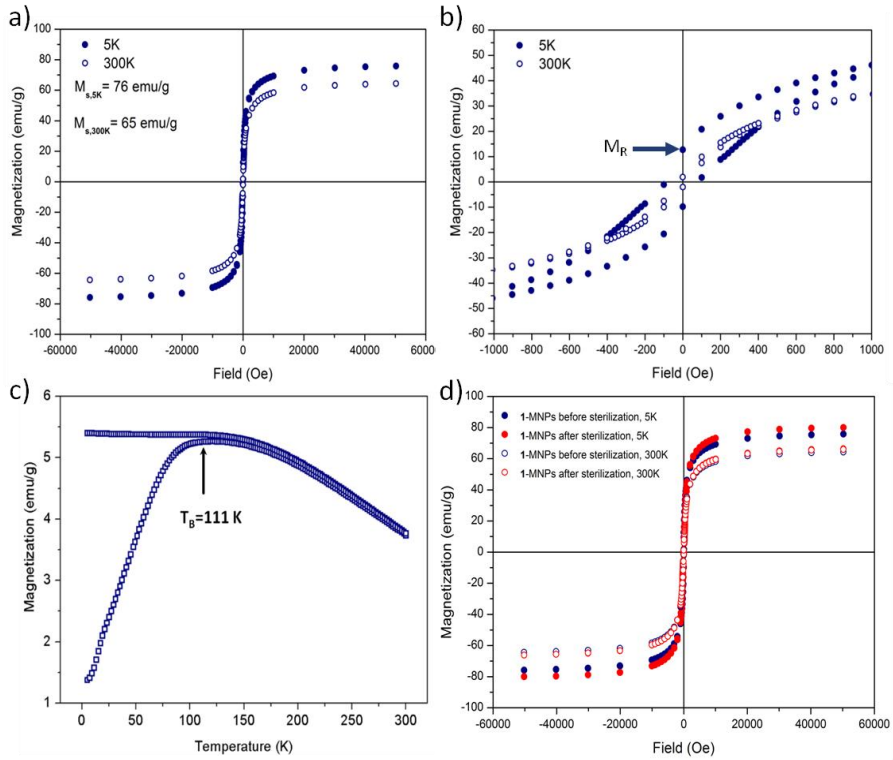

Figure 5.7 a) Hysteresis cycles recorded at low temperature (5 K) and room temperature (300K) for 1-MNPs; b) zoom of the hysteresis cycle at low fields; c) Zero field cooled (ZFC) and field cooled (FC) curves of 1-MNPs at 50 Oe; d) Hysteresis cycles recorded at low temperature (5 K) and room temperature (300K) for 1-MNPs before (blue) and after (red) the autoclave sterilization process

important point to be addressed in the use of MNPs for medical applications and consequently on their sterilization for their application on cultures, is to learn on the fate of the MNPs and their ligands, particularly on what occurs to Fe^{2+} upon the autoclave sterilization process, and to this purpose it is necessary to learn on the fate of functionalized MNPs at room temperature and after the autoclave sterilization process. To this aim, magnetic measurements of **1**-MNPs were done and the results are displayed in Figure 5.7. Figures 5.7a and 5.7b show a typical magnetization curve at 300 K for superparamagnetic nanoparticles in which neither remanent magnetization (magnetization at zero field, M_R) nor coercivity (hysteresis

loop, H_c) were observed. The saturation magnetization value of **1**-MNPs at 300 K was 65 emu/g, that indicates a high degree of crystallinity, as well as 29.8% of Fe^{2+} by comparison with the ferromagnetic iron. This value is comparable to the 25.1% of Fe^{2+} of the total $Fe^{2+/3+}$ that was obtained by chemical titration of freshly prepared **1**-MNPs; this indicates that **1**-MNP is made of a ratio of 2:1 mols of magnetite (Fe_3O_4) per 1 mol of maghemite (Fe_2O_3). Maghemite exhibits ferrimagnetic ordering and as magnetite is also used in biomedicine. As expected, saturation magnetization was higher at 5K (76 emu/g **1**-MNPs) and the **1**-MNPs present M_R ferromagnetic features of 12 emu/g (Figure 5.7b).

Superparamagnetism was also proved by the ZFC-FC magnetization curves (Figure 5.7c). The zero field cooled magnetization (ZFC) increased with temperature until reaching the maximum value corresponding to the blocking temperature (T_B) at 111 K. The field cooled (FC) curve increases as the temperature decreases and never reaches saturation at low temperature, suggesting that interparticles' interactions do not significantly affect the relaxation dynamics. These studies were done with the **1**-MNPs before autoclave sterilization.

On the other hand, little information is available on MNPs after sterilization in autoclave, and definitively is necessary for their medical application. We will take advantage of the chemical nature of the carboranylphosphinic acid, having uncommon atoms B and P, to learn on the evolution of the ligand's shell following autoclave sterilization. Three main targets are thus sought: Is the initial $Fe^{2+/3+}$ pre-sterilization distribution of the MNPs core maintained after sterilization? What happens with the ligand shell? Is the magnetic response comparable to the starting one?. To answer these questions, magnetic properties of **1**-MNPs were measured after the autoclave sterilization process. Magnetization curves of **1**-MNPs before (blue) and after (red) autoclave sterilization process at 5 K and 300 K as function of the applied 6 Tesla magnetic field are displayed in (Figure 5.7d). The graph demonstrates that the sterilization process does not produce significant changes on magnetic properties of **1**-MNPs. The saturation magnetization value of **1**-MNPs at 300 K was 65 emu/g and 66 emu/g before and after sterilization respectively. As expected, saturation magnetization was higher at 5 K (76 emu/g before and 80

emu/g after sterilization). These results would suggest that no changes or just minor modifications in the structure and composition would have occurred upon applying the autoclave sterilization conditions, but we shall see that this is not the case.

A redox titration of an aqueous suspension of **1**-MNPs (following autoclave sterilization) was performed and shows that there was partial oxidation of Fe^{2+} to Fe^{3+}. It was observed that the Fe^{2+} content decreases from 25.1 % to 14.7 % while Fe^{3+} increases from 74.9 % to 85.3 % indicating that autoclave sterilization of **1**-MNPs leads to partial oxidation of the **1**-MNPs core, and increase the amount of maghemite (Tables 5.1 and 5.2). This leads to a chemical composition $Fe_3O_4 \cdot 2Fe_2O_3$.

Table 5.2. Redox titration analysis results of **1**-MNPs after autoclave sterilization

n	Fe^{2+} content, wt.%$_{Fe2+/totFe}$	Fe^{3+} content, wt.%$_{Fe3+/totFe}$
1	14.31	85.69
2	15.94	84.05
3	13.89	86.11
MEAN	14.71	85.28

5.1.3 Determination of the ligand shell morphology of **1**-MNPs using EDX before and after sterilization in autoclave.

Geometry calculations. First was estimated the amount of carborane clusters that may fit one nanoparticle, considering the nanoparticle core and the carborane cluster as ideal spheres, and the square packing of carborane clusters onto the surface of MNP (Figure 5.8).

Dimentions of *meta*-carboranylphosphinate were measured from its crystal structure, and determined as 0.5 nm ($Ø_{carboranylphosphinate}$) in diameter for carborane cluster “sphere” and 0.7 nm (L) in length including the phosphinate group (Figure 5.8). The diameter of the core of **1**-MNPs was found subtracting the two lengths of carboranylphosphinate ligand, 2L, from mean diameter of **1**-MNPs found by TEM, $Ø_{TEM}$ = 7.6 ± 0.6 nm, that resulted as 6.2 ± 0.6 nm ($Ø_1$).

$Ø_1 = Ø_{TEM} - 2L = 6.2 \pm 0.6$ nm, $R_1 = 3.1 \pm 0.3$ nm;

$Ø_2 = Ø_{TEM} - 2(L - \frac{1}{2}Ø_{carboranylphosphinate}) = 7.1 \pm 0.6$ nm, $R_2 = 3.55 \pm 0.3$ nm;

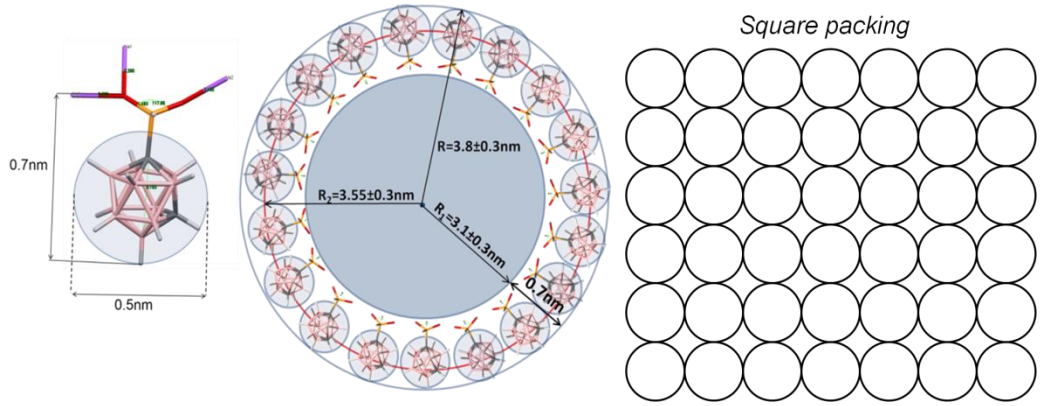

Figure 5.8 Dimentions of the *meta*-carboranylphosphinate and its distribution on the surface of nanoparticles, square packing model.

$A_2 = 4\pi R_2^2 = 132.73 \div 186.27$ nm^2 (159.50 ± 26.77 nm^2);

For squire packing: $A_{carboranylphosphinate} = Ø_{carboranylphosphinate}{}^2 = 0.5 \times 0.5 = 0.25$ nm^2;

$n_{max} = A_2/A_{carboranylphosphinate} = 530.92 \div 745.08$ (638.00 ± 107.08) – maximum number of *meta*-carboranylphosphate ligands that can fit one nanoparticle with core diameter of 6.2 ± 0.6 nm.

Surface coverage values calculations before and after autoclave sterilization.

Energy Dispersive X-ray (EDX) analysis of **1**-MNPs before autoclave sterilization was performed for 3 (n = 3) bathes, prepared following the same synthesis. Average:

Fe 92,89 (At %) – 13 Fe

P 7.11 (At %) – 1 P

Fe:P = 13:1

By chemical titration was found that the core composition of freshly prepared **1**-MNPs is $2Fe_3O_4 \cdot Fe_2O_3$ (Fe_8O_{11}).

Fe_8O_{11} : $C_2B_{10}H_{11}$-P(H)OO^- = 1.625 : 1

(from geometry calculations) d = 6.2 ± 0.6 nm - diameter of the nanoparticle core.

$m_{MNPs} = (1/6)\pi d^3 \rho_{MNPs}$ = (66.4 ± 19)E-20 g (taking the density of magnetite to be $\rho_{Magnetite}$=5.175 g/cm^3 according to https://www.mindat.org/min-2538.html).

$Mole_{MNPs} = m_{MNPs}/M_{2Fe3O4\cdot Fe2O3} = N_{Fe8O11}/N_A$, where M_{Fe8O11} = 622.75 g/mol is molecular weight of magnetite/maghemite couple $2Fe_3O_4.Fe_2O_3$, N_{Fe8O11} – number of Fe_8O_{11} units that contains one nanoparticle core with diameter 6.2 ± 0.6 nm.

$N_{Fe8O11} = m_{MNPs}.N_A/M_{Fe8O11}$ = 642 ± 182 Fe_8O_{11}/NP

Taking into account EDX results before sterilization, Fe_8O_{11} : $C_2B_{10}H_{11}$-P(H)OO^- = 1.625 : 1, each nanoparticle bears $n_{carboranylphosphinate} = N_{Fe8O11}/1.625$ = 395 ± 112 *meta*-carboranylphosphinates. The saturation of surface of the nanoparticles core (%) $s_{carboranylphosphinate} = n_{carboranylphosphinate}/n_{max}\cdot 100$ % = 61.29 ± 7.43 %.

Energy Dispersive X-ray (EDX) analysis of **1**-MNPs after sterilization was performed for 3 (n = 3) bathes, prepared following the same synthesis. Average:

Fe 55,34 (At %) – 70 Fe

P 0.79 (At %) – 1 P

Fe:P = 70:1

By chemical titration was found that the core composition of **1**-MNPs after sterilization is $Fe_3O_4.2Fe_2O_3$ (Fe_7O_{10}).

Fe_7O_{10} : $C_2B_{10}H_{11}$-P(H)OO^- = 10 : 1. $Mole_{MNPs} = m_{MNPs}/M_{Fe7O10} = N_{Fe7O10}/N_A$, where M Fe_7O_{10} = 550.91 g/mol is molecular weight of magnetite/maghemite couple Fe_7O_{10}, N_{Fe7O10} – number of Fe_7O_{10} units that contains one nanoparticle core with diameter 6.2 ± 0.6 nm.

$N_{Fe7O10} = m_{MNPs}.N_A/M_{Fe7O10}$ = 726 ± 205 Fe_7O_{10}/NP

Taking into account EDX results after sterilization, Fe_7O_{10} : $C_2B_{10}H_{11}$-P(H)OO^- = 10 : 1, each nanoparticle bears $n_{carboranylphosphinate}$ = 73 ± 21 *meta*-carboranylphosphinates. The saturation of surface of the nanoparticles core (%) $s_{carboranylphosphinate} = n_{carboranylphosphinate}/n_{max}\cdot 100\%$ = 11.21 ± 1.41 %.

To conclude, the composition of **1**-MNPs before and after auticlave sterilization was analyzed by means of Energy Dispersive X-ray spectroscopy (EDX) and redox titration. The EDX ratio before autoclave sterilization was 1P:13Fe, and after autoclave sterilization was 1P:70Fe indicating that practically 80% of the ligand shell had been removed from the surface. Using a spherical geometrical model and considering the major circle area of the carborane, the first ratio corresponds to a surface coverage of 61.3 ± 7.4% whereas after autoclave

sterilization the surface coverage by the carboranyl ligands has been reduced to 11.2 ± 1.4% (Table 5.3).

Table 5.3. Surface coverage values before and after autoclave sterilization.

	Before sterilization	After sterilization
Core composition	$2Fe_3O_4.Fe_2O_3$	$Fe_3O_4.2Fe_2O_3$
Number of *meta*-carboranylphosphinate ligands per NP	395 ± 112	73 ± 21
Surface coverage, %	61.3 ± 7.4	11.21 ± 1.41

To know what had happened with the liberated ligand the mother liquor was analyzed by means of ^{11}B and ^{31}P-NMR spectroscopy. ^{11}B-NMR indicated that the *meta*-carboranyl cluster of the released ligand remained intact after sterilization. $^{1}H\{^{11}B\}$-NMR and ^{31}P-NMR indicated that the *meta*-carboranylphosphinate had been deprotonated and formed a salt, $[NMe_4][1\text{-}OPH(O)\text{-}1,7\text{-}closo\text{-}C_2B_{10}H_{11}]$ (Figure 5.9).

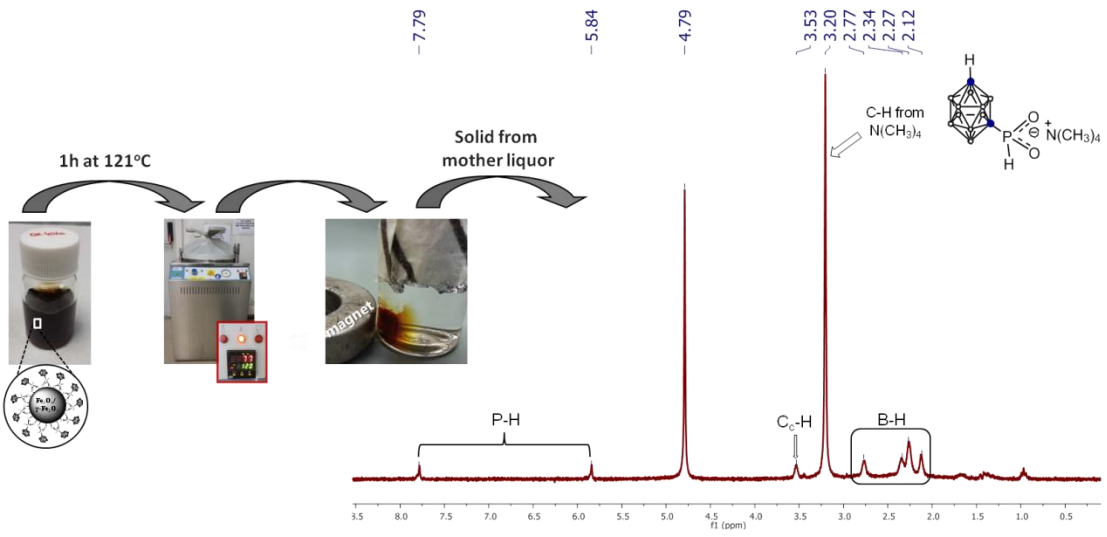

Figure 5.9 $^{1}H\{^{11}B\}$-NMR spectrum in D_2O of the solid from mother liquor after sterilization of **1**-MNPs

5.1.4 Studies of colloidal stability of the **1**-MNPs suspension in aqueous medium at different pH and during the autoclave sterilization process.

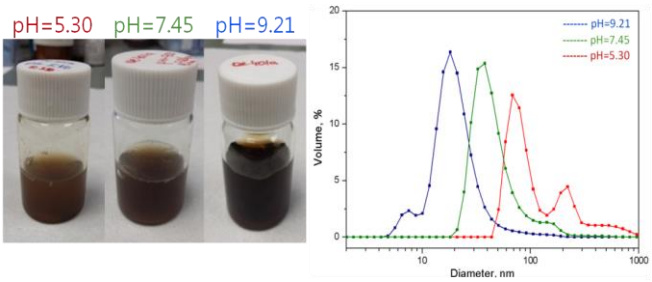

Figure 5.10 DLS graphs of the **1-**MNPs in aqueous medium at different pH

The control of the monodisperse size of magnetic nanoparticles is very important because their biological properties strongly depend on their polydispersity, charge, and nature of the coating in addition to their size and shape. The surface charge of the nanoparticles was determined by measuring their ζ-potential values at different pH, by means of Dynamic light scattering (DLS). The pH of the solution was adjusted using aqueous $[NMe_4]OH$ solution (25 wt.%). DLS technique also provides information on the hydrodynamic diameter and, thus, on the colloidal behaviour of the 1-MNPs in a different environment. As the mean effective diameter of the particles depends on the size of the core, the size of the shell, particle concentration as well as the type of ions in the medium, the influence of pH on the stability of colloidal aqueous dispersion of **1**-MNPs was studied and their results collected in Table 5.4. DLS analysis reveals that the hydrodynamic diameter radius of the particle increases when decreasing the pH, which indicates the particles aggregate when pH decreases. On the other hand, when pH is basic, the electrostatic repulsion force seems to be higher (ζ= -44 ± 5 mV), therefore the

Table 5.4. Hydrodynamic diameter, Zeta potential and Diffusion coefficient values of **1**-MNPs colloidal aqueous dispersion at different pH measured by DLS.

pH	$Ø_{HYD}$, (nm)	PdI	Zeta potential, ζ (mV)	Diffusion Coefficient, ($\mu m^2/s$)
5.30	> 60	0.446	+17	1.77
7.45	45 ± 20	0.454	-30 ± 4	3.77
9.21	23 ± 11	0.482	-44 ± 5	7.49

dimensions of the aggregates ($Ø_{HYD}$ = 23 ± 11 nm) are closer to the size of particles determined by TEM ($Ø_{TEM}$) that is 7.6 ± 0.6 nm. At physiological pH, the size of aggregates are $Ø_{HYD}$= 45 ± 20 nm and Zeta potential value, ζ= -30 ± 4 mV, that was enough to avoid the aggregation with further precipitation of colloid. This fact can be attributed to the negatively charged surface of the core of magnetic nanoparticles and by the hydrophobicity due to the carboranyl spheres coordinated to the surface $Fe^{2+/3+}$ ions through the phosphinate binding sites.

The colloidal behaviour of an aqueous solution at the pH range 7.4-7.6 of the **1**-MNPs (0.5 mg/mL) that had been under autoclave sterilization process conditions (steam heated to 121 °C under pressure during 1 hour) were studied by DLS measurements. Figure 5.11 shows that the dimensions of the aggregates are the same before and after the autoclave sterilization and, as said earlier, the magnetic properties of **1**-MNPs remain unaltered after the autoclave sterilization process. What has changed is the composition of the MNPs from $2Fe_3O_4{\cdot}Fe_2O_3$ before autoclave sterilization to $Fe_3O_4{\cdot}2Fe_2O_3$ following autoclave sterilization. It has also changed the degree of ligands' MNPs coverage that has been reduced nearly a 80%.

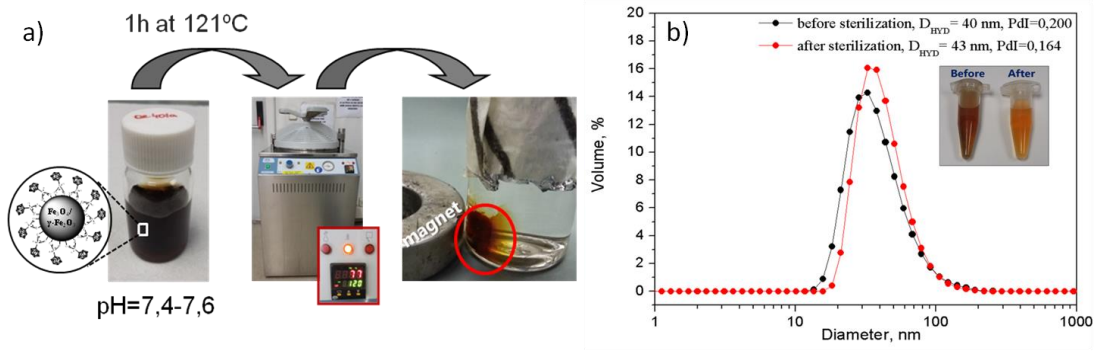

Figure 5.11 a) **1**-MNPs display magnetic properties after the autoclave sterilization process. b) DLS of **1**-MNPs before and after the autoclave sterilization process

5.1.5 Studies of colloidal stability of the **1**-MNPs suspension at culture media.

It has been proven above that pH produces an effect on hydrodynamic diameter radius of the aqueous **1**-MNPs suspensions. There are many studies

revealing that MNPs behave differently in biological media than in water at physiological pH (7.45)[8] because of the presence of inorganic salts, proteins, amino acids or polysaccharides in biological media.[9]

Prior to testing the *in vitro* toxicity of **1**-MNPs, it was important to perform colloidal stability assays of **1**-MNPs in commonly used biological media for cell culturing (DMEM-F12-1% FBS, DMEM-1% FBS, EGM2-2%FBS and RPMI) as well as with the well known phosphate buffered saline (PBS) solution that contains inorganic salts (NaCl, Na_2HPO_4, KH_2PO_4, KCl). So, the stability of colloidal dispersions of **1**-MNPs (50 μg **1**-MNPs/mL) in PBS and culture media was studied at different times (10 min. and 24 h.) and temperatures (room temperature (r.t.) and 37 ºC) by means of Dynamic light scattering (DLS). The results are on display in Figure 5.12 and Table 5.5.

Figure 5.12 DLS studies of the **1-**MNPs in different biological media and PBS solution

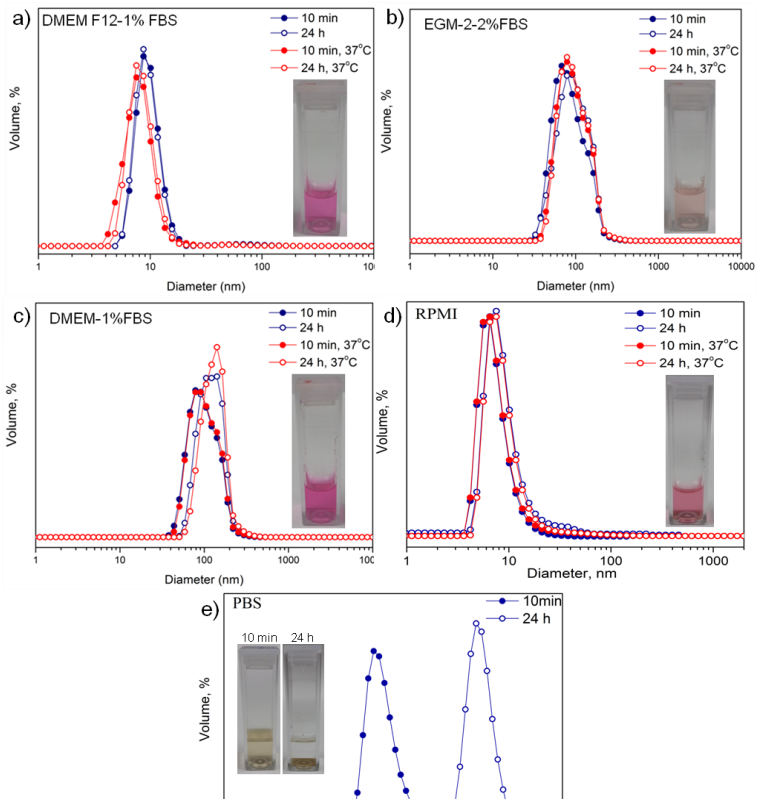

In all culture media no precipitation was observed neither after 10 min nor after incubating 24 h at r.t. or at 37 ºC while in PBS **1**-MNPs sedimented within 24 h. In the case of DMEM F12–1% FBS, 1% non-essential amino acids and 1% antibiotics, and in RPMI the size of detected particles was close to the mean particle diameters determined by TEM, $Ø_{TEM}$ = 7.6 ± 0.6 nm. In EGM-2 medium with 2%FBS and in DMEM-1%FBS **1**-MNPs rapidly formed aggregates with hydrodynamic diameters in the range of 50-140 nm and 60-170 nm respectively, maintaining the invariable size was for 24 h. Comparing results at r.t. and 37 ºC, a slight increase in hydrodynamic diameters was observed in all culture media.

Table 5.5. Hydrodynamic diameter and Diffusion coefficient values of **1**-MNPs suspensions at different culture media and temperatures (r.t. and 37 ºC) measured by DLS.

Media	T, ºC	$Ø_{HYD}$, (nm)	Diffusion Coefficient, (μ^2/s)
10 min			
DMEM F12–1% FBS	r.t	9.8 ± 2.5	3.40
	37	8.2 ± 2.6	3.63
EGM-2 medium with 2%FBS;	r.t	90.3 ± 40.7	4.43
	37	98.7 ± 41.6	5.69
DMEM-1% FBS	r.t	103.4 ± 40.7	4.14
	37	106.6 ± 42.9	5.13
RPMI	r.t	9.0 ± 2.3	4.16
	37	8.4 ± 2.0	4.19
PBS	r.t	76.1 ± 31.1	4.90
24 hours			
DMEM F12–1% FBS	r.t	9.5 ± 2.2	3.50
	37	8.5 ± 2.3	4.03
EGM-2 medium with 2%FBS;	r.t	99.5 ± 41.9	4.31
	37	101.0 ± 42.6	5.54
DMEM-1% FBS	r.t	123.6 ± 40.8	3.42
	37	133.3 ± 43.4	4.24
RPMI	r.t	10.8 ± 4.4	3.92
	37	11.0 ± 12.9	4.09
PBS	1276 ± 435 (precipitated)		

5.2 Application of *meta*-carboranylphosphinate MNPs and biological systems

5.2.1 Cell cultures

To illustrate the potential biomedical application of *meta*-carboranylphosphinate MNPs, we aimed to study the cellular uptake of these **1**-MNPs from culture media by a human cell line related to the nervous system, capillary-derived human brain endothelial cells (hCMEC/D3). To explore its potential ability to penetrate into malignant tumours as drug carriers or in Neutron Capture Therapy for treating cancer locally, glioblastoma multiforme cell line A172 was used as a model of tumor cells.

5.2.2 Cytotoxicity: MTT assays

The hybrid nature of the MNPs is conceptually divided into the inorganic core, the engineered surface coating comprising the ligand shell and the corona of adsorbed biological molecules. Empirical evidence shows that all these three components may degrade individually *in vivo* and can drastically modify the life cycle and biodistribution of the whole heterostructure. Thus, the MNPs may be decomposed into different parts, whose biodistribution and fate would need to be analyzed individually.

The first step of the biological studies was to confirm the uptake of as sterilized **1**-MNPs by the cultured cells (hCMEC/D3 and A172). As shown in the right panels of Figure 5.13, the Prussian blue stain enables us to identify the presence of intracellular iron after 24 h treatment with **1**-MNPs. These experiments suggest that there has been cytoplasmatic endocitosis of the iron core of the **1**-MNPs.[10–12]

To determine the highest non toxic dose of **1**-MNPs for two studied cell lines: hCMEC/D3 and A172, we tested different **1**-MNPs concentrations (10, 25, 50 and 100 μg $Fe^{2+/3+}$/mL) and times (6 h and 24 h of incubation with cells). Cell viability assay shows that brain endothelial (hCMEC/D3) cells were more sensitive to **1**-MNPs toxicity than glioblastoma A172 cells (Figure 5.13A and 5.13B) since doses of 25 μg $Fe^{2+/3+}$/mL significantly reduced endothelial cell viability. The reduction in

hCMEC/D3 viability could be only partially explained by the vehicle solution, but certainly the **1**-MNPs nanohybrid induced cell toxicity starting at 25 μg/mL. At the same administration doses of **1**-MNPs, glioblatoma A172 cells presented full viability as observed in Figure 5.13B. However higher doses already induced cell toxicity to this cancer cells, maybe due to the acidity of *m*-carboranylphosphinic acid present in the vehicle solution.

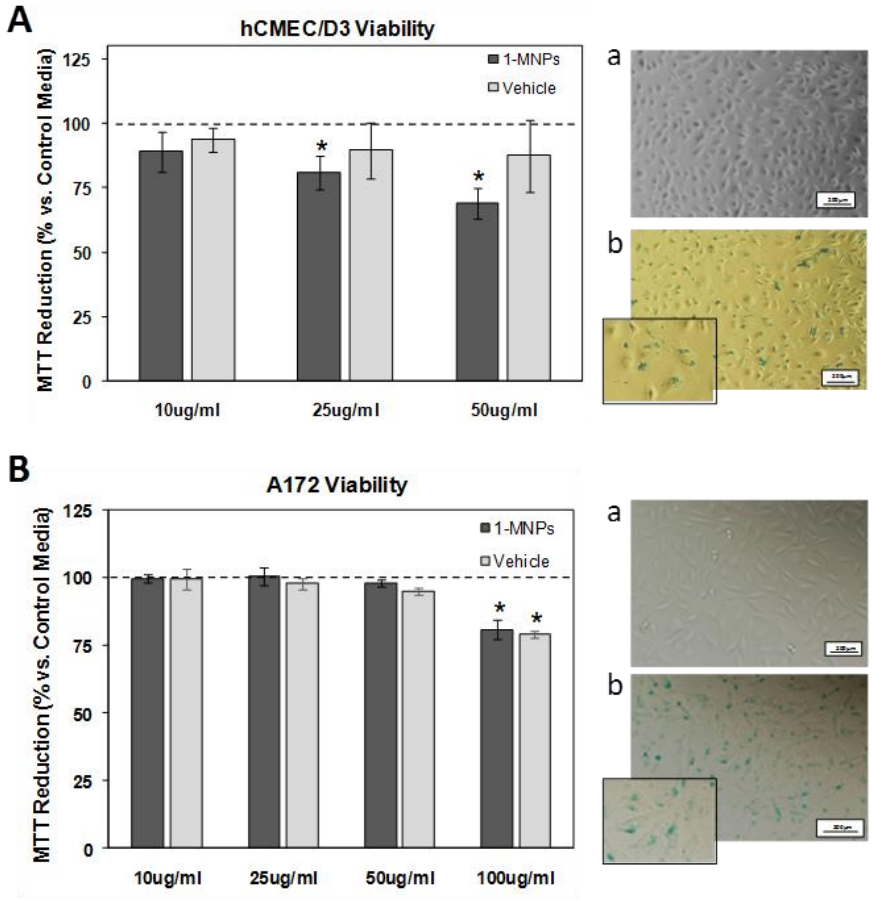

Figure 5.13: Cell viability was tested after exposing brain endothelial cells (A), and Glioblastoma cells (B) to increasing doses of **1**-MNPs and corresponding vehicle solutions for 24 hours. Data is expressed as mean ±SD of n=3/4 per condition; * $p<0.05$ indicates differences vs. control media (dashed line). Right panels correspond to images of each cell line (a) and to iron deposits observed after Prussian Blue Stain (b, treatment dose 10 μg/mL).

It was important to know about the toxicity of the ligand shell coating the **1**-MNPs core. In this regard, the toxicity of only the sodium salt of the carboranylphopshinate ligand, Na[1-OPH(O)-1,7-*closo*-$C_2B_{10}H_{11}$], Na[**1**], was determined in both A172 and hCMEC/D3 cells in a dose-response cell viability assay (Figure 5.14). Endothelial cells were more sentitive to the Na[**1**] salt than the glioblastoma cells A172 since Letal Dose 50 (LD_{50}) was around 1mM compared to the 7.5mM observed in the case of A172 cells. Those doses correspond to 230 μg Na[**1**]/mL and 1725 μg Na[**1**]/mL of Na[**1**], respectively.

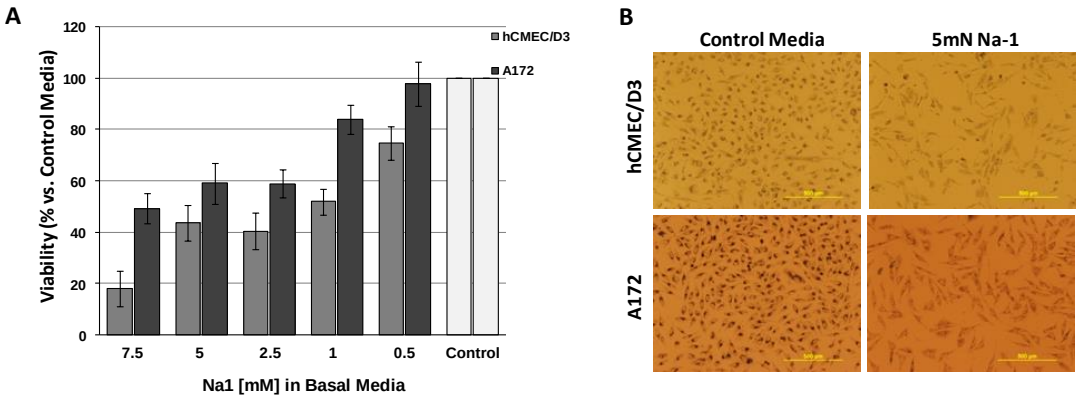

Figure 5.14 Cell viability was tested after exposing brain endothelial cells (hCMEC/D3 cells) and glioblastoma cells (A172) to increasing concentrations of the Na[**1**] salt and compared to control treatment (vehicle). A) bar graph representing cell viability after 24h treatment (mean ±SD). B) representative images of cells after MTT reduction

5.2.3 Quantification and visualization of *meta*-carboranylphosphinate MNPs uptake by cells

To confirm the uptake of MNPs core by the hCMEC/D3 and A172 cells after 6 or 24 h of incubation in the presence of **1**-MNPs, the cells were dried and magnetization measurements were run. To prepare dried cells total cells collected from the cell count cultures were centrifuged at 1500 rpm for 5 minutes, then the cell pellet was resuspended in 50 μL of each cell culture media, and transferred into a polycarbonate capsule (Figure 5.15) to be dried at 60 °C using a speed vacuum centrifuge (1500 rpm for 1 hour).

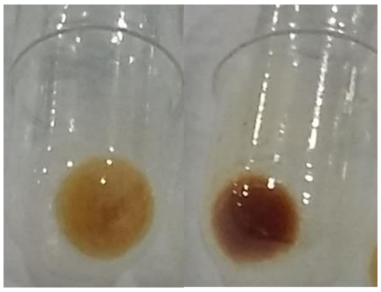

Figure 5.15 Dry cell samples used for magnetization measurements

The as-prepared dry cells sample (Figure 5.15) was inserted into the SQUID magnetometer sample holder for cell remanent magnetization measurement (M_R) that was made at 5 K after the material has been magnetically saturated up to 6T. The uptake of **1**-MNPs was measured through the MNPs core and calculated as follows: first, dividing the M_R value of the treated cells by the total number of cells which provides the magnetization per cell (emu/cell), then further dividing this value by the remanent magnetization of the **1**-MNPs (emu/g **1**-MNPs) at 5 K to give the amount of iron per cell:

$$\textbf{1}\text{-MNPs content /cell} = \frac{M_{Rcapsula}}{N_{total\ cells} \cdot M_{R\ \textbf{1}\text{-MNPs}}}$$

The results determine the amount of iron per cell and show a clear time- and dose-dependent relationship with both endothelial and glioblastoma cell lines as shown in Figure 5.16A. Moreover at the same tested dose of **1**-MNPs (25 μg/ml) glioblastoma A172 cells presented higher cellular iron content than endothelial cells (a 6-fold and 4-fold increase after 6 and 24 hours, respectively) as shown in Figure 5.15B, indicating a higher capacity for cell labelling with iron oxides without toxic effects. These are interesting results suggesting that by using low doses of **1**-MNPs, glioblastoma cancer cells might be largely labelled with the **1**-MNPs compound compared to other neighbouring cells in the tissue.

The presence of cytoplasmatic MNPs core and its intracellular localization into endothelial hCMEC/D3 and glioblastoma A172 cells were visualized by TEM analysis in membrane-bound compartments matching with endosomal or lysosomal organelles (Figure 5.17) at least 24 hours after labeling, as described for other iron oxide compounds.[12,13,14] However, the presence of the *meta*-carboranyl cluster surrounding the observed MNPs core present in the glioblastoma A172 and endothelial hCMEC/D3 cytoplasma cells' sample could not be confirmed by means of TEM analysis. Neither EELS nor EFTEM elemental maps of the same samples

could detect the presence of *meta*-carboranyl cluster probably because of the low levels of boron, thus only Fe was was clearly detected.

A

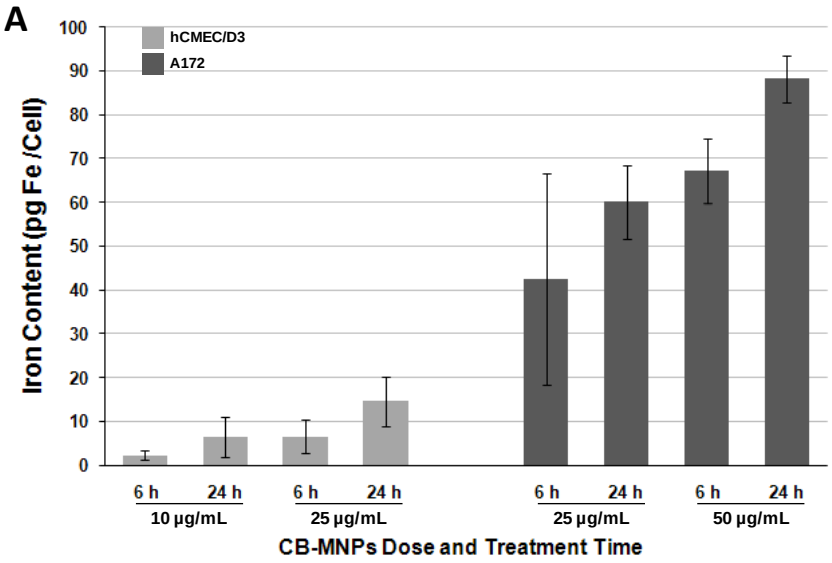

B

	hCMEC/D3				A172			
	10µg/mL		25µg/mL		25µg/mL		50µg/mL	
	6h	24h	6h	24h	6h	24h	6h	24h
MEAN	2.32	6.56	6.61	14.66	42.49	60.07	67.38	88.26
SD	1.16	4.52	3.73	5.69	24.14	8.27	7.33	5.37

Figure 5.16 The amount of Fe per viable cell was determined after treating cells with increasing doses of **1**-MNPs for 6 or 24 hours. Bar graph (**A**) shows that the amount of Fe/cell was time- and dose-dependent in both brain endothelial and glioblsatoma cell lines. The tested glioblastoma cells (A172) were capable to uptake the largest amounts of iron at all sub-toxic tested doses (**B**). Data is expressed as mean ±SD pg Fe/Cell of n=3 independent experiments per condition

To overcome this drawback and unambiguously prove the presence of the meta-carboranyl cluster coordinated at the MNPs core, high resolution XPS and EELS spectra on the A172 dry cells sample were run. Peaks at 189 and 133 eV in the XPS spectrum, which are characteristic of B-B[15] and P-O bonding, were observed that, clearly confirmed the presence of *meta*-carboranyl phosphinate (Figure 5.18). But it could not give the final prove that meta-carboranyl phosphinate was coordinated to the MNPs core. EELS analysis on the A172 dried-cells sample (Figures 5.19 and 5.20) also showed the B-K and PL2,3 edges present in the

sample proving that carboranylphosphinate was found around MNPs, that could be a prove of its coordination onto the MNPs surface in cytoplasm of the cells.

a)

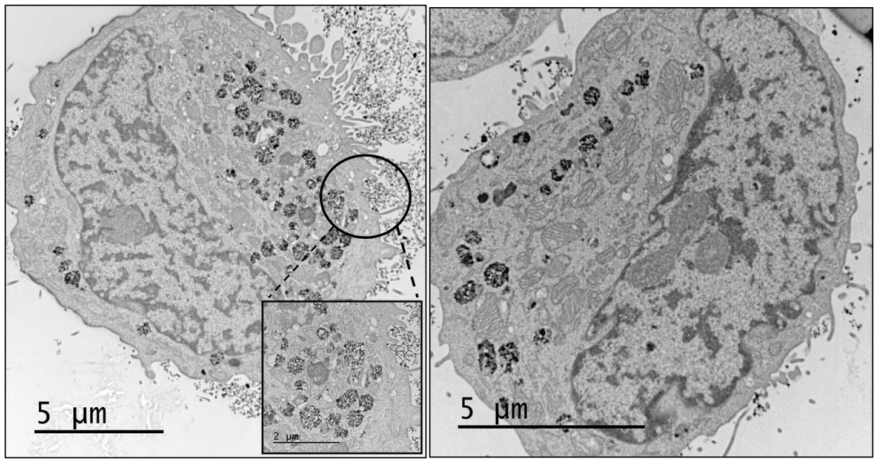

b)

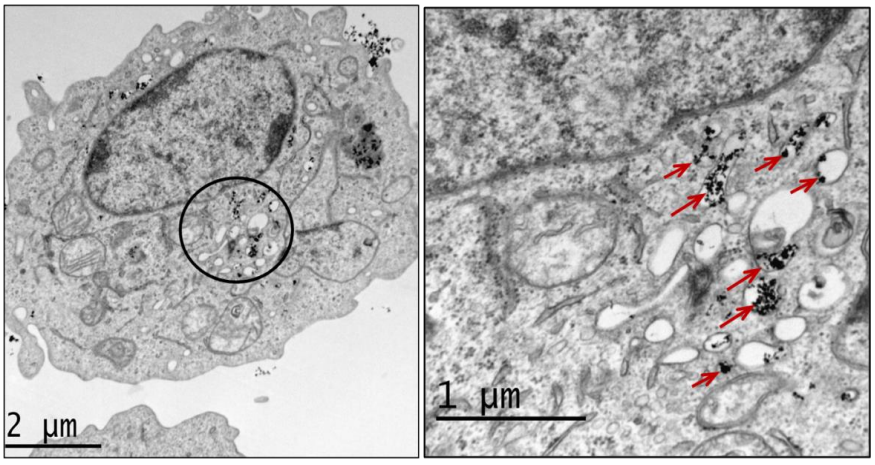

Figure 5.17 Transmission electron microscope (TEM) images of a) glioblastoma cells (A172) and b) endothelial hCMEC/D3 cells showing the presence of **1**-MNPs into the cytoplasm

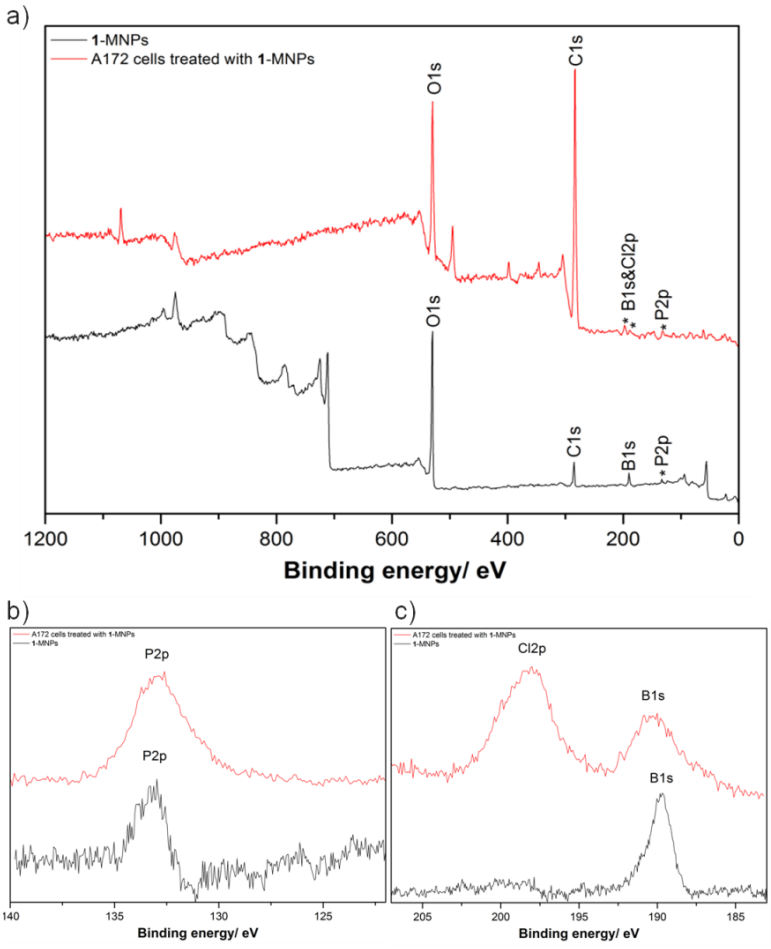

Figure 5.18 a) High resolution spectra XPS of **1**-MNPs (black) and A172 cells treated with **1**-MNPs (red). High resolution spectra XPS of **1**-MNPs and A172 cells treated with **1**-MNPs in the B 1s and P 2p regions, (b) and (c) respectively.

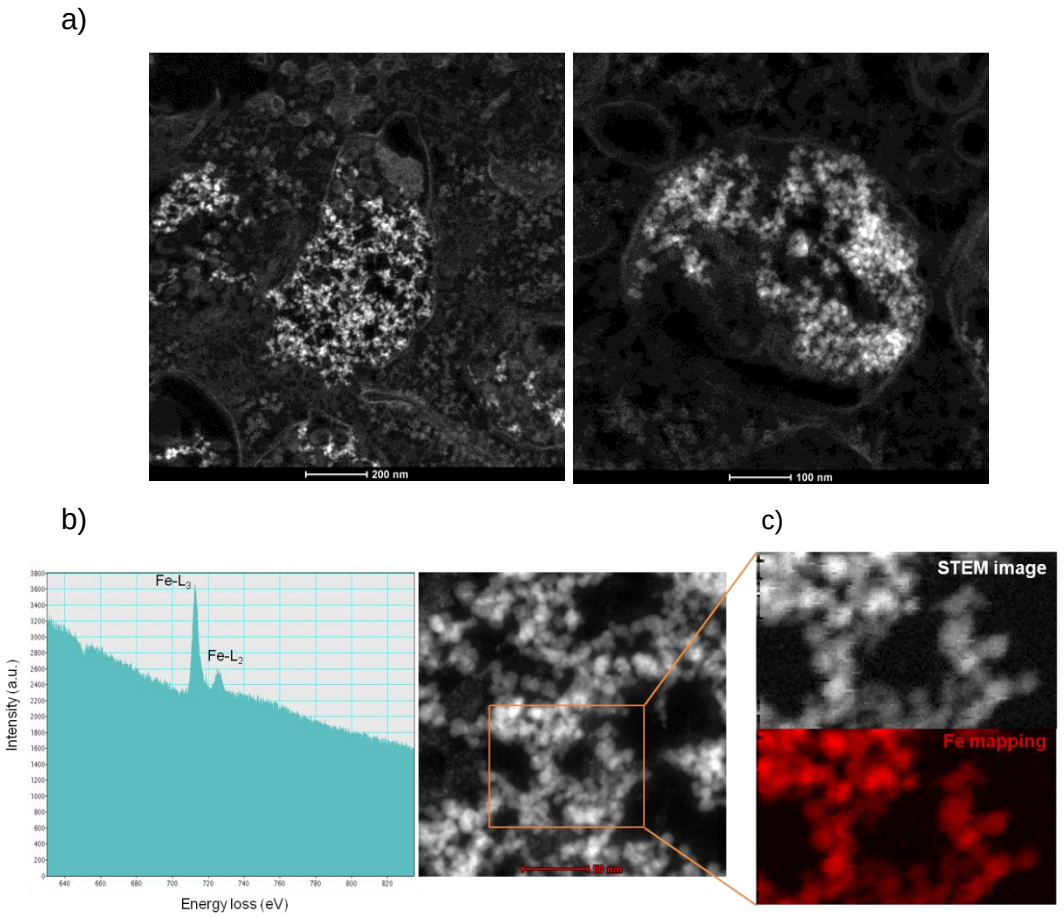

Figure 5.19 a) STEM images of glioblastoma cells (A172) with different magnification. b) EELS analysis spectrum on the square area showing the characteristic peaks for Fe. c) EFTEM elemental map of glioblastoma cells (A172); Fe (in red) can be observed on the cells samples.

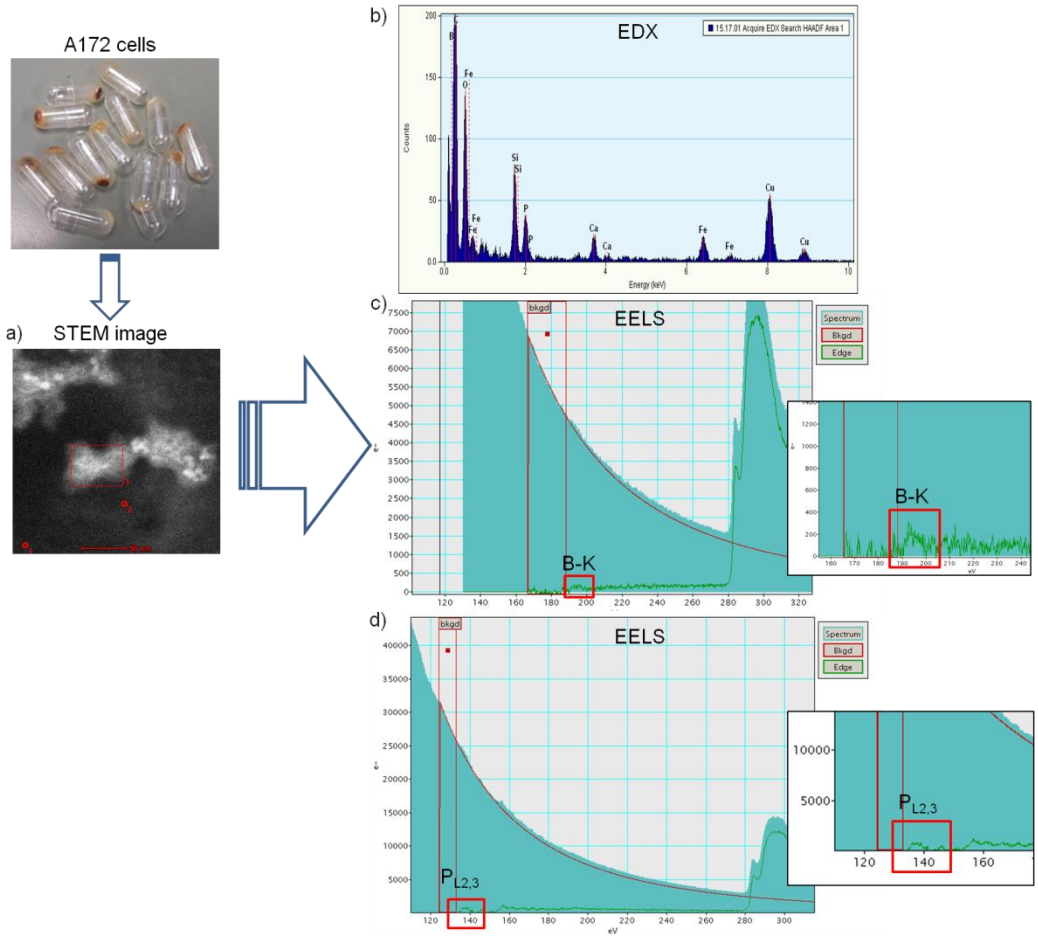

Figure 5.20 a) High-angle annular dark-field scanning transmission electron microscopy (HAADF-STEM) image of A172 cells and b) EDX spectrum on the square area showing the characteristic peaks for Fe and P. c) EELS spectrum on the square area. Energy loss peaks with onsets at 188 eV correspond to B containing in the sample. d) EELS spectrum on the square area. Energy loss peaks with onsets at 133 eV correspond to $P_{L2,3}$ containing in the sample.

5.2.4 Evaluation of *in vivo* toxicity of *meta*-carboranylphosphinate MNPs in mice

Before testing a drug or compound in a person we must find out the potential harm effects in experimental models, and rodents have been widely used for this purpose. We aimed at proving that the **1**-MNPs was well tolerated and did not induce major toxicity signs such as death or seizures but also acute pain, distress or dehydratation by monitoring body weight before and after treatment. Briefly, mice

received 80μL of **1**-MNPs intravenously which corresponds to 0.58±0.03 mg/kg of body weight, very close to the approved dose for Feridex® in humans (0.56 mg/Kg of body weight) and previously tested in other in vivo studies.[16] Importantly, all mice survived the study-period (10 days) with no major signs of toxicity. In particular we found that the individual body weight of the 2 treated groups were comparable with the control group (naïve mice) by fluctuating from day to day without clear trend of increasing or decreasing (Figure 5.21a). No statistic difference in final body weight increase/decrease was detected between groups: 0.53±0.69 for **1**-MNPs-treated, 0.55±0.57 gr for vehicle-treated and 0.40±0.65 for naïve mice (Figure 5.21b). Therefore, no major treatment-related side effects were observed after in vivo administration of **1**-MNPs in mice at clinically-relevant doses. In spite of the relevance of this in vivo testing, additional studies in pre-clinical models are needed including longer follow-up, repeated doses or organ-specific toxicity studies.

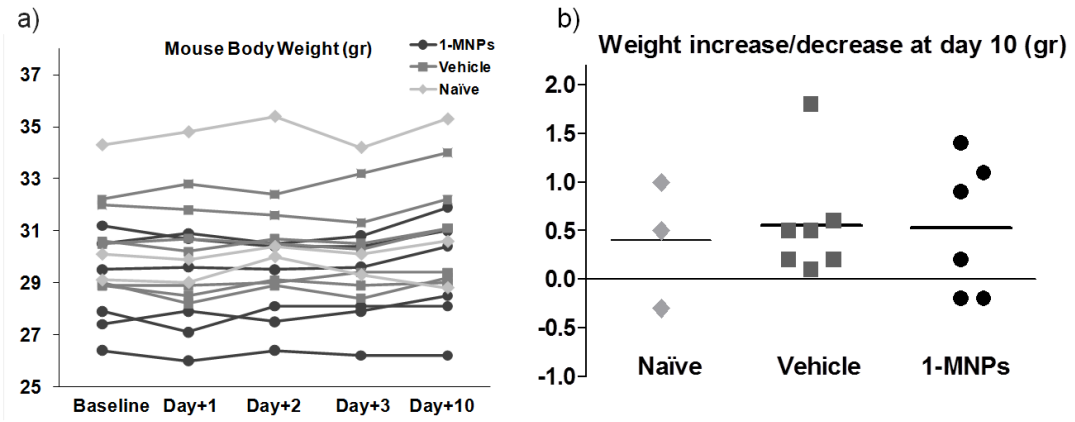

Figure 5.21 Mouse weight after in vivo administration of 1-MNPs or vehicle in mice. a) Mice were weighted before 1-MNPs (n=6) or Vehicle (n=7) intravenous administration, and followed-up at 1, 2, 3 and 10 days of injection. A group of naïve mice who did not receive any treatment were also weighted at the same days (n=3). b) The Individual weight increase or decrease at day 10 was calculated for each mouse and represented, showing no differences between treatment

(1) Leites, L. A. *Chem. Rev.* **1992**, *92* (2), 279–323.

(2) Pothiraja, R.; Shanmugan, S.; Walawalkar, M. G.; Nethaji, M.; Butcher, R. J.; Murugavel, R. *Eur. J. Inorg. Chem.* **2008**, *2008* (11), 1834–1845.

(3) Pothiraja, R.; Sathiyendiran, M.; Butcher, R. J.; Murugavel, R. *Inorg. Chem.* **2005**, *44* (18), 6314–6323.

(4) Lu, X.; Liu, W.; Ouyang, J.; Tian, Y. *Appl. Surf. Sci.* **2014**, *311* (October), 749–752.

(5) Joseph, D.; Sachar, S.; Kishore, N.; Chandra, S. *Colloids Surfaces B Biointerfaces* **2015**, *135*, 596–603.

(6) O'Handley, R. C. *Modern magnetic materials : principles and applications*; Wiley, 2000.

(7) Ho, D.; Sun, X.; Sun, S. *Acc. Chem. Res.* **2011**, *44* (10), 875–882.

(8) Aires, A.; Ocampo, S. M.; Cabrera, D.; Cueva, L. de la; Salas, G.; Teran, F. J.; Cortajarena, A. L.; Garwood, M.; Bischof, J. C.; Morales, M. d. P.; Teran, F. J. *J. Mater. Chem. B* **2015**, *3* (30), 6239–6247.

(9) Salvati, A.; Pitek, A. S.; Monopoli, M. P.; Prapainop, K.; Bombelli, F. B.; Hristov, D. R.; Kelly, P. M.; Åberg, C.; Mahon, E.; Dawson, K. A. *Nat. Nanotechnol.* **2013**, *8* (2), 137–143.

(10) Sundstrøm, T.; Daphu, I.; Wendelbo, I.; Hodneland, E.; Lundervold, A.; Immervoll, H.; Skaftnesmo, K. O.; Babic, M.; Jendelova, P.; Sykova, E.; Lund-Johansen, M.; Bjerkvig, R.; Thorsen, F. *Cancer Res.* **2013**, *73* (8).

(11) Matuszak, J.; Zaloga, J.; Friedrich, R. P.; Lyer, S.; Nowak, J.; Alexiou, C.; Cicha, I. *J. Magn. Magn. Mater.* **2015**, *380*, 20–26.

(12) Carenza, E.; Barceló, V.; Morancho, A.; Levander, L.; Boada, C.; Laromaine, A.; Roig, A.; Montaner, J.; Rosell, A. *Nanomedicine Nanotechnology, Biol. Med.* **2014**, *10* (1), 225–234.

(13) Wilhelm, C.; Gazeau, F. *Biomaterials* **2008**, *29* (22), 3161–3174.

(14) Angelopoulos, I.; Southern, P.; Pankhurst, Q. A.; Day, R. M. *J. Biomed. Mater. Res. Part A* **2016**, *104* (10), 2412–2419.

(15) Lu, X.; Liu, W.; Ouyang, J.; Tian, Y. *Appl. Surf. Sci.* **2014**, *311*, 749–752.

(16) Wang, Y.-X. J. *Quant. Imaging Med. Surg.* **2011**, *1* (1), 35–40.

Universitat Autònoma de Barcelona

Carboranylphosphinic acids: A New Class of Purely Inorganic Ligands to Generate Polynuclear Compounds and Multifunctional Nanohybrid Materials for Biomedical Applications

Elena Oleshkevich

TESI DOCTORAL

Programma de Doctorat de Química

Directora: Prof. Clara Viñas i Teixidor

Tutor: Dr. Lluis Escriche Martinez

Departament de Química

Facultat de Ciències

2017

Memòria presentada per aspirar al Grau de Doctor per

Elena Oleshkevich

Vist i plau

Prof. Clara Viñas i Teixidor (Directora)

Dr. Lluis Escriche Martinez (Tutor)

Bellaterra, 11 de Maig de 2017

La Professora CLARA VIÑAS i TEIXIDOR, Professora d'Investigació del Consejo Superior de Investigaciones Científicas a l'Institut de Ciència de Materials de Barcelona

CERTIFICA

Que en Elena Oleshkevich, llicenciat en Enginyeria Química, ha realitzat sota la meva direcció la Tesí Doctoral que porta per títol "*Carboranylphosphinic acids: A New Class of Purely Inorganic Ligands to Generate Polynuclear Compounds and Multifunctional Nanohybrids Materials for Biomedical Applications*" i que recull aquesta memòria per optar al títol de Doctor en Química per la Universitat Autònoma de Barcelona.

I, perquè consti i tingui els efectes corresponents, signa aquest certificat a Bellaterra, a 11 de Maig de 2017.

Prof. CLARA VIÑAS i TEIXIDOR

ICMAB (CSIC)

Campus de la Universitat Autònoma de Barcelona
08193 Bellaterra, Catalunya, Espanya
Telf.: +34 935 801 853
Fax.: +34 935 805 729
http://icmab.es/

Aquest treball de recerca ha estat finançat per la Comisión Interministerial de Ciencia y Tecnología, CICYT, mitjançant els projectes CTQ2013-44670-R i CTQ2016-75150-R; per la Generalitat de Catalunya amb el projecte 2014/SGR/149 i al projecte concedit per l'ALBA (ref.: 2015091372). Agraïr la beca de Formació de Personal Universitari (FPU, ref.: AP-2012-3828) concedida pel Ministerio de Ciencia e Innovación, durant el període maig del 2013 al abril del 2017.

Aquest treball d'investigació, amb la data de defensa del 23 de Juny de

2017 , té com a membres del tribunal a:

- President: Prof. Olivier Diat, Investigador CEA, Institut de Chimie Séparative de Marcoule.

- Secretari: Dra. Mercé Capdevila, Professora Titular d'Universitat de la Universitat Autònoma de Barcelona.

- Vocal: Dra. Fernanda Marujo Marques, Investigador científic, Departamento de Ciências e Tecnologias Nucleares, Campus Tecnológico e Nuclear, Instituto Superior Técnico da Universidade de Lisboa.

Com a membres suplents:

- Suplent 1: Prof. Joan Suades Ortuño, Catedràtic de la Universitat Autònoma de Barcelona.

- Suplent 2: Dra. Montserrat Rodríguez, Professora Titular de Química de la Universitat de Girona.

ACKNOWLEDGEMENTS

To begin I would like to point that I am in debt to many people for the accomplishment of this PhD thesis. First of all I want to thank Prof. Clara Viñas, my PhD director, who accepted me with lots of care, who always believed in me, who always encouraged me, always gave lots of scientific ideas and supported mines, so I had a chance to learn many techniques, participate in many conferences and training scientific schools, and work on application part of ligands synthesized in this PhD thesis. I would also like to thank Prof. Francesc Teixidor, who also supported, motivated, and directed me during these 5 years of PhD thesis, for his predisposition to solve any of my doubts at any moment. To both of them I would like to express my appreciation!

To Dr. Rosario Núñez and Dr. José Giner for their collaboration and kind advices.

To Dr. Anna Rosell, thank you for accepting our collaboration with all your passion (and incredible energy) for research. To Dr. Anna Morancho, who performed many biological tests for us, it was a great pleasure to learn from you. To Dr. Koen Galenkamp, who also realized many biological studies for us with cancer cells, thank you for the many ideas and explanations you provided me during our collaboration.

To Dr. Lluis Escriche from Universitat Autònoma de Barcelona for accepting to be my PhD tutor.

To Dr. Ana Paula Candiota from Universitat Autònoma de Barcelona for being so welcome always and providing autoclave sterilization of our samples.

To Dr. Xavier Fontrodona, Prof. Reijo Sillanpää, DR. Duane Choquesillo-Lazarte, Prof. Matti Haukka for the resolution of the crystalline structures presented in this work, in spite of some of them were really challenging.

Special thanks to Dr. Isabel Romero García! Your help was essential for the work with coordination polymers! Thank you also for being so helpful and providing me many explanations and experience during our work, for the private advices as well.

I am thankful to Prof. Xavier Obradors, the director of ICMAB for accepting me in the institute and giving me the opportunity to use all the services within the institute as well as to all the ICMAB´s personnel for doing their best for me.

I wish also to thank to Anna Fernández for all the patience in doing and sometimes repeating NMR analysis, for her advices and nice atmosphere always in her “lab”, and to Jordi Cortés, without him the work in the laboratory would not be possible! Gracias Jordi!!!

To my colleagues who became my friends also! To Radu Popescu for training me in the lab and explaining many details about NMR and chemistry in general, to Màrius Tarrés for his help in the lab always and with catalan, motivation in general and funny company in SAF, to Ivy and Adnana for their attention and friendly talks that made my days in the lab. Especially to Adnana, you taught me to be patient! To Arpita and Abhishek, thank you both for help with English! Also to Arpita and Ines (my students ☺) who became good friends for me! To Isa and Bego for their support, funny talks and help with catalan. And all other students in our group (Albert, Ana Cioran, David, Ana Daniela, Marius Lupu, Flavia, Lei, Mahdi, Victor, Justo) for all your collaboration and good atmosphere in the group! I wish also to give thanks to Elena Laukhina, for her taking care of me and encouraging me.

Also my thoughts bring to my friends (Katia, Jane, Stamatis, Pablo) and one's nearest and dearest (Victor), who made my life last 5 years, and motivated in difficult moments. To Victor, who always supported me and has been there with me, for me in good, in bad. Thank you moi miliy! Вите, которому я благодарна за его терпение и за то, что он рядом!

The last, but one of the most important to my mother, without whom I would not be who I am now. Мама, спасибо за все терпение и поддержку, понимание и любовь!

Thank you all for you've done for me and for all I've learnt!

ORGANITZACIÓ DEL MANUSCRIT

D’acord amb la normativa vigent i prèvia acceptació de la comissió de Doctorat de la Universitat Autònoma de Barcelona, aquesta Memòria es presenta com a recull de publicacions, que va ser aprovada per aquesta comissió el dia 26 d'abril de 2017 (Addendum I). A més d'incloure les publicacions aprovades, també s'han inclòs els treballs realitzats en el marc d'aquesta tesi doctoral que estan enviats o en procés de elaboració (Addenium II).

Addendum I. Articles publicats i presentats a la Comissió de Doctorat de la Universitat Autònoma de Barcelona al 26 de abril de 2017:

1. “Carboranylphosphinic Acids: A New Class of Purely Inorganic Ligands”. Elena Oleshkevich, Francesc Teixidor, Duane Choquesillo-Lazarte, Reijo Sillanpää, and Clara Viñas. *Chemistry- A European Journal*, **2016**, *22*, 3665-3670.

2. “*m*-Carboranylphosphinate as Versatile Building Blocks to Design All Inorganic Coordination Polymers”. Elena Oleshkevich, Clara Viñas, Isabel Romero García, Duane Choquesillo-Lazarte, Matti Haukka, and Francesc Teixidor. *Inorganic Chemistry*, **2017**, DOI: 10.1021/acs.inorgchem.7b00610.

Addendum II. Articles d'aquesta tesi doctoral que estan enviats o en procés de elaboració:

1. “Merging Icosahedral Boron Clusters and Magnetic Nanoparticles: Aiming towards Multifunctional Nanohybrid Materials”. Elena Oleshkevich, Francesc Teixidor, Anna Rosell and Clara Viñas.

2. ”Biocompatible Fully Inorganic Nanohybrids for Biomedical Applications: Combining Magnetic Nanoparticles and Icosa-hedral Boron Clusters”. Elena Oleshkevich, Anna Morancho, Koen M. O. Galenkamp, Alba Grayston, Joan X. Comella, Francesc Teixidor, Anna Rosell, and Clara Viñas.

Numbering of the compounds

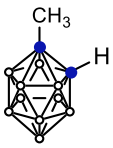

(1)

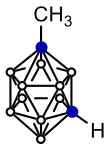

(2)

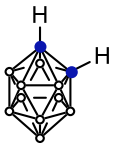

(3)

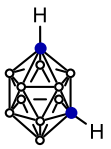

(4)

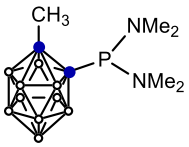

(5)

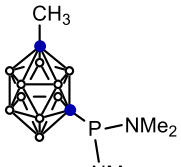

(6)

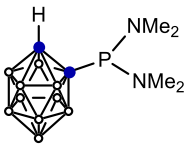

(7)

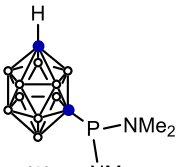

(8)

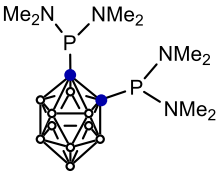

(9)

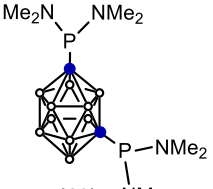

(10)

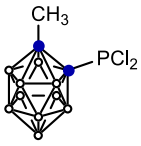

(11)

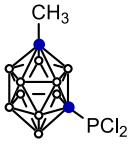

(12)

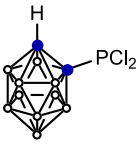

(13)

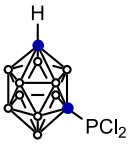

(14)

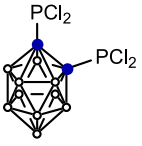

(15)

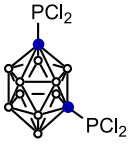

(16)

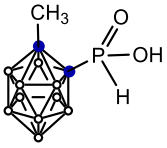

(17)

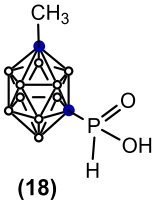

(18)

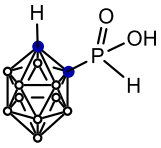

(19)

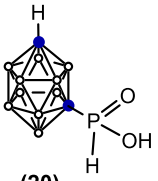

(20)

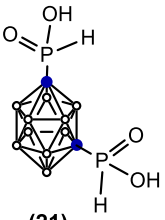

(21)

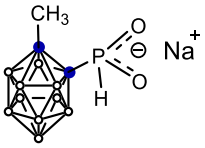

(22)

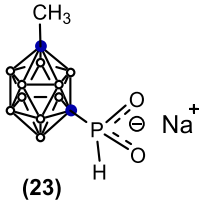

(23)

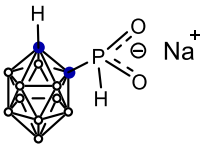

(24)

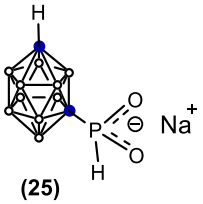

(25)

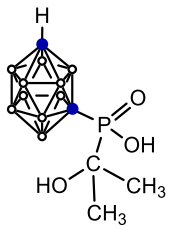

(26)

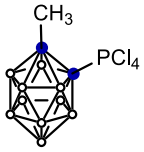

(27)

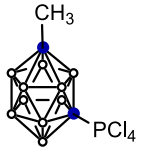

(28)

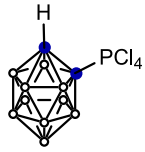

(29)

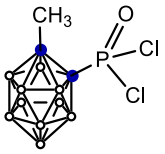

(30)

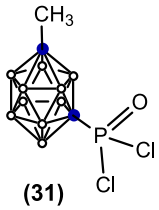

(31)

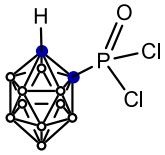

(32)

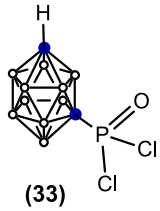

(33)

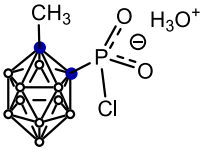

(34)

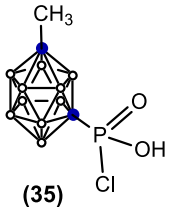

(35)

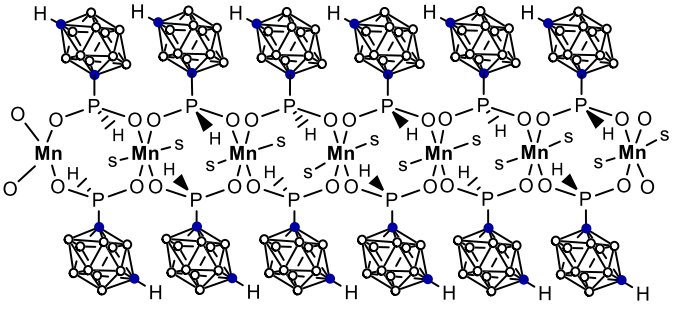

(36) s = MeOH

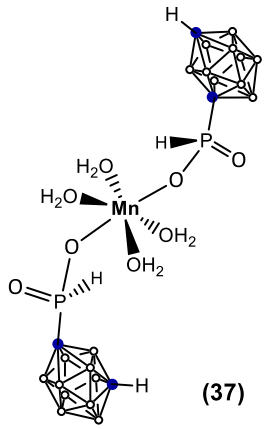

(37)

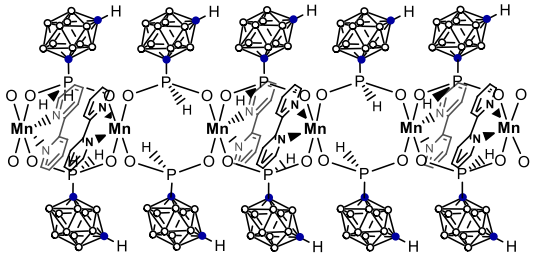

(38)

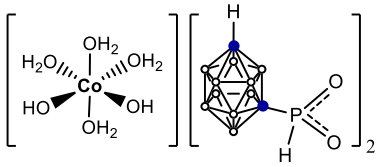

(39)

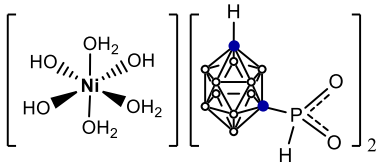

(40)

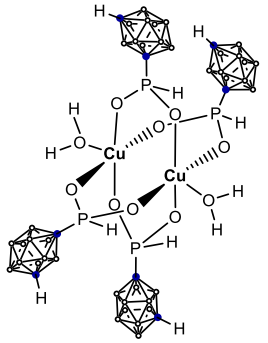

(41)

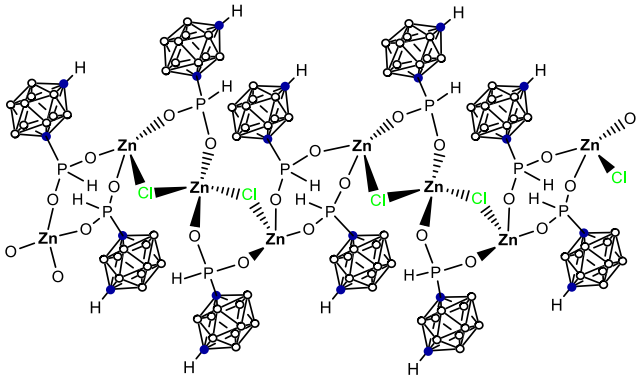

(42)

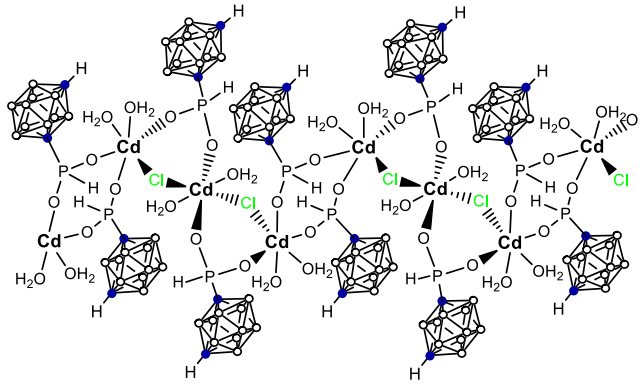

(43)

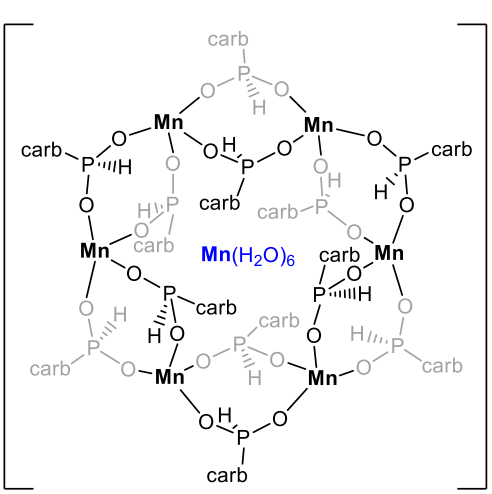

(44)

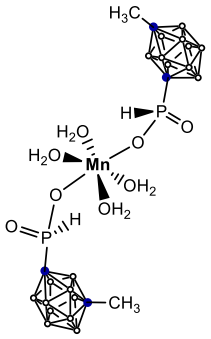

(45)

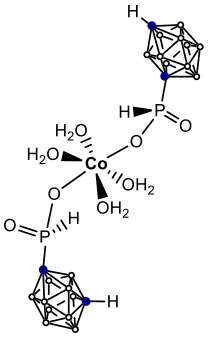

(46)

carb =

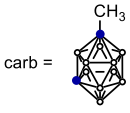

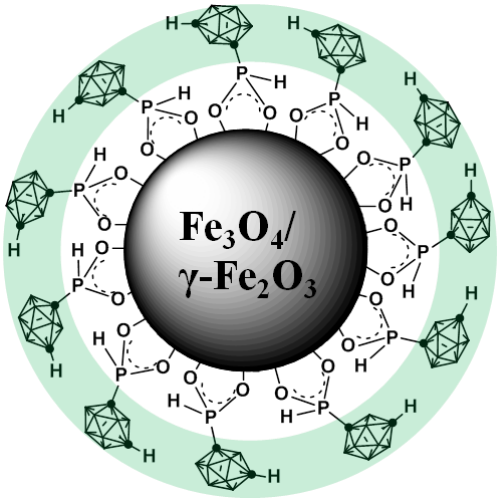

1-MNPs

Abbreviations

δ – NMR chemical shift

BNCT – Boron Neutron Capture Therapy

bipy – 4,4-bipyridine

C_c – carbon atom belonging to carborane cluster

C_{bpy} – carbon atom belonging to 2,2´-bipyridine

DSC – Differential Scanning Calometry

2,2´-bpm – 2,2´-bipyrimidine

2,2´-bpy – 2,2´-bipyridine

H_{CH3} – proton atom belonging to methyl group

IR – InfraRed

^{i}Pr – *iso*-propyl

MNPs – magnetic nanoparticles

1-MNPs – *meta*-carboranylphosphi-nate MNPs

Me – methyl

NCT – Neutron Capture Therapy O_w – oxigen atom belonging to water

NMR – Nuclear Magnetic Resonance

Ph – phenyl

n-BuLi – *normal*-butyl lithium

t-Bu – *tert*-buthyl

STEM-HAADF – High-angle annular dark-field (HAADF) scanning transmission electron microscopy (STEM)

TGA – ThermoGravimetric Analysis

TEM – Transmission Electron Spectroscopy

XPS – X-ray photoelectron Spectroscopy

$Ø_{carborane}$ – diameter of carborane cluster

Table of contents

Introduction

1.1 Carboranes

1.1.1 Boron chemistry and the nature of the B-B bonding

In the periodic table of elements, boron lines next to carbon. Both, boron and carbon have the property to catenate. Carbon forms cycles and polymers and is the base of organic chemistry. Boron forms clusters and induces a huge discipline of chemistry: Boron science. Boranes, boron clusters, and in particular, icosahedral dicarba-*closo*-dodecaboranes with impirical formula $C_2B_{10}H_{12}$ are of special interest. Boron clusters were considered as electron deficient compounds till Lipscomb´s discovery. William N. Lipscomb was awarded with the Nobel Prize in Chemistry 1976 "for his studies on the structure of boranes illuminating problems of chemical bonding". Lipscomb proposed the mechanism to understand the three-center two-electron (3c-2e) bond in boron clusters[1]. In 3c-2e a pair of electrons is shared between three atoms. The three atoms can be a boron atom at either end and a hydrogen atom in the middle as in the case of the diborane B-H-B bonds or the three atoms can be three boron atoms as in the polyhedral clusters. 3D aromaticity of boron or carborane clusters gives them unique properties that are not common in organic chemistry[2,3,4].

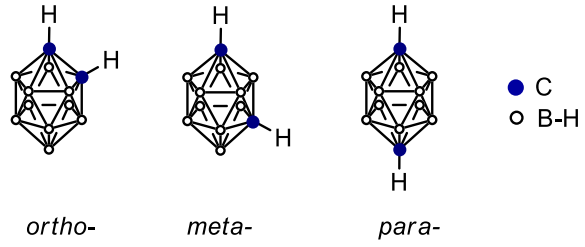

Figure 1.1 The three isomers of icosahedral dicarba-*closo*-dodecarboranes ($C_2B_{10}H_{12}$).

Relation between hydrocarbon and borohydride chemistries have been recently reported.[5,6] The idea is based on keeping the same number of valence electrons in a confined space. Thus “addition” of an extra electron to each boron atom in borohydrides yields molecular analogues of hydrocarbons. As a result, for any given hydrocarbon in organic chemistry can be find its borohydride analogue in

boron chemistry.[5] Following this direction, recently was reported the work that establishes a direct connection between Wade-Mingos rule of tridimensional aromatic *closo* boron hydride clusters and Hückel´s rule of planar aromatic annulenes, showing that they share a common origin regulated by the number of valence electrons in a electronic confined space[6].

1.1.2 Carboranes: Synthesis, properties and reactivity

Although *ortho*- and *meta*-carborane clusters are remarkable stable, in certain reaction conditions they exhibit high synthetic reactivity. From point of view of electrophilic substitution at the C_c-H vertices (C_c: carbon atom belonging to carborane cluster), both isomers display similar chemical reactivity. In both carborane isomers, the hydrogen atoms of the C_c-H units are more acidic than the ones bonded to B-H vertices, due to more electronegative character of carbon with respect to boron (2.5 and 2.0 respectively, according to Pauling scale). Thus, hydrogen atoms attached to carbon can be considered as acidic while those bonded to boron as hydride. The acidity of the C_c-H vertices decreases in the order of *ortho*-, *meta*- and *para*-carborane. In the same order decreases its vulnerability to get deprotonated.

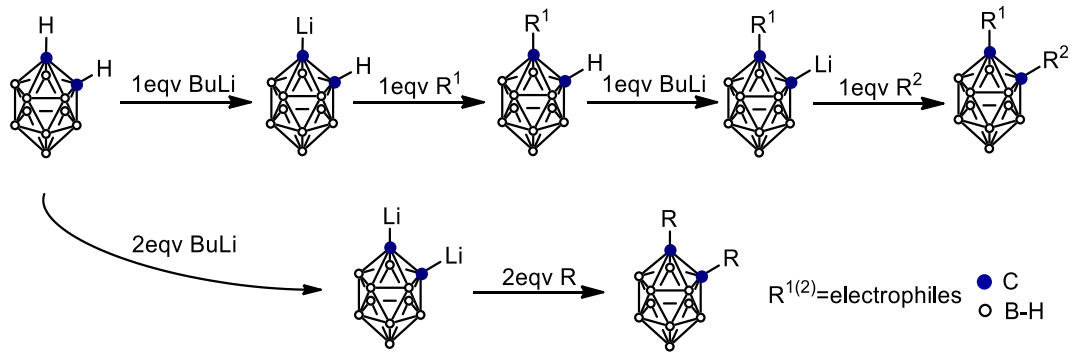

Scheme 1.1. Deprotonation reaction of C_c-H units followed by substitution with electrophilic agents.

This relatively acidic character of C_c-H units allows their deprotonation by strong alkali and alkaline earth metal bases, like for example *n*-butyllithium or Grignard reagents. The generated negative charge on the carbon atom of the

cluster, C_c, attracts electrophilic reagents, opening the way to the introduction of funcional groups at the C_c position of the cluster.

Scheme 1.1 shows the two possible pathways for substitutions at one or both of the C_c atoms. After dilithiation of the carborane cluster it is possible to introduce simultaneously twice the same substituent, which leads to symmetrically substituted carborane. The other pathway (top) demonstrates monosubstitution of the carborane cluster or the unsymmetrical disubstitution. The synthesis of monosubstituted carborane derivatives is more complicated compared to disubstituted. The reason is the disproportionation of Li[1,2-$C_2B_{10}H_{11}$] into Li_2[1,2-$C_2B_{10}H_{10}$] and 1,2-$C_2B_{10}H_{12}$ how it was found for *ortho*-carborane[7]. Several approaches have been developed to overcome this problem. Among them is using the way of protection/deprotection methodologies with dimethoxyethane as the solvent or by doing the reaction at high dilution[8,9,10]. Perhaps more simple method is carrying the monosubstitution reactions in ethereal solvents at low temperature and specific carborane concentration. It was suggested that depending on type of electrophile it is possible to find combination of conditions (ethereal sovent, temperature, carborane concentration) that facilitate the largest degree of monosubstitution[11].

The coupling to a boron atom of a carborane cluster can be performed through iodo-substituted carborane with following palladium-catalyzed cross-coupling reaction (Scheme 1.2).[7]

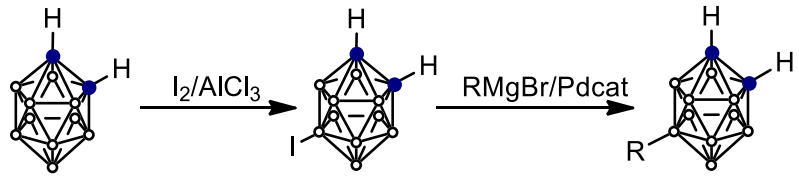

Scheme 1.2. *Ortho*-carborane substitution in the B(9) position through iodo-derivative.

1.2 *Closo* – Carboranylphosphorus compounds

1.2.1 General aspects on *closo*-carboranylphosphines

Since their discovery phosphines continue to be the most significant class of ligands in coordination chemistry and catalysis. Nowadays a big choice of different phosphine ligands[12] is commercially available from chemical products suppliers: monodentate, bidentate, Buchwald, cataCXium, Dalphos ligands.

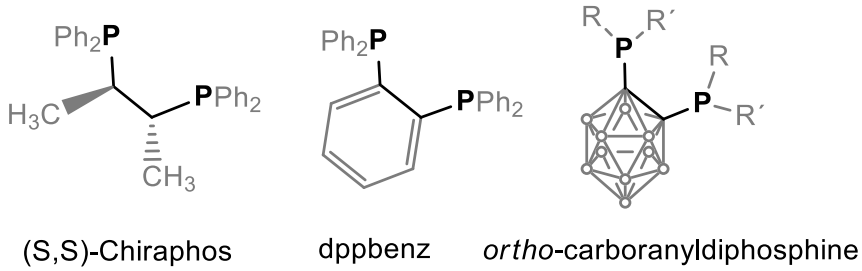

(S,S)-Chiraphos dppbenz *ortho*-carboranyldiphosphine

Figure 1.2 C_2-symmetric backbone of different phosphine ligands.

Bidentate phosphine ligands play an important role in catalysis. C_2-symmetric backbone of phosphine ligand is favored because it allows the formation of stable five-membered rings by coordination to transition metal through phosphorus atoms. Due to its C_2 symmetry 1,2-dicarba-*closo*-dodecaborane, or *ortho*-carborane, same way as ethylene and *ortho*-phenylene attracted lot of attention as a platform do produce chelating bidentate phosphine ligands (Figure 1.2).

Our group and others were interested in the exploration of the properties of phosphinate ligands synthesized on the *ortho*-carborane platform[13]. Among them P(III) and P(V) derivatives of *ortho*-carboranylphoshines[14]. Substituting conventional organic entities by boron clusters to produce new compounds could lead to remarkable properties as high rigidity, space occupancy and hydrophobicity of the cluster group. Carboranylphosphines is one of the examples[13]. By changing groups bonded to phosphorus, the steric and electronic effects can be modified, so it is possible to “tailor” properties of the phosphines as ligands. A representative drawing of the carboranyl phosphines, carboranyl phosphine oxides, carboranyl phosphinates and carboranyl phosphonates is shown in Figure 1.3.

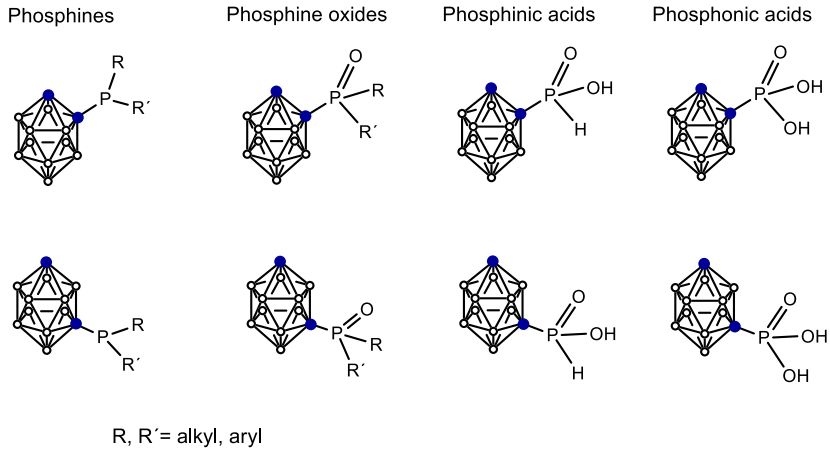

Figure 1.3 Phosphorus-substituted *closo*-carboranes.

1.2.2 *Closo* – Carboranylphosphines with P(III) moieties

The chemistry of *closo*-carboranylphosphines started in 1963[15], almost immediately after discover of *ortho*-carborane, when the first P(III) derivative, 1,2-$(PPh_2)_2$-1,2-*closo*-$C_2B_{10}H_{10}$, was synthesized by R. P. Alexander and H. Schroeder in a reaction between dilithio-*ortho*-carborane and two equivalents of diphenylchlorophosphine. This reaction became a fundamental for the synthesis of numerous symmetrical 1,2-bis(phosphino)-*closo*-carboranes.

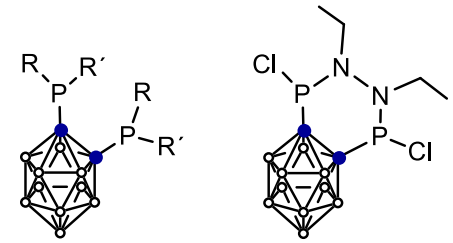

R= Ph; R´=Cl
R= t-Bu; R´=Cl
R= NEt_2; R´=Cl

Figure 1.4 1.2-bis(phosphino)-*closo*-carboranes.

P-chiral 1,2-bis(chlorophosphino)-*closo*-carboranes and cyclic compound showed on Figure 1.4 were obtained in the same reaction between dilithio-*ortho*-carborane and appropriate phosphine[16]. In many cases was possible to isolate each diastereomer.

Considering that chlorophosphines are good starting products for the synthesis of other organophosphorus compounds (phosphonate esthers and amides, phosphinic and phosphonic acids and their esters) it appeared of interest to synthesize *closo*-carboranylchloro-phosphine derivatives[15]. By the same scientists,

R. P. Alexander and H. Schroeder, it was found that equimolar quantities of dilithio-*ortho*-carborane and PCl_3 form a cyclic dimer [1,2-PCl-1,2-*closo*-$C_2B_{10}H_{10}]_2$. However, in the reaction of dilithio-*meta*-carborane with PCl_3 they found 1,7-bis(dichlorophosphino)-*closo*-carborane and *meta*-carborane containing polymer (Scheme 1.5). It can be explained by the fact that in *ortho*-carborane two carbon atoms of the cluster, C_c, are in adjacent position, while in *meta*-carborane they are separated by one B-H vertice.

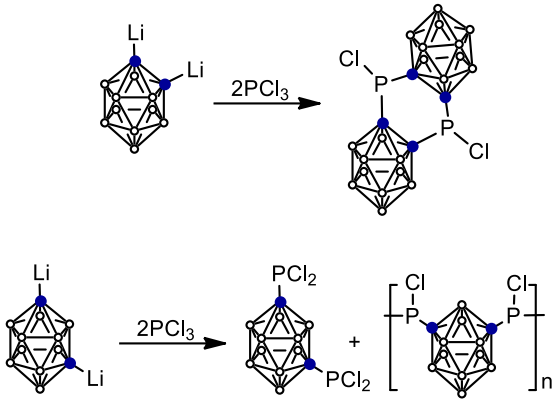

Scheme 1.5 Reaction of dilithiated *ortho*- and *meta*-carboranes and PCl_3.

In the same period of time Russian scientists also were investigating the chemistry of *closo*-carboranylchlorophosphines. They discovered that equimolar quantities of monolithio-*ortho*-carborane and PCl_3 gives a mixture of *closo*-carboranyldichlorophosphines and dicarboranylchlorophosphines[17] (Scheme 1.6). These results revealed that substitution of one chlorine atom in PCl_3 by carboranyl group increases reactivity of the other chlorine bonded to phosphorus. As a result, isolation of the dichlorophosphine in pure form was complicate, and the method mentioned above became not efficient for the synthesis of diclorophosphine derivative of carborane. Instead was developed the other method based on reaction

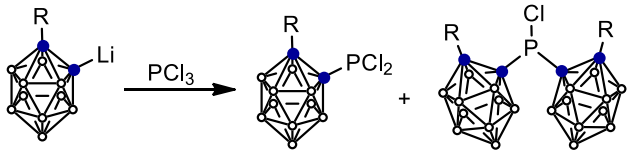

Scheme 1.6 Reaction of monolithio-*ortho*-carborane and PCl_3.

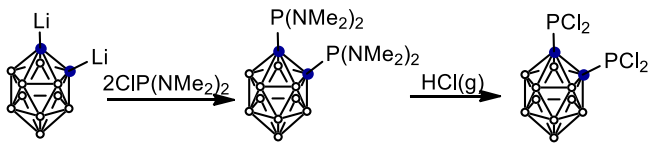

Scheme 1.7 Synthesis of 1,2-$(PCl_2)_2$-1,2-*closo*-$C_2B_{10}H_{10}$.

between dialkylaminophosphine derivative of carborane and dry HCl acid (Scheme 1.7).

Thus, diclorophosphine derivative, 1,2-$(PCl_2)_2$-1,2-*closo*-$C_2B_{10}H_{10}$, was obtained quantitatively from 1,2-$(P(NMe_2)_2$-1,2-*closo*-$C_2B_{10}H_{10}$ upon reaction with dry HCl in benzene solution.[18] 1,2-$(P(NMe_2)_2$-1,2-*closo*-$C_2B_{10}H_{10}$ was also synthesized in the reaction of dilithio-*ortho*-carborane with $ClP(NMe_2)_2$.

In contrast to organic dichlorophosphines, both alkyl- and aryl-, *closo*-carboranyldichlorophosphines were found to be stable in front of atmospheric oxygen at room temperature. Also they do not react with sulfur at temperatures below 200°C. However, they easily (exothermically) react with chlorine at ambient temperature producing *closo*-carboranyltetrachlorophosphines (Scheme 1.8).[19]

1.2.3 *Closo* – Carboranylphosphines with P(V) moieties

The first derivatives of carboranes that contain pentavalent phosphorus were synthesized by hydrolysis of diclorophosphine derivatives, 1-R-2-PCl_2-1,2-*closo*-$C_2B_{10}H_{10}$ (R=Me, Ph), producing phosphinic acids of *ortho*-carborane[18,20]. The same starting compounds in the reaction with chlorine gave tetrachlorophosphine derivative of carborane. Although tetrachlorophosphine derivatives were not isolated their existence was proved by the products of their hydrolysis, 1-R-2-$POCl_2$-1,2-*closo*-$C_2B_{10}H_{10}$ (R=Me, Ph) (Scheme 1.8).[21] Interestingly, that attempts to produce *closo*-

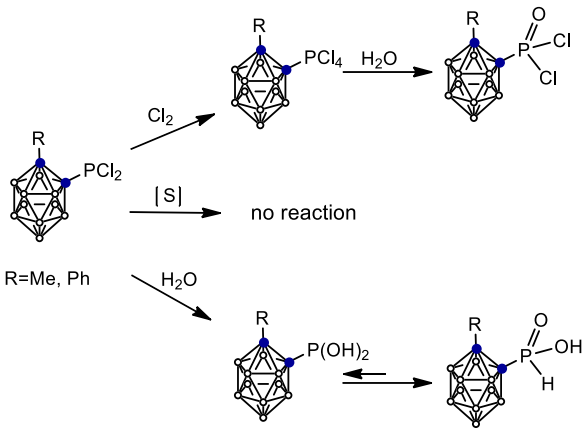

Scheme 1.8 Synthesis of the first *closo*–carboranylphosphines with P(V) moieties.

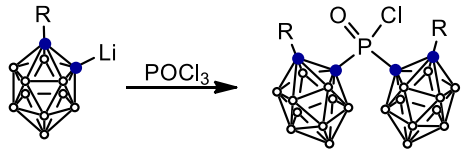

Scheme 1.9 Reaction of monolithio-*ortho*-carborane and $POCl_3$.

carboranyldichlorophosphonates by reaction of lithiated *ortho*-carborane and $POCl_3$ did not work how it was expected, giving a product of substitution of one chlorine atom by carboranyl group (Scheme 1.9). Even a big excess of $POCl_3$ gave products of substitution of two chlorine atoms producing dicarboranylchlorophosphonate, (1-R-1,2-*closo*-$C_2B_{10}H_{10})_2POCl$ (R=Me, Ph)[21].

Also P(V) derivatives can be achieved by oxidation of *closo*-carboranylchlorophosphines with chalcogens: oxygen (using H_2O_2), sulfur and selenium. The first product of oxidation by sulfur was produced upon reaction of 1-R-2-PPhCl-1,2-*closo*-$C_2B_{10}H_{10}$ (R = Me, Ph) with elemental sulfur in decane at 180ºC. The reaction of the same compound with chlorine followed by hydrolysis gives the P(V) derivative with oxygen[22] (Scheme 1.10).

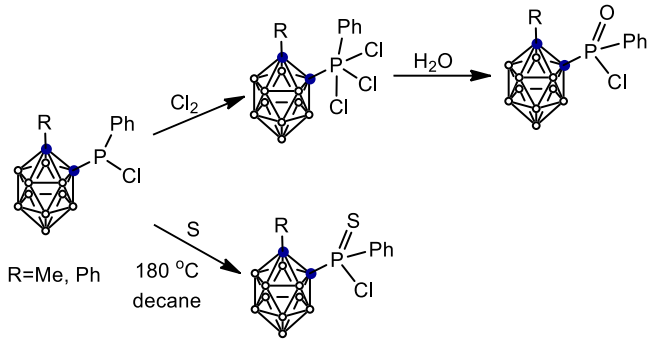

Scheme 1.10 Synthesis of oxidized carboranylphosphines.

Later in 2011 was reported a comprehensive study of the oxidation of *closo*-carboranylphosphines with H_2O_2, S and Se.[14] Oxidation of *closo*-carboranylmonophosphines with H_2O_2, S and Se yielded in all the cases the resulting oxidized monophosphine, whereas, for *closo*-carboranyldiphosphines different results were obtained. In the oxidation with H_2O_2 in acetone, both P atoms were oxidized, the reaction time depended on the organic groups bonded to the P atoms (e.g. longer time is needed for Ph than for ^{i}Pr) (Scheme 1.11). Different behavior was observed for dialkylcarboranyl and diarylcarboranyldiphosphines in oxidation with S and Se (Scheme 1.12). Oxidation of 1,2-$(PPh_2)_2$-1,2-*closo*-$C_2B_{10}H_{10}$ with sulfur produced three different species after purification: 1-$SPPh_2$-2-PPh_2-1,2-*closo*-

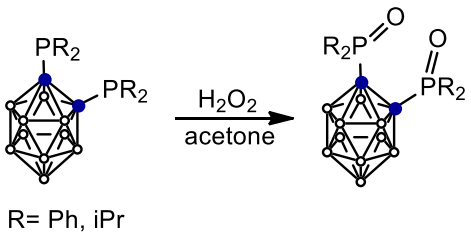

Scheme 1.11 Oxidation of *closo*-carboranyldiphosphines with H_2O_2.

$C_2B_{10}H_{10}$, 1,2-$(SPPh_2)_2$-1,2-*closo*-$C_2B_{10}H_{10}$ and 1-$SPPh_2$-2-$OPPh_2$-1,2-*closo*-$C_2B_{10}H_{10}$. Oxidation of 1,2-$(PiPr_2)_2$-1,2-*closo*-$C_2B_{10}H_{10}$ with S produced first the compound in which only one P atom is oxidized, respectively, 1-$SPiPr_2$-2-$PiPr_2$-1,2-*closo*-$C_2B_{10}H_{10}$ and if the reaction is prolonged, the C_c—P^iPr_2 bond cleavage takes place, yielding the monophosphine derivative, 1-SP^iPr_2-1,2-*closo*-$C_2B_{10}H_{11}$. Oxidation of 1,2-$(PPh_2)_2$-1,2-*closo*-$C_2B_{10}H_{10}$ with Se led only to 1-$SePPh_2$-2-PPh_2-1,2-*closo*-$C_2B_{10}H_{10}$ that remains intact even after refluxing in toluene for days. Oxidation of 1,2-$(P^iPr_2)_2$-1,2-*closo*-$C_2B_{10}H_{10}$ with selenium produces C_c— P bond cleavage, yielding the oxidized monophosphine 1-SeP^iPr_2-1,2-*closo*-$C_2B_{10}H_{11}$.

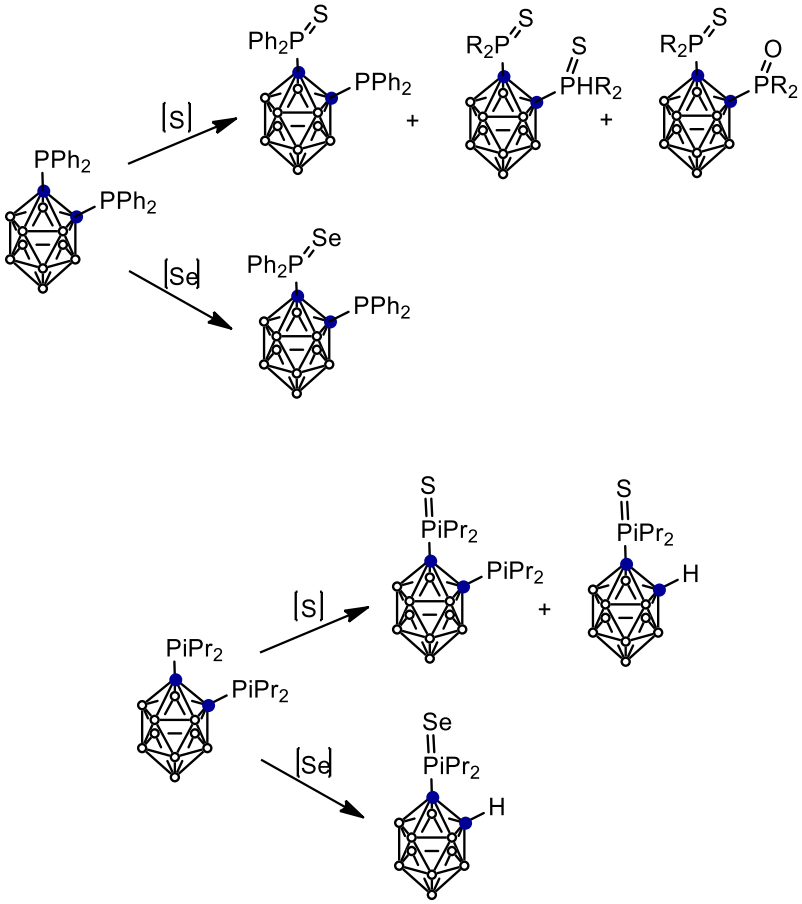

Scheme 1.12 Reaction of *closo*-carboranyldiphosphines with sulfur and selenium.

1.3 Coordination polymers incorporating icosahedral boron clusters

According to IUPAC Recommendations 2013 the definition of coordination polymer is: "*a coordination compound with repeating coordination entities extending in 1, 2, or 3 dimensions"*.[23] Coordination polymers are relevant to many fields such as organic and inorganic chemistry, biochemistry, material science, electrochemistry, pharmacology, being currently of great scientific interest and having many applications[24]. These structures are highly dependent on metal center and the nature of ligands.

Because carboranes exhibit an unusual combination of properties such as low nucleophilicity, chemical inertness, thermal stability,[25,26] electron-withdrawing via bonding at the carboranyl carbon atoms,[27,28] and electron-donating via bonding at the carborane boron atoms,[29,30] *closo*-carborane clusters can play a variety of roles in coordination polymers. They can be as guests that are accommodated by a coordination polymer. Anionic *closo*-carboranes can be incorporated into coordination polymers via B-H⋯M interactions directing a polymer chain.[31,32] Carboranes fuctionalized with the metal-binding group directly bonded to the cage (carboxylato, phosphino, thiolato) have been used to introduce C_2B_{10}-icosahedrons into the backbone of 1D coordination polymers. In this way, was found that carboranylcarboxilate ligands, 1-R-2-CO_2-1,2-*closo*-$C_2B_{10}H_{20}$ (R=CH_3, H) in the reaction with $MnCO_3$ in water produce air-stable water soluble polymeric compounds[33,34]. Depending on the substituent, -CH_3 or –H, on one of the C_c of the carboranylcarboxylate ligand, two different polymeric compounds were obtained: [Mn(μ-H_2O)(μ-1-CH_3-2-CO_2-1,2-*closo*-$C_2B_{10}H_{10})_2]_n{\cdot}(H_2O)_n$ and [Mn(H_2O)(μ-1-CO_2-1,2-*closo*-$C_2B_{10}H_{11})_2]_n{\cdot}2H_2O$ (Figure 1.5). To be noted that compound [Mn(μ-H_2O)(μ-1-CH_3-2-CO_2-1,2-*closo*-$C_2B_{10}H_{10})_2]_n{\cdot}(H_2O)_n$ was the first polynuclear Mn^{II} complex with carboxylate and aqua ligands bridging two Mn^{II} centers.

The polymeric nature of both polymers can be fragmented by coordination solvents, e.g. diethyl ether or Lewis bases, such as 2,2´-bipyridine, forming new compounds with low (mono-, di-, tri-) nuclearity, due to breakage of the corresponding polymer. The reactivity of [Mn(μ-H_2O)(μ-1-CH_3-2-CO_2-1,2-*closo*-

$C_2B_{10}H_{10})_2]_n\cdot(H_2O)_n$ with 2,2´-bipyrimidine leads to the formation of a new hybrid polymer $[Mn(1\text{-}CH_3\text{-}2\text{-}CO_2\text{-}1,2\text{-}closo\text{-}C_2B_{10}H_{10})_2(bpm)]_n$ (Figure 1.6).

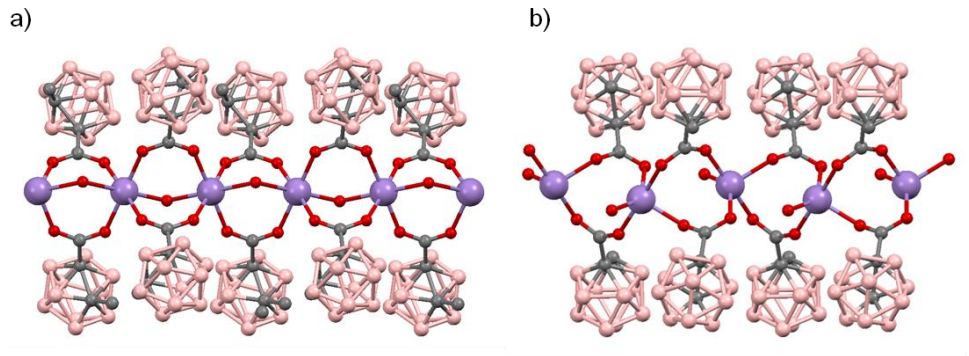

Figure 1.5 Structure of polymers $Mn(\mu\text{-}H_2O)(\mu\text{-}1\text{-}CH_3\text{-}2\text{-}CO_2\text{-}1,2\text{-}closo\text{-}C_2B_{10}H_{10})_2]_n\cdot(H_2O)_n$ (a) and $[Mn(H_2O)(\mu\text{-}1\text{-}CO_2\text{-}1,2\text{-}closo\text{-}C_2B_{10}H_{11})_2]_n\cdot 2H_2O$ (b) showing the monodimensional arrangement (H atoms are omitted for clarity).

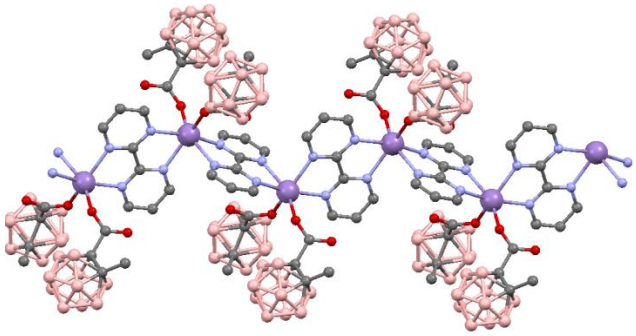

Figure 1.6 The polymer chain of the hybrid $[Mn(1\text{-}CH_3\text{-}2\text{-}CO_2\text{-}1,2\text{-}closo\text{-}C_2B_{10}H_{10})_2(bpm)]_n$ (H atoms are omitted for clarity).

Coordination properties of phosphino-functionalized carboranes $1,2\text{-}(PR_2)_2\text{-}1,2\text{-}C_2B_{10}H_{10}$ are well studied. And in the chemistry of coordination polymers, a few examples exist with this type of ligands. The synthesis of novel 1D chain was reported by Dou et al. in 2011 starting from $1,2\text{-}(PPh_2)_2\text{-}1,2\text{-}C_2B_{10}H_{10}$ and $HgCl_2$[35], $\{[Hg_5(1,2\text{-}(PPh_2)_2\text{-}1,2\text{-}C_2B_{10}H_{10})_2(\mu\text{-}Cl)_8]\cdot 2CH_2Cl_2\}_n$. The same year was reported other chain-like polymer, $[Ag_2(SCN)_2\{1,2\text{-}(PCy_2)_2\text{-}1,2\text{-}C_2B_{10}H_{10}\}_2]_n\cdot CH_2Cl_2$, prepared from $1,2\text{-}(PCy_2)_2\text{-}1,2\text{-}C_2B_{10}H_{10}$ (Cy = cyclohexyl) with silver salt AgSCN[36] (Figure 1.7).

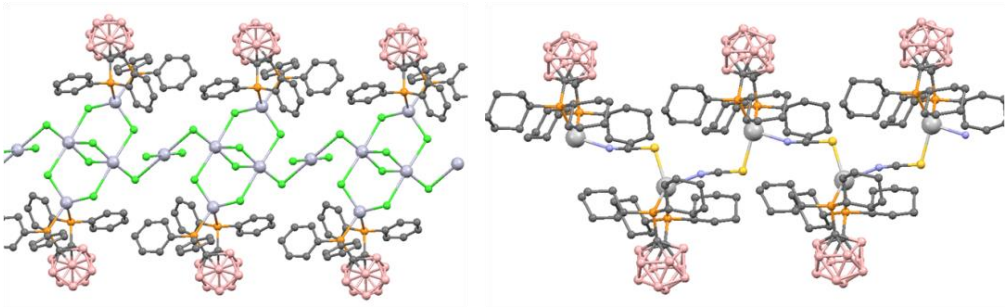

Figure 1.7 The 1D polymer chain structure of complexes $\{[Hg_5(1,2\text{-}(PPh_2)_2\text{-}1,2\text{-}C_2B_{10}H_{10})_2(\mu\text{-}Cl)_8]\cdot 2CH_2Cl_2\}_n$ and $[Ag_2(SCN)_2\{1,2\text{-}(PCy_2)_2\text{-}1,2\text{-}C_2B_{10}H_{10}\}_2]_n\cdot CH_2Cl_2$ (H atoms are omitted for clarity).

1.4 Characteristics and applications of phosphinate complexes

Phosphinic acids are of the general formula $R_2P(O)OH$ where R can be H, alkyl or aryl group or combination of any two. They are related to other P (V) compounds, such as phosphine oxides, phosphonic acids and phosphoric acid (Figure 1.8). Industrially, these types of phosphorus compounds and their esters are used for the separation and purification of different metals.[37]

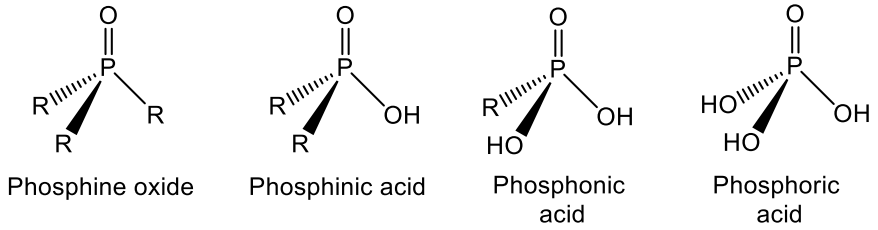

Figure 1.8 Schematic representation of P(V) compounds.

Mixtures of bis(2,4,4-trimethylpentyl)phosphinic acid and tri(2,4,4-trimethyloctyl)phosphine oxide are sold by Cytec Industries Inc. with the name *Cyanex 272* and are used for the extraction and purification of different metals. Notably, *Cyanex 272* is most commonly used in the separation of cobalt from nickel.[38] Despite their extensive use in the purification of different metals, the coordination chemistry of phosphinic acids is relatively unexplored.

Although phosphinic acids and related P (V) compounds are generally drawn with a phosphorus-oxygen double bond its nature has been the subject of intense studies for many years. Experimental and theoretical calculations clearly suggest the absence of conventional double bonding in the phosphorus-oxygen bond. The recent investigations emphasize that P=O unit is better described with the highly polar structure $P^{+}–O^{-}$.[39–41]

In some way phosphinic and carboxylic acids are structurally related (Figure 1.9). Both compounds are oxoacids in which the acidic moiety consists of an oxide and hydroxide bonded to a central atom that is electron deficient. Due to this deficiency, the hydroxyl group can ionize relatively easily to form either a phosphinate or carboxylate anion and a proton. Where carboxylic and phosphinic acids differ is in their geometry and nature of their bonding. Phosphinic acids are always tetrahedral in shape with four different moieties bonding to the central phosphorus atom. The identities of the two moieties that are not the oxide or hydroxide can have profound effects on the steric nature of the phosphinic acids, this could change how the phosphinic acid or phosphinate coordinates to metal atoms.

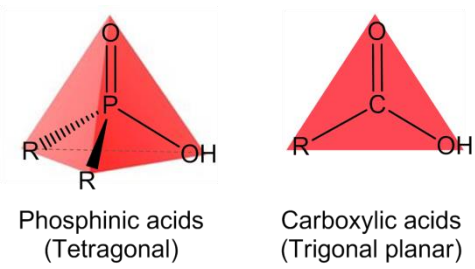

Figure 1.9 Geometry of phosphinic and carboxylic acids.

Carboxylic acids on the other hand, are trigonal planar compounds with only three moieties bonded to the central carbon atom. The identity of the one moiety that is not the hydroxide or oxide can also have similar steric effects on the coordination of the carboxylic acid or carboxylate to metal atoms. Unlike the O=P bond, the O=C double bond in carboxylic acids is in fact a true double bond consisting of one σ-bond and one π-bond. The carboxylate anion, when compared to the phosphinate anion, would have less electron density spread over its two oxygens due to its resonance structures. This would presumably decrease the

amount of electron density that can be donated to a metal center potentially lowering its effectiveness in stabilizing high oxidation state metals.

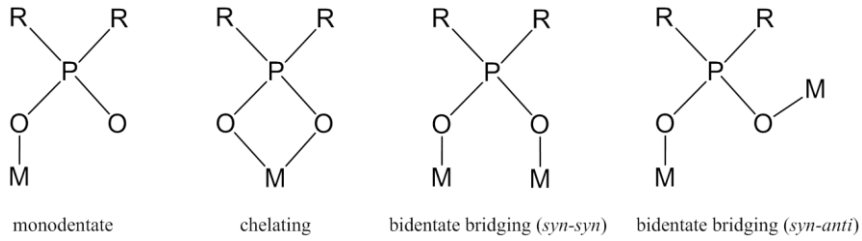

Figure 1.10 Examples of coordination modes of phosphinates.

Phosphinate anion exhibits a versatile coordination behavior displaying various bonding modes toward metal cations. Some of the more common modes are presented in Figure 1.10. Coordination chemistry of phosphinic acids type $R_2P(O)OH$ (R= alkyl, aryl) is more frequent then of type RPH(O)OH. A search at the Cambridge Structural Database (CSD), On February 9th 2017 shows 102 hits for phosphinic acid $R_2P(O)OH$ (R=alkyl, aryl) and 211 for its transition metal complexes, but only 20 hits for phosphinic acids R-P(H)O(OH) (R=alkyl, aryl) and 47 hits were found for its transition metal complexes. On the other hand, a search at the Cambridge Structural Database (CSD version 5.38) shows 375 hits for phosphonic acid $R\text{-}PO(OH)_2$ (R=alkyl, aryl) and >2200 hits for its transition metal complexes (Figure 1.11).

Figure 1.11 Relative percentage of hits of $R_2P(O)OH$, P(H)O(OH) and $R\text{-}PO(OH)_2$ and its corresponding complexes found at the Cambridge Structural Database (CSD), On February 9th 2017.

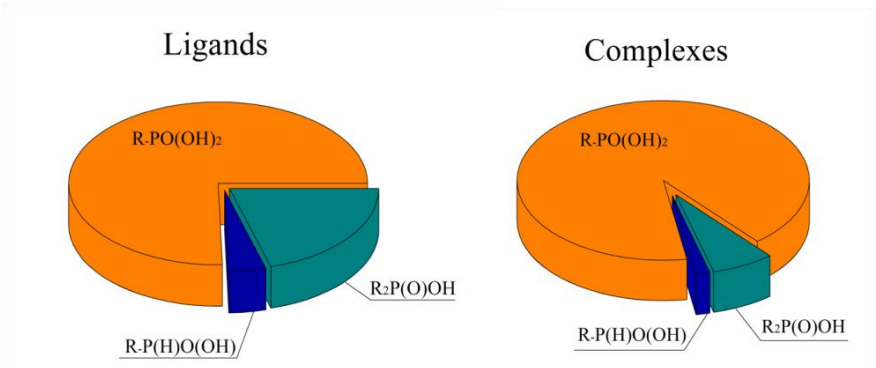

Most of a few complexes of phosphinic acids of the formula RPH(O)OH that have been found in the literature are formed with phenylphosphinate ligand, PhPH(O)OH and transition metals such as Mn^{II},[42,43,44,45] Sb^{II},[46,47] Co^{II},[48,49] Cu^{II},[48] Gd^{II},[50] Zn^{II},[51] Al^{III}.[52] In these metal phosphinate complexes, the phosphinate ligand is monodentate or bridging two metal centers.

Isotope	Cross section (barns)
^{10}B	3837
^{11}B	0.005
^{12}C	0.0035
^{1}H	0.33
^{14}N	1.7
^{35}Cl	43.6
^{23}Na	0.534
^{157}Gd	25400
^{153}Gd	0.02

Table 1.1 Thermal Neutron Cross Sections.

1.5 Boron Neutron Capture Therapy for tumor targeting

Neutron Capture Therapy (NCT) is a bimodal therapy that utilizes a neutron source to generate an internal destroying radiation in tumor cells that leads to their death. As opposed to conventional radiation therapy using X rays or γ rays where an external radiation source is required, a big advantage of NCT is that the surrounding healthy tissue is not exposed to the radiation that can be a big issue in treatment of tumors in deep parts of the body. Thus, NCT requires the use of an isotope with high neutron capture cross section. The “organic” elements such as C, H, O, N have very low neutron capture cross section (< 2 barn). In contrast, isotopes of other elements such as boron and gadolinium, ^{10}B and ^{157}Gd, are good at absorbing neutrons (capture cross section for ^{10}B is 3840 barn, for ^{157}Gd- 25400 barn). Also ^{10}B isotope was an attractive element due to its high

natural abundance of 20%. ^{157}Gd isotope also has a natural abundance of 15.7% that can be effective to capture neutrons. Up to now GdNCT has never been used clinically (i.e., in humans), the reason being the toxicity concern of gadolinium. On the other hand, over 900 patients have already undergone Boron Neutron Capture Therapie, BNCT, worldwide and effects of BNCT on malignant tumors and healthy surrounding tissue seemed to be established.

The history of BNCT started in 1932 since the discovery of the neutron by Chadwick,[53] followed by Locher´s proposal to use neutron capture reactions in cancer treatment (Figure 1.12).[54]

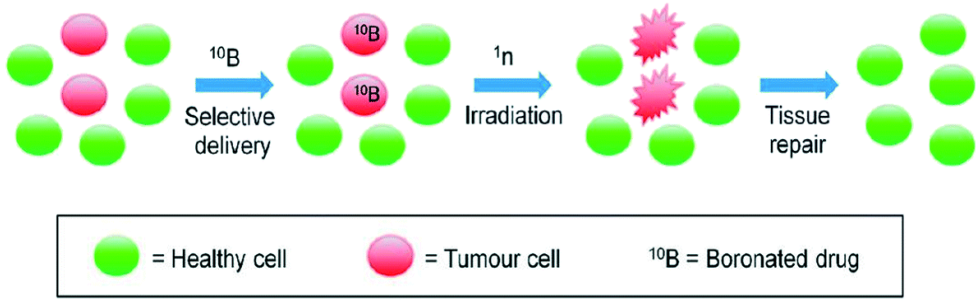

Figure 1.12 BNCT steps: the selective delivery of ^{10}B-containing drugs to tumor cells is followed by irradiation with thermal neutrons (^{1}n) to initiate the destruction of cancer cells and to allow tissue repair (figure from ref.[74]).

BNCT technique consists of two steps: the selective delivery of ^{10}B-containing agents to tumor cells followed by their irradiation with low-energy neutrons, which results into the prompt nuclear reaction. The predominant products of this reaction are ^{7}Li nuclei and high liner energy transfer (LET) α particles. LET particles are lethal but their effect is concentrated mostly inside of host cells due to their short path length in tissues (4.5-10μm).

Research in the area of development of boron-containing delivery agents for BNCT started ~ 60 years ago with the investigation of a large number of boron compounds, that were regarded as “first-generation” agents for BNCT.[55] The most important requirements for a BNCT delivery agent are: i) low toxicity, ii) water solubility, iii) good tumor-cell selectivity, with a tumor: normal tissue and tumor: blood rations higher than 3, iv) be deliverable at around 20 μg ^{10}B/g (tumor tissue),

v) persistence in tumor cells during the course of neutron irradiation, vi) capacity to penetrate biological barriers, such as the blood-brain barrier (BBB).

So far, clinically for the treatment of patients with malignant brain tumors and malignant melanoma has been used two main boron delivery agents: sodium borocaptate, $Na_2B_{12}H_{11}SH$ (BSH), and boronophenylalanine (BPA) which formulas are displayed in the Figure 1.13. And during the last 20 years a big number of boron delivery agents have appeared using different approaches. Among them are derivatives of biological molecules (aminoacids, nucleic acids, peptides, DNA-binding molecules), porphyrin derivatives, nanovehicles (liposomes), dendrimers. Also other delivery systems such as nanoparticles are currently under research. Hosmane et al. attempted to use magnetic nanoparticles for boron delivery into tumor cells.[56]

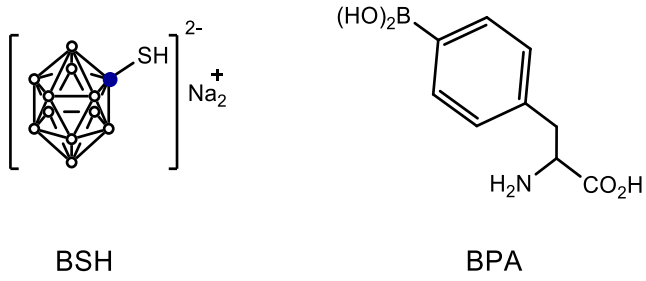

Figure 1.13 Chemical structures of boron compounds used in BNCT clinical trials.

1.6 Magnetic nanomaterials: properties and applications in biomedicine

Since the first synthesis of a magnetic fluid that was reported in 1965 in the pioneering work by Papell,[57] an increase of scientific production took place in this area (Figure 1.14).

The research field of magnetic nanoparticles is multi-disciplinary: chemists work on the synthetic part, physicists and engineers study their physical properties and their

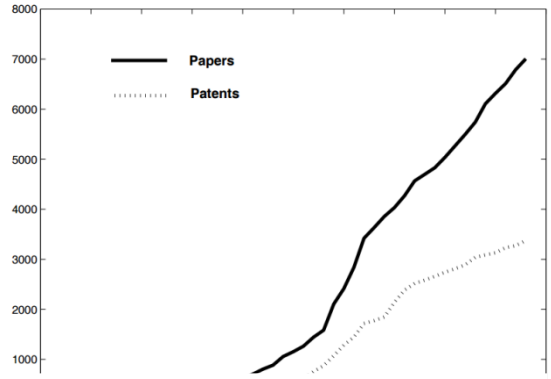

Figure 1.14 Increase in production of papers and patents on magnetic nanoparticles (figure from ref.[75]).

applicability, and biologists study their possibility in biomedical applications such as magnetic drug targeting, hyperthermia, Magnetic Resonance Imaging (MRI).[58–65]

What makes magnetic nanoparticles (MNPs) interesting for biomedical application? Most applications of MNPs are based on the following properties: i) their high surface/volume ratio; their size is at the scale of the important biomolecules such as proteins and DNA and 10^3 times smaller cells ii) MNPs follow the magnetic field; iii) MNPs absorb electromagnetic energy and heats up.

1.6.1 Magnetic property

The base of magnetism arises from two important characteristics of electrons: the orbital movement of the electron around the atomic nucleus and the movement of the electronic spin around its axis. This association of an orbital and a spin magnetic moments makes an electron to behave like a tiny magnet. Magnetization is the sum of all magnetic moments (m) of the atoms in a material per unit volume (V), $\mathrm{M} = \frac{\mathrm{m}}{\mathrm{V}}$ (emu/cm^3). For practical reasons, magnetization (M) is often referred to unit mass and expressed as emu/g.

All materials respond differently when they are exposed to an externally applied magnetic field, and according to this they can be classified into diamagnetic, paramagnetic, ferromagnetic, antiferromagnetic and ferromagnetic (Figure 1.15). In *diamagnetic* materials an applied magnetic field creates an induced magnetic field in the opposite direction, so they are repelled by a magnetic field. Materials whose atomic magnetic moments are uncoupled are *paramagnetic*. These materials are slightly attracted by a magnetic field and they do not retain the magnetic properties when the external field is removed. *Ferromagnetic* materials have aligned atomic magnetic moments of equal magnitude. In the presence of a magnetic field, they have a strong net magnetization that partially remains when the magnet is not longer applied. In *ferrimagnets* atomic magnetic moments align antiparallel but have different strength. *Antiferromagnetic* substances show zero net

magnetization even being under the influence of a magnetic field due to the antiparallel alignment of magnetic moments of equal magnitude.

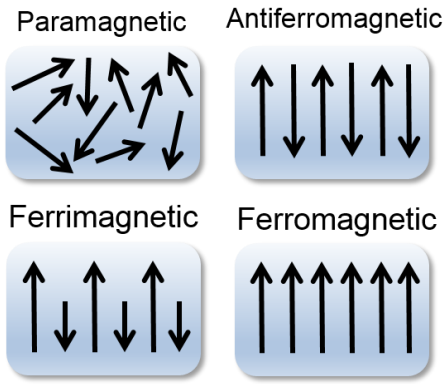

Figure 1.15 Types of magnetic materials (arrows represent the atomic magnetic moments orientation).

The domain structure of a ferromagnetic material determines the size dependence of its magnetic behavior (Figure 1.16). When the size of a ferromagnetic material is reduced below a critical value, it becomes a single domain. For single domain magnetic nanoparticles their magnetic energy becomes comparable to its thermal energy.

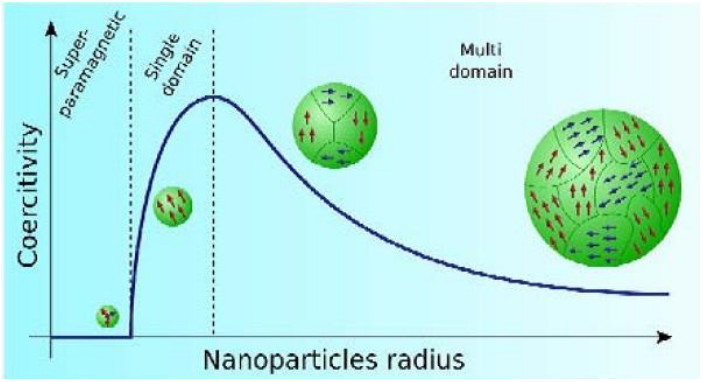

Figure 1.16 Schematic illustration of the coercivity-size relations of small particles (figure from ref.[76])

The respond of ferromagnetic materials on an applied magnetic field is described by hysteresis loop, which is characterized by two main parametrs: remanence (M_R) and coercivity (H_C). When the size of particles is below the size of

single-domain, its thermal energy overcomes its magnetic energy, so the magnetization vector of single-domain nanoparticles can be reversed spontaneously. As a result, the coercivity becomes zero, and particles become *superparamagnetic*. Superparamagnetism is a size effect of ferromagnetism. Superparamagnetic particles become magnetic in the presence of an external magnetic field, but demagnetize when the external magnetic field is removed, thus they have no hysteresis (Figure 1.17). This property makes superparamagnetic particles very attractive for applications in biological systems since they can be "activated" or "disactivated" depending on the applied external magnetic field.

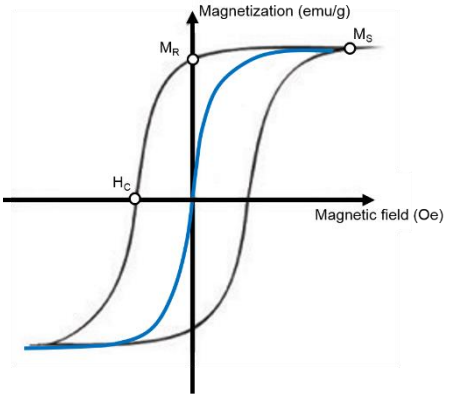

Figure 1.17 Magnetization *vs*. applied magnetic field for a ferromagnetic (black) and a superparamagnetic (blue) material.

The temperature plays an important role in defining the superparamagnetic state of magnetic nanoparticles. At some point at low temperatures in superparamagnetic materials, the thermal energy becomes smaller than its magnetic energy, and material is not superparamagnetic anymore. The temperature above which nanoparticles are in superparamagnetic state calls *blocking temperature*, T_B. The blocking temperature value in a superparamagnetic material can be found from zero-field cooling (ZFC) and field cooling (FC) measurements of

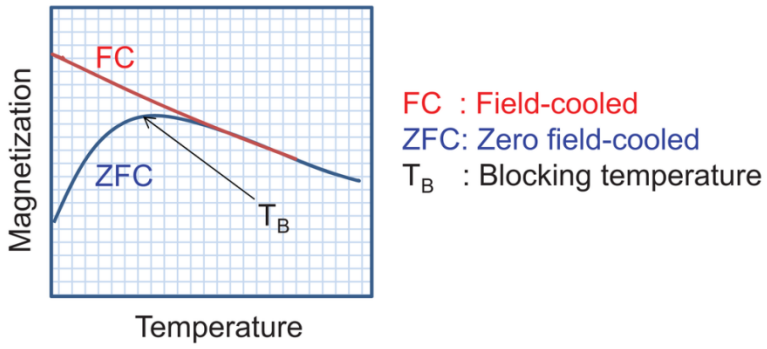

Figure 1.18 Zero-field cooling field cooling curves of superparamagnetic nanoparticles (figure from ref [77])

magnetization *vs* temperature (Figure 1.18), performed by heating the sample under a constant magnetic field in *Superconductive Quantum Interference Device* (SQUID). In ZFC curve, the magnetic moment increases with the temperature and then decreases, while the moment decreased in FC curve. The temperature at the peak point of ZFC curve is the Blocking temperature.

Magnetite, Fe_3O_4, is the most magnetic of all the naturally occurring minerals on earth, and it is widely being investigated in the form of superparamagnetic nanoparticles (SPIONs or MNPs) during the last 20 years for numerous *"in vivo"* and *"in vitro"* applications such as magnetic resonance imaging (MRI) contrast enhancement,[66,67] tissue repair, detoxification of biological fluids, hyperthermia, drug delivery, immunoassays and cell separation techniques.[68–70] Further developments in the synthesis and bioorthogonal chemistry of nanoparticles have broadened MNPs applications to the therapeutic areas.[71,72]

1.7 Objectives and justification of the thesis

From the brief introduction presented above it is clear that the chemistry of the carborane derivatives with phosphorus moieties have been well studied except carboranylphosphinic and carboranylphosphonic acids. This doctoral thesis symbolized the introduction a new research line to the existing ones in the research group and has been developed centered in the:

- Synthesis and characterization of carboranylphosphinic and carboranylphosphonic acids to use them as a versatile purely inorganic building blocks.

- Study of the coordination chemistry of *m*-carboranylphosphinate ligands with the first and the second raw transition metals, aiming to generate purely inorganic coordination polymers (CPs).

- Using possibilities offered by the phopshinate coordinating group, and properties bestowed by the *m*eta-carboranyl unit (spherical nature, hydrophobicity), we aimed to produce boron cluster-Magnetic Nanoparticles nanohybrids functionalized with *m*-carboranylphosphinate (**1**-MNPs), then learn on their structural and physicochemical properties. To illustrate their potential biomedical applications as drug carriers or in Boron Neutron Capture Therapy (BNCT) was planned to study the cytotoxicity and cellular uptake of these **1**-MNPs from culture media by different human cell lines.

(1) Eberhardt, W. H.; Crawford, B.; Lipscomb, W. N. *J. Chem. Phys.* **1954**, *22* (6), 989–985.

(2) Teixidor, F.; Viñas, C.; Demonceau, A.; Nuñez, R. *Pure Appl. Chem.* **2003**, *75* (9), 1305–1313.

(3) Scholz, M.; Hey-Hawkins, E. *Chem. Rev.* **2011**, *111* (11), 7035–7062.

(4) Poater, J.; Solà, M.; Viñas, C.; Teixidor, F. *Angew. Chemie Int. Ed.* **2014**, *53* (45), 12191–12195.

(5) Poater, J.; Solà, M.; Viñas, C.; Teixidor, F. *Chem. - A Eur. J.* **2013**, *19* (13), 4169–4175.

(6) Poater, J.; Solà, M.; Viñas, C.; Teixidor, F. *Chem. - A Eur. J.* **2016**, *22* (22), 7437–7443.

(7) Grimes, R. N. *«Carboranes» 2nd Edition, Academic Press: Burlington, MA*; Burlington, MA, 2011.

(8) Gomez, F. A.; Hawthorne, M. F. *J. Org. Chem.* **1992**, *57* (5), 1384–1390.

(9) Vinas, C.; Benakki, R.; Teixidor, F.; Casabo, J. *Inorg. Chem.* **1995**, *34* (14), 3844–3845.

(10) Valliant, J. F.; Guenther, K. J.; King, A. S.; Morel, P.; Schaffer, P.; Sogbein, O. O.; Stephenson, K. A. *Coord. Chem. Rev.* **2002**, *232* (1), 173–230.

(11) Popescu, A.-R.; Musteti, A. D.; Ferrer-Ugalde, A.; Viñas, C.; Núñez, R.; Teixidor, F. *Chem. - A Eur. J.* **2012**, *18* (11), 3174–3184.

(12) Aldrich.com. .

(13) Popescu, A. R.; Teixidor, F.; Viñas, C. *Coord. Chem. Rev.* **2014**, *269*, 54–84.

(14) Popescu, A.-R.; Laromaine, A.; Teixidor, F.; Sillanpää, R.; Kivekäs, R.; Llambias, J. I.; Viñas, C. *Chem. - A Eur. J.* **2011**, *17* (16), 4429–4443.

(15) Alexander, R. P.; Schroeder, H. *Inorg. Chem.* **1963**, *2* (6), 1107–1110.

(16) Sterzik, A.; Rys, E.; Blaurock, S.; Hey-hawkins, E. **2001**, *20*, 3007–3014.

(17) Zakharkin, L. I.; Bregadze, V. I.; Okhlobystin, O. Y. *J. Organomet. Chem.* **1965**, *4* (3), 211–216.

(18) L.I. Zakharkin, A.V. Kazantsev, M. N. Z. *Izv. Akad. Nauk SSSR, Ser. Khim.* **1969**, *9*, 2056–2057.

(19) Zakharkin, L. I.; Bregadze, V. I.; Okhlobystin, O. Y. *J. Organomet. Chem.*

1965, *4* (3), 211–216.

(20) A.V. Kazantsev, M.N. Zhubekova, L. I. Z. *Zh. Obs. Khim.* **1971**, *42*, 1570–1571.

(21) L.I. Zakharkin, M.N. Zhubekova, A. V. K. *Zh. Obs. Khim.* **1971**, *41*, 588–592.

(22) A.V. Kazantsev, M.N. Zhubekova, L. I. Z. *Zh. Obs. Khim.* **1971**, *41*, 2027.

(23) Batten, S. R.; Champness, N. R.; Chen, X.-M.; Garcia-Martinez, J.; Kitagawa, S.; Öhrström, L.; O'Keeffe, M.; Paik Suh, M.; Reedijk, J. *Pure Appl. Chem.* **2013**, *85* (8), 1715–1724.

(24) Fromm, K. M. *Coord. Chem. Rev.* **2008**, *252* (8), 856–885.

(25) Plesek, J. *Chem. Rev.* **1992**, *92* (2), 269–278.

(26) Grimes, R. N. *Carboranes. Third Edition*; Elsevier Inc.: New York/Oxford, 2016.

(27) Núñez, R.; Farràs, P.; Teixidor, F.; Viñas, C.; Sillanpää, R.; Kivekäs, R. *Angew. Chemie Int. Ed.* **2006**, *45* (8), 1270–1272.

(28) Teixidor, F.; Núñez, R.; Viñas, C.; Sillanpää, R.; Kivekäs, R. *Angew. Chemie* **2000**, *39* (23), 4290–4292.

(29) Teixidor, F.; Barberà, G.; Vaca, A.; Kivekäs, R.; Sillanpää, R.; Josep Oliva, A.; Viñas, C. *J. Am. Chem. Soc* **2005**, *127* (29), 10158–10159.

(30) Spokoyny, A. M.; Machan, C. W.; Clingerman, D. J.; Rosen, M. S.; Wiester, M. J.; Kennedy, R. D.; Stern, C. L.; Sarjeant, A. A.; Mirkin, C. A. *Nat. Chem.* **2011**, *3* (8), 590–596.

(31) Hardie, M. J. *J. Chem. Crystallogr.* **2006**, *37* (1), 69–80.

(32) Núñez, R.; Romero, I.; Teixidor, F.; Viñas, C.; Xie, Z.; Viñas, C.; Aliaga-Alcalde, N.; Matějíček, P.; Hosmane, N. S.; Beavis, P.; Heeney, M. *Chem. Soc. Rev.* **2016**, *45* (19), 5147–5173.

(33) Fontanet, M.; Rodríguez, M.; Romero, I.; Fontrodona, X.; Teixidor, F.; Viñas, C.; Aliaga-Alcalde, N.; Matějíček, P. *Dalt. Trans.* **2013**, *42* (22), 7838.

(34) Fontanet, M.; Rodríguez, M.; Fontrodona, X.; Romero, I.; Teixidor, F.; Viñas, C.; Aliaga-Alcalde, N.; Matějíček, P. *Chem. - A Eur. J.* **2014**, *20* (43), 13993–14003.

(35) Kong, L.; Zhang, D.; Su, F.; Lu, J.; Li, D.; Dou, J. *Inorganica Chim. Acta* **2011**, *370* (1), 1–6.

(36) Yang, L.-G.; Zhu, C.-C.; Zhang, D.-P.; Li, D.-C.; Wang, D.-Q.; Dou, J.-M. *Polyhedron* **2011**, *30* (9), 1469–1477.

(37) Kalina, D. G.; Horwitz, E. P.; Kaplan, L.; Muscatello, A. C. *Sep. Sci. Technol.* **1981**, *16* (9), 1127–1145.

(38) Tait, B. K. *Hydrometallurgy* **1993**, *32* (3), 365–372.

(39) Gilheany, D. G. *Chem. Rev.* **1994**, *94* (5), 1339–1374.

(40) D. B. Chesnut*, †; Savin‡, A. **1999**.

(41) Chesnut†, D. B. **2003**.

(42) Richeter, S.; Larionova, J.; Long, J.; van der Lee, A.; Leclercq, D. *Eur. J. Inorg. Chem.* **2013**, *2013* (18), 3206–3216.

(43) Kevin Bernot, †,‡; Javier Luzon, †; Roberta Sessoli, *,†; Alessandro Vindigni, §; Julien Thion, ǁ; Sébastien Richeter, ǁ; Dominique Leclercq, ǁ; Joulia Larionova, ǁ and; Lee⊥, A. van der. **2008**.

(44) Taylor, S. M.; McIntosh, R. D.; Beavers, C. M.; Teat, S. J.; Piligkos, S.; Dalgarno, S. J.; Brechin, E. K. *Chem. Commun. (Camb).* **2011**, *47* (5), 1440–1442.

(45) Inglis, R.; Dalgarno, S. J.; Brechin, E. K. *Dalt. Trans.* **2010**, *39* (20), 4826.

(46) Srungavruksham, N. K.; Baskar, V. *Eur. J. Inorg. Chem.* **2013**, *2013* (24), 4345–4352.

(47) Svoboda, T.; Jambor, R.; Růžička, A.; Padělková, Z.; Erben, M.; Dostál, L. *Eur. J. Inorg. Chem.* **2010**, *2010* (33), 5222–5230.

(48) Liu, M.-J.; Cao, D.-K.; Liu, B.; Li, Y.-Z.; Huang, J.; Zheng, L.-M. *CrystEngComm* **2012**, *14* (14), 4699.

(49) Lukeš, I.; Císařová, I.; Vojtíšek, P.; Bazakas, K. *Polyhedron* **1995**, *14* (20–21), 3163–3166.

(50) Kotková, Z.; Pereira, G. A.; Djanashvili, K.; Kotek, J.; Rudovský, J.; Hermann, P.; Vander Elst, L.; Muller, R. N.; Geraldes, C. F. G. C.; Lukeš, I.; Peters, J. A. *Eur. J. Inorg. Chem.* **2009**, *2009* (1), 119–136.

(51) Pothiraja, R.; Shanmugan, S.; Walawalkar, M. G.; Nethaji, M.; Butcher, R. J.; Murugavel, R. *Eur. J. Inorg. Chem.* **2008**, *2008* (11), 1834–1845.

(52) Y. Wang; S. Parkin, and; Atwood*, D. **2002**.

(53) Chadwick, J. *Proc. R. Soc. London A Math. Phys. Eng. Sci.* **1932**, *136* (830).

(54) G.L. Locher. *Am J Roentgenol Radium Ther. 1936* (36), 1–13.

(55) Hawthorne, M. F.; Maderna, A. **1999**.

(56) Zhu, Y.; Lin, Y.; Zhu, Y. Z.; Lu, J.; Maguire, J. A.; Hosmane, N. S. *J. Nanomater.* **2010**, *2010*, 1–8.

(57) Papell, S. S. Low Viscosity Magnetic Fluid Obtained by Colloidal Suspension of Magnetic Particles. U. S. Patent no. 3. 215, 1965.

(58) Feliu, N.; Docter, D.; Heine, M.; del Pino, P.; Ashraf, S.; Kolosnjaj-Tabi, J.; Macchiarini, P.; Nielsen, P.; Alloyeau, D.; Gazeau, F.; Stauber, R. H.; Parak, W. J.; Star, A.; Shvedova, A. A.; Ruiz-Lozano, P.; Serpooshan, V.; Shokrgozar, M. A.; Nienhaus, G. U.; Parak, W. J.; Star, A.; Shvedova, A. A. *Chem. Soc. Rev.* **2016**, *45* (9), 2440–2457.

(59) Lee, N.; Hyeon, T.; Park, Y. I.; Lee, N.; Li, F.; Song, C.; Choi, S. H.; Na, K.; Hyeon, T.; Kim, J.; Hyeon, T.; Beisiegel, U.; Adam, G.; Weller, H.; Choi, S. H.; Hyeon, T. *Chem. Soc. Rev.* **2012**, *41* (7), 2575–2589.

(60) Haun, J. B.; Yoon, T.-J.; Lee, H.; Weissleder, R. *Wiley Interdiscip. Rev. Nanomedicine Nanobiotechnology* **2010**, *2* (3), 291–304.

(61) Kaittanis, C.; Santra, S.; Santiesteban, O. J.; Henderson, T. J.; Perez, J. M. *J. Am. Chem. Soc.* **2011**, *133* (10), 3668–3676.

(62) Faivre, D.; Bennet, M. *Nature* **2016**, *535* (7611), 235–236.

(63) Ling, D.; Hyeon, T. *Small* **2013**, *9* (9–10), 1449–1449.

(64) Mahmoudi, M.; Sahraian, M. A.; Shokrgozar, M. A.; Laurent, S. *ACS Chem. Neurosci.* **2011**, *2* (3), 118–140.

(65) Lee, N.; Yoo, D.; Ling, D.; Cho, M. H.; Hyeon, T.; Cheon, J. *Chem. Rev.* **2015**, *115* (19), 10637–10689.

(66) Casula, M. F.; Floris, P.; Innocenti, C.; Lascialfari, A.; Marinone, M.; Corti, M.; Sperling, R. A.; Parak, W. J.; Sangregorio, C. *Chem. Mater.* **2010**, *22* (5), 1739–1748.

(67) Lee, N.; Hyeon, T. *Chem. Soc. Rev.* **2012**, *41* (7), 2575–2589.

(68) Ling, D.; Hyeon, T. *Small* **2013**, *9* (9–10), 1450–1466.

(69) Yoo, D.; Lee, J.-H.; Shin, T.-H.; Cheon, J. *Acc. Chem. Res.* **2011**, *44* (10), 863–874.

(70) Jun, Y.; Lee, J.; Cheon, J. *Angew. Chemie Int. Ed.* **2008**, *47* (28), 5122–5135.

(71) Mahmoudi, M.; Sahraian, M. A.; Shokrgozar, M. A.; Laurent, S. *ACS Chem. Neurosci.* **2011**, *2* (3), 118–140.

(72) Sosnovik, D. E.; Nahrendorf, M.; Weissleder, R. *Circulation* **2007**, *115* (15), 2076–2086.

(73) Weber, L.; Kahlert, J.; Brockhinke, R.; Böhling, L.; Halama, J.; Brockhinke, A.; Stammler, H.-G.; Neumann, B.; Nervi, C.; Harder, R. A.; Fox, M. A. *Dalt. Trans.* **2013**, *42* (30), 10982.

(74) Gianpiero, C.; Anis, D.; Aikaterini, R.; Eirini, T.; Ioannis, V. S.; Dimitrios, F. G.; John, T. *Med. Chem. Commun.* **2017**, *8* (1), 67–72.

(75) Scherer, C.; Figueiredo Neto, A. M. *Brazilian J. Phys.* **2005**, *35* (3A).

(76) Akbarzadeh, A.; Samiei, M.; Davaran, S. *Nanoscale Res. Lett.* **2012**, *7*, 144.

(77) Kolhatkar, A.; Jamison, A.; Litvinov, D.; Willson, R.; Lee, T. *Int. J. Mol. Sci.* **2013**, *14* (8), 15977–16009.